Summer 5-17-2012

Evaluating Vegetation Response to Water Stress Using Close-Range and Satellite Remote Sensing

Sharmistha Swain
University of Nebraska-Lincoln, sharmisthaswain@gmail.com

EVALUATING VEGETATION RESPONSE TO WATER STRESS USING CLOSE-RANGE AND SATELLITE REMOTE SENSING

by

Sharmistha Swain

A DISSERTATION

Presented to the Faculty of

The Graduate College at the University of Nebraska

In Partial Fulfillment of Requirements

For the Degree of Doctor of Philosophy

Major: Geography

Under the Supervision of Professors Sunil Narumalani and Brian D. Wardlow

Lincoln, Nebraska

May, 2012

EVALUATING VEGETATION RESPONSE TO WATER STRESS USING CLOSE-RANGE AND SATELLITE REMOTE SENSING

Sharmistha Swain, Ph.D.

University of Nebraska, 2012

Advisors: Sunil Narumalani and Brian D. Wardlow

Drought is a weather related natural disaster that occurs in virtually all climatic zones of the world. In the last century, almost all parts of the contiguous United States have experienced several prolonged drought events with considerable impacts on the agricultural economy and environment. With changing climates, the droughts are expected to be more severe, longer, and widespread in many parts of the world including sections of the United States. Understanding the response of vegetation to water stress using remote sensing technologies will enhance our ability to detect and monitor drought. This research evaluates the response of vegetation to drought-related water stress at the leaf, canopy, and landscape scales using remotely sensed reflectance and/or thermal data. At the leaf level, a crop water stress index model was developed using high spatial resolution thermal imagery to estimate Relative Water Content (RWC) in soybean leaves. The model showed a higher accuracy in RWC determination (85%) compared to the raw temperature based RWC determination (69%). At the canopy level, multi-year close-range reflectance based vegetation indices (VIs) were correlated with soil moisture measured at four depths of maize and soybean root zone. Results indicated that maize VIs were significantly related to soil moisture at deeper depths and kept the soil moisture memory up to previous 45-days. Soybeans VIs were significantly related to soil moisture

at shallower depths and kept a relatively shorter (5-days) memory of soil moisture compared to maize. At the landscape scale, Terra-MODIS Land Surface Temperature (LST) and Normalized Difference Vegetation Index (NDVI) products were used to detect drought-induced stress in vegetation including corn, soybeans, and three grassland cover types across the state of Nebraska. Results indicate that the majority of the land cover pixels experienced significantly higher daytime and nighttime LSTs and lower NDVI during the drought-year growing season compared to the non-drought year. The findings of this dissertation research will contribute toward the development of more robust tools for monitoring drought stress in vegetation.

ACKNOWLEDGEMENTS

I am indebted to all those people whose contribution in assorted ways made this dissertation possible. It is a true pleasure to convey my gratitude to them all in my humble acknowledgment.

At the outset, I would like to record my sincere gratitude to my dissertation co-advisor, Dr. Sunil Narumalani, Professor and Associate Dean of College of Arts & Sciences, for his supervision, advice, and guidance throughout my graduate study. Certainly, this dissertation would not have taken place had he not afforded me this opportunity. He continued to provide me unflinching encouragement and support in various ways during this work and his true researcher intuition and passion in exploring new areas of study inspired and enriched my growth as a student and also as a researcher that I ever wanted to be. I am obliged to him more than he knows.

I extend my deepest gratitude to my co-advisor, Dr. Brian D. Wardlow, Assistant Professor, School of Natural Resources (SNR), for his mentorship that was paramount in providing me a comprehensive experience consistent with my long-term career goals. His expertise and knowledge in the field of remote sensing helped me to not only grow as an experimentalist and a geographer but also as an independent thinker. His involvement with his originality has elicited and nourished my intellectual maturity that I will benefit from, forever.

I owe sincere and earnest thankfulness to my dissertation committee member Dr. Donald Rundquist, Professor, SNR, for his insightful comments, suggestions, and recommendations that helped improve the overall quality of this dissertation. Having

taken two remote sensing courses and worked as a teaching assistant with Dr. Rundquist in one of his courses, I found an amazing teacher and meticulous researcher in him. He taught me the fundamental principles of conducting close-range remote sensing research and always managed to find time to read through my research manuscripts, listen to my research questions, and to provide me the much needed guidance when I was up against the wall during this dissertation research. I regard him as a personal *guru*, and I highly commend him for his academic achievements.

I would like to express my gratitude to the other committee member, Dr. Michael Hayes, Director, National Drought Mitigation Center (NDMC), for being supportive about my research and encouraging me to think critically about the potential application of this research. Dr. Hayes, I am thankful to you in every possible way and I hope to keep up our collaboration in the future.

I honestly appreciate Dr. Timothy J. Arkebauer, Dr. Anatoly Gitelson, Dr. Tsegaye Tadesse, and Dr. Qingfeng Guan for their suggestions and enthusiasm to share their bright thoughts with me, that was rewarding for shaping up my ideas and research.

I gratefully acknowledge the funding sources and institutional support that made my Ph.D. work possible. I was funded by the Center for Advanced Land Management Information Technologies (CALMIT) for the first year and by the NDMC for the rest of my graduate study. I am thankful to the Institute of Agriculture and Natural Resources (IANR), SNR, Department of Geography, and NDMC for awarding me the student travel grants.

I would like to especially thank Dave Scoby for extending wholehearted support to my greenhouse experiments. To CALMIT research staff Bryan Leavitt and Rick Perk,

I appreciate your technical assistance in data collection during my experiments. I owe a special appreciation to Andy Boateng, Travis Yiek, David Gibbs, and Sonisha Sharma who helped me for long hours in taking greenhouse measurements. It is also my pleasure to thank the former and current CALMIT graduate students: Lesli Rawlings, Amy Wright (Zoller), Paul Merani, Daniela Gurlin, Yi Peng, Ruopu Li, and Nwakaku Ajaere for their friendship that made my experience in the University of Nebraska pleasant and memorable.

To Joyce Hurst, Bernice Goemann, Ann Fiedler, Leonita Masek, I thank you all for your help and support during my graduate study in the School of Natural Resources.

Earning a Ph.D. degree is a major milestone in my life for which I wish to thank my parents and family, without whom this would not have been simply possible. My parents and parents-in-law deserve special mention for their inseparable support and prayers. I am at loss of words to express my deepest gratitude and appreciation to my parents, Shashadhara and Debahuti Swain for their love and generosity. I am also grateful to my parents-in-law and relatives who continued to give me their emotional support and encouragement.

I am indebted to my husband, Ajay Swain, for sharing with me this wonderful journey of life. He encouraged me to pursue my dream of earning a doctoral degree. His thorough dedication, unconditional love, and persistent confidence in me, has helped me sail through the difficult times in my life. I am grateful to him for his moral support and creative suggestions that enabled me to stand up and bounce back during my entire graduate study.

Finally, I owe a very special appreciation and gratitude to our loving son, Ainesh who had to stay with his grandparents over one year back in India, away from us, so that I could finish my course work here at UNL. I cannot thank him enough.

Sharmistha Swain

May 17, 2012

DEDICATION

This dissertation is dedicated to my dear husband, Ajay and our loving son, Ainesh.

TABLE OF CONTENTS

LIST OF FIGURES

CHAPTER 1

INTRODUCTION

1.1. Background and Rationale

Water is one of the fundamental requirements for the healthy growth of vegetation. Green plants utilize light energy from the sun along with water and atmospheric carbon dioxide (CO_2) to perform photosynthesis. The energy generated from photosynthesis is essential for the growth of the plants, and plants in turn serve as the basic nutrient source for all other forms of life on this planet. Water, drawn from below ground by roots and transported to the leaves by xylem, is exchanged to the atmosphere through the process called transpiration. Transpiration substantially increases the partitioning of energy into latent heat fluxes and influences the local climate through formation of clouds. Availability of water in the plant's root zone and its movement in the soil-plant-atmosphere continuum is one of the important factors limiting crop productivity (Boyer, 1982). Under water-deficit conditions, most plants close their stomata to decrease their transpiration rate, which have detrimental effects on the physiological development of plants (Bowne et al., 2012). Determination of water status in plants is important to agriculturalists, particularly as it relates to irrigation management, in order to optimize crop yields.

The United States (U.S.) is a leading producer and exporter of corn (*Zea mays*) and soybeans (*Glycine max*). About 20 percent of the corn and 54 percent of the soybeans produced in the U.S. is exported (USDA, 2010). Therefore, the production of corn and soybeans in the U. S. largely influences the supply, demand, trade, and prices of these

crops in the world market. The U.S. Corn Belt is an agriculturally productive region. Within the U.S. Corn Belt, states including Iowa, Illinois, Nebraska, Minnesota, Indiana, and Ohio, collectively contribute approximately 70% of the total U.S. corn production (USDA-NASS, 2009). The vast stretches of grasslands in the U.S. Central Great Plains provide forage for the cattle population, critical for sustaining the cattle based industries. Unfortunately, drought is a regular climatic feature affecting the crop and forage production in these regions. The periodic drought events have serious impacts on the agricultural sector as farming is the major economic driver in the U.S. Corn Belt. Agricultural drought conditions primarily develop because of the deficiency of precipitation over an extended period of time that adversely affect crop and range productivity (Wilhite, 1982). Several other meteorological factors including temperature, humidity and wind speed and biophysical factors such as available soil moisture, and the water holding capacity of soil may play important roles in the initiation and severity of drought.

Most parts of the U.S. are vulnerable to drought, and more than 25% of the contiguous U.S. is affected by severe and extreme droughts in one out of every four years (Wilhite et al., 2000). During the historic drought of 1934, about 65% of the contiguous U.S. and 95% of the Great Plains region was under the grip of severe and extreme drought (Wilhite et al., 2000). The recent drought of 2002, with its peak in July, affected approximately half of the contiguous U.S. (NCDC, 2002). Drought is one of the costliest weather related disasters in the U.S., accounting for an average annual loss of about $6-8 billion (FEMA, 1995). Climate projections forecast more frequent, severe, longer, and wide spread drought events in many parts of the world including sections of the U.S.

(IPCC, 2007; Romm, 2011), indicating a greater need to understand the response of vegetation to drought at multiple spatial and temporal scales.

Detection and monitoring of drought is challenging because its onset is relatively slow compared to the other natural disasters and each drought event is distinct based on its duration, intensity, and spatial extent (Wilhite and Glantz, 1985). Traditional methods of monitoring drought involve the use of climate data including precipitation, air temperature, stream flow, water holding capacity of the soil collected at meteorological stations. These data sets are usually transformed into a single numerical value, termed as a drought index that indicates the drought severity at a particular area. Widely used climate-based operational agricultural drought indices include the Palmer Drought Severity Index (PDSI), the Standardized Precipitation Index (SPI), and the Crop Moisture Index (CMI). The PDSI is based on the supply-and-demand concept of the water balance equation and is computed using precipitation, temperature, and local Available Water Content (AWC) of the soil (Palmer, 1965). The rest of the terms in the water balance equation including evapotranspiration, soil moisture recharge, runoff, and soil moisture loss are derived from the precipitation, temperature, and soil AWC data. Although the PDSI is widely used in the U.S., it suffers from numerous limitations. Arbitrary categorization of drought intensity and duration, crude division of soil layers, exclusion of snow cover and frozen ground in the index calculation, ignoring precipitation and runoff time lag are some of the major deficiencies highlighted in the scientific literature (Alley, 1984; Hayes et al., 1999). Many of the drought indices developed after PDSI were designed to address some of the weaknesses of the PDSI. For example, the SPI is calculated at multiple time scales (3, 6, 12, 24 and 48 months) to identify short-term

changes in soil moisture as well as changes in ground water, stream flow, and reservoir storage which reflect longer-term changes in precipitation. The index value reflects the anomalies in the moisture supply by comparing the current rainfall amount with the long term precipitation record (30 years or more), fitted into a probability distribution function (McKee et al., 1995). The CMI is designed to monitor short term moisture changes in the crops during the crop growing season by using the weekly mean temperature and total precipitation, contrary to the PDSI which reflects the longer-term moisture status.

These discrete, point-based climatological drought indices have to be interpolated to provide a continuous spatial coverage of the drought conditions across a given region. These spatially interpolated map products are more representative of the ground conditions where the density and distribution of weather stations is high (Brown et al., 2008). Regions with mountainous topography or low populations typically do not have a dense network of weather stations to adequately characterize detailed spatial patterns of drought conditions. Since the launch of the Landsat-1 satellite in 1972, remotely sensed data have supplemented the ground based observations in monitoring vegetation health and dynamics across landscapes. Remote sensing data provide a spatially contiguous and temporally repetitive view of the earth surface, essential for monitoring drought stress on vegetation over large areas. Vegetation indices computed from multispectral data collected by satellite sensors have been used in many vegetation drought assessment studies. One such index, the Normalized Difference Vegetation Index (NDVI), is based on the normalized difference between the absorption of radiation in red wavelengths by the chlorophyll pigments and the reflectance in the near infrared (NIR) in the spongy mesophyll layer within the leaf (Rouse et al., 1974).

Time-series NDVI data derived from the Advanced Very High Resolution Radiometer (AVHRR) and Moderate Resolution Imaging Spectroradiometer (MODIS) have shown strong relationships with climatological and biophysical variables including precipitation, temperature, and soil moisture that affect the vegetation conditions and therefore can be used for vegetation drought assessments. Rundquist and Harrington (2000) reported significant relationships between AVHRR monthly NDVI and one month lagged precipitation at two grassland sites in the U.S. Central Great Plains.

Wang et al. (2001) evaluated the responses of AVHRR bi-weekly NDVI to precipitation and temperature during a 9-year period in the U.S. Central Great Plains and found that the spatial pattern of NDVI corresponded well with the spatial pattern of average annual precipitation. They also found that the NDVI during the growing season had the strongest correlations with the accumulated antecedent precipitation summed over 14 biweekly periods, and that the NDVI was influenced by the minimum temperature in early summer and towards the end of the growing season.

Ji and Peters (2003) compared the AVHRR based growing season monthly NDVI with 1 through 12 month SPI over a period of 10 years to assess cropland and grasslands drought conditions in the Northern Great Plains of the U.S. Their study confirmed the relationship of NDVI with precipitation and showed the strongest relationships of NDVI with three month SPI. They also found that the NDVI and precipitation relationship was time and space dependent as higher correlations were noticed in areas with low soil water holding capacity and during the middle of the growing season.

Wang et al. (2007) examined the relationship between MODIS based 8-day composited NDVI and the root zone soil moisture from 2000 through 2004 growing

seasons at three locations representing semiarid and humid climates and grassland and shrub land cover types. Results indicated that grassland NDVI responded quickly (about 5 days) to the changes in the soil moisture at the water limited semiarid site compared to the humid site (about 10 days).

The normalized difference water index (NDWI) combines the NIR and short wave infrared (SWIR) channels and is sensitive to the water content in vegetation canopies (Gao, 1996). The time-series NDWI data have also been used to detect and monitor drought-related stress in vegetation over large areas. For example, Gu et al. (2007) compared the performance of MODIS-derived NDVI and NDWI in monitoring drought in grasslands over the Flint Hills ecoregion in the U. S. Great Plains. They reported a larger decrease in NDWI values in response to drought conditions than those of NDVI, which suggest that NDWI may be a more sensitive indicator of approaching drought compared to NDVI.

Several other indices were also developed using the historical time series vegetation indices and canopy temperature information and applied for monitoring drought globally. For example, Kogan (1995) computed the Vegetation Condition Index (VCI) and Temperature Condition Index (TCI) using average, minimum, and maximum AVHRR based NDVI and brightness temperature data, respectively, over a temporal composite period of interest. The VCI and TCI were successfully applied for crop yield assessments in United States and other parts of the world including Asia, Europe, and South America (Kogan, 1995; Kogan, 1997). The Vegetation Health Index (VHI) was developed by combining the AVHRR-based VCI and TCI information and applied globally for drought assessment in parts of Asia, Africa, Europe, and the Americas

(Kogan, 2002). Peters et al. (2002) developed the Standardized Vegetation Index (SVI) by quantifying the per-pixel deviation of current NDVI from the "normal," computed from the historical NDVI data record and applied for assessing drought related vegetation conditions in the U.S. Great Plains. Available literature suggests that most of the vegetation stress assessment studies in the U.S. Great Plains are based on broad land cover types such as forest, croplands, and grasslands. Relatively little research has been conducted to understand the response of different grassland cover types or crop types with different management practices to drought stress at local and regional levels.

1.2. Objectives

The goal of this dissertation research is to evaluate the response of vegetation to drought-related water stress at multiple spatial scales including the leaf, canopy, and landscape scales using remotely sensed reflectance and/or thermal data.

In the context of drought monitoring, knowledge about the amount of water held in plants tissues is important, as it provides an indication about the plant's susceptibility to drought stress. The volume of water held in leaf tissues is generally expressed in terms of relative water content (RWC). The RWC compares the actual water content in a leaf against the content at full turgor and provides a direct measure of water status in leaf tissue. The first objective of this dissertation is to estimate RWC in soybean leaves using close-range, high spatial resolution thermal imagery. The sub-objectives include:

1. To evaluate the thermal response of leaves of soybean plants subjected up to eight days of water deficit and compare the leaf temperatures of progressively water stressed plants against the control (well watered) plants.

2. To develop models using both raw leaf temperatures and leaf temperature based indices extracted from thermal images to estimate RWC.

Soil moisture status in the plant's root zone is one of the important factors determining the plants vulnerability to drought stress. In rainfed farming systems, precipitation primarily controls the amount of moisture present in the soil profiles available for plants to use in photosynthesis. Deficiency of soil moisture within the plants' root zone limits their photosynthetic capacity and ultimately results in drought stress in plants. Understanding the connections between root zone soil moisture and plant spectral signals will improve our ability to detect and monitor drought stress in vegetation. The second objective of this dissertation is to evaluate the relationships between vegetation indices and soil moisture for corn and soybean crops grown under rainfed farming systems in southeastern Nebraska using close-range spectral reflectance data taken approximately at one week intervals during the crop growing cycles. The sub-objectives include:

1. To assess the relationship between corn and soybean spectral reflectance-based VIs with same-day soil moisture measured at four different depths within the root zone.
2. To assess the relationship between corn and soybean spectral reflectance-based VIs with antecedent soil moisture with lags up to 60 days at 5-day increments at four different depths within the root zone.

In natural and managed ecosystems, different vegetation cover types respond uniquely to drought stress. Some vegetation cover types are more drought resistant

compared to the others. Knowledge about the relative susceptibility of different vegetation cover types to drought stress may contribute to the formulation of better drought detection and planning efforts. In this context, the third objective of this dissertation research is to evaluate the response a few select crop and grassland cover types to drought across the state of Nebraska through the analysis of data collected by Moderate Resolution Imaging Spectroradiometer (MODIS) on board Terra satellite platform. The sub-objectives include:

1. To compare the Terra-MODIS derived cumulative daytime and nighttime Land Surface Temperature (LST) and NDVI response of irrigated and rainfed corn and soybeans and three grassland cover types during the growing seasons of contrasting drought (2002) and non-drought (2007) years.
2. To examine the differential response of the aforementioned land cover types to drought stress.

1.3. Study Area

The study area of this research is focused on the state of Nebraska in the United States. The state covers an area of about 200 thousand km^2 and constitutes a part of the Central Great Plains region of North America. Agriculture and ranching are important economic activities. Grasslands and croplands constitute approximately 54% (10.9 million ha) and 39% (7.9 million ha) of the state's total area, respectively (Henebry et al., 2008). The distribution of grassland cover types across the state is influenced by the gradient in precipitation. The tall grass prairie in the east is transitioned to mixed and short grass toward the drier western part of the state. Corn and soybeans are the major crops grown in the state, and the other minor crops include winter wheat (*Triticum*

aestivum), sorghum (*Sorghum bicolor*), and alfalfa (*Medicago sativa*). Specific cropping pattern and management practices are strongly influenced by the amount of precipitation received during the major crop growing season and vary widely across the state. Because of a favorable precipitation regime, non-irrigated corn and soybeans thrive in the eastern part of the state. In contrast, the majority of crops in the much drier western and central Nebraska are irrigated from both surface and ground water sources.

Drought is a regular climatic occurrence in the state affecting the crop and pasture productivity. According to the U.S. Drought Monitor, severe and extreme drought conditions were experienced in at least some parts of Nebraska at some period during the crop growing season in seven out of past 12 years between 2000 and 2011 (http://droughtmonitor.unl.edu/). During the drought of 2002, entire state of Nebraska was under moderate to exceptional drought conditions (http://droughtmonitor.unl.edu/, July 30, 2002). During this period more than 80% of the range and pasture lands in the state were reported to be under poor to very poor condition (USDA, 2002).

This dissertation research was carried out at the leaf, canopy, and landscape scales; therefore the areal unit of each level of study was different. The leaf level study was performed in a greenhouse located at the University of Nebraska-Lincoln (40.82°N, 96.68°W, and elevation 370.03 m above sea level), USA. The canopy level study was carried out at the University of Nebraska Agricultural Research and Development Center (ARDC), located in the southeastern part of Nebraska, USA. The study site is a rainfed cropland (41°10'46.8″ N, 96°26'22.7″ W) covering an area of 65.4 ha with a yearly crop rotation pattern of corn and soybeans. The landscape level study covered the entire state

of Nebraska. More detailed description of the study area is provided in the respective research chapters.

1.4. Data

This research was conducted using a number of remotely sensed and *in situ* data sets. The leaf level study included high spatial resolution thermal imagery and *in situ* data on leaf gas exchange and RWC. The leaf temperature information of the soybean plants was acquired using a thermal camera (FLIR ThermaCAM 640, FLIR Systems, Inc.). Leaf gas exchange measurements including the leaf photosynthetic rate (A), stomatal conductance (g_s), and intercellular CO_2 concentration (C_i) were taken on specific leaves using a portable open-path gas exchange measurement system (model LI-6400, Li-Cor Inc., Lincoln, NE, USA). Water content of the leaves was determined by gravimetrically measuring RWC. The canopy level study was carried out by using high spectral resolution reflectance data taken approximately at 6 m above the corn and soybean canopies and volumetric soil moisture data measured at four depths (10, 25, 50, and 100 cm) in the soil profile. The spectral reflectance data were acquired by using a dual-fiber, inter-calibrated Ocean Optics USB2000 radiometers attached to the sensor platform. Soil moisture data were collected using Vitel and Theta probes. In the landscape level study, Terra-MODIS eight-day composite LST (MOD11A2, collection 5) and surface reflectance (MOD09Q1, collection 5) products spanning the 2002 and 2007 growing season periods (May 15 through September 28) covering Nebraska (tile h10v04) were used. The detailed description about the data and methods are presented in the respective research chapters.

1.5. Dissertation Structure

This dissertation is organized into five chapters. Chapter 1 provides an introduction to the research background, rational, and objectives of this dissertation. It also presents an overview of the study area and the data used in this dissertation research. Chapter 2 presents the determination of relative water content in soybean leaves using close-range thermal infrared imagery. Chapter 3 analyzes the relationships among the corn and soybean based vegetation indices and root zone soil moisture using above canopy hyperspectral reflectance data. Chapter 4 presents the response of different vegetation cover types to drought stress in Nebraska using Terra-MODIS Land Surface Temperature and NDVI products. Chapter 5 summarizes the important findings of this work and provides recommendations for future research.

References

Alley, W. M., 1984. The Palmer Drought Severity Index: Limitations and assumptions. *Journal of Climate and Applied Meteorology*, 23: 1100-1109.

Boyer, J. S., 1982, Plant productivity and environment. *Science*, 218: 443-448.

Bowne, J., T. Erwin, J. Juttner, T. Schnurbusch, P. Langridge, A. Bacic, and U. Roessner, 2012. Drought responses of leaf tissues from wheat cultivars of differing drought tolerance at the metabolite level. *Molecular Plant* 5: 418-429.

Brown, J.F, B. D. Wardlow, T. Tadesse, M. J. Hayes, and B. C. Reed, 2008. The Vegetation Drought Response Index (VegDRI): A new integrated approach for monitoring drought stress in vegetation. *GIScience & Remote Sensing*, 45: 16-46.

Federal Emergency Management Agency, 1995. National mitigation strategy–partnerships for building safer communities, 26 pp.,Washington, D. C.

Gao, B., 1996. NDWI-A normalized difference water index for remote sensing of vegetation liquid water from space. *Remote Sensing of Environment*, 58: 257-266.

Gu, Y., J. F. Brown, J. P. Verdin, and B. D. Wardlow, 2007. A five-year analysis of MODIS NDVI and NDWI for grassland drought assessment over the Central Great Plains of the United States. *Geophysical Research Letters*, 34, L06407 [doi:10.1029/2006GL029127].

Hayes, M. J., M. D. Svoboda, D. A. Wilhite, and O. V. Vanyarkho, 1999. Monitoring the 1996 drought using the Standardized Precipitation Index. *Bulletin of the American Meteorological Society*, 80: 429-438.

Henebry, G., M. Vaitkus, and J. Merchant, 2008. Nebraska Gap Analysis Project, Reston, VA: U.S. Geological Survey [http://digitalcommons.unl.edu/cgi/viewcontent.cgi?article=1030&context=usgspubs].

IPCC, 2007, Climate change: the physical science basis. Contribution of working group I to the fourth assessment report of the Intergovernmental Panel on Climate Change, edited by S. Solomon et al., Cambridge Univ. Press, Cambridge, U. K.

Ji, L., and A. J. Peters, 2003. Assessing vegetation response to drought in the Northern Great Plains using vegetation and drought indices. *Remote Sensing of Environment*, 87: 85-98.

Kogan, F. N., 1995. Droughts of the late 1980s in the United States as derived from NOAA polar orbiting satellite data. *Bulletin of the American Meteorological Society*, 76: 655-668.

Kogan, F. N., 1997. Global drought watch from Space. *Bulletin of the American Meteorological Society*, 78: 621–636.

Kogan, F. N., 2002. World Droughts in the new millennium from AVHRR-based Vegetation Health Indices. *EOS, Transactions, American Geophysical Union*, 83: 557-564.

McKee, T. B., N. Doesken, and J. Kleist, 1995. Drought monitoring with multiple time scales. *in Preprints 9th Conference on Applied Climatology*, Dallas, TX, 233–236.

NOAA National Climatic Data Center, State of the Climate: Drought for July 2002, published online August 2002, retrieved on December 24, 2011 from http://lwf.ncdc.noaa.gov/sotc/drought/2002/7.

Palmer, W. C., 1965. Meteorological Drought, Washington, DC: U.S. Department of Commerce Weather Bureau, Research Paper No. 45.

Peters, A. J., E. A. Walter-Shea, L. Ji, A. Viña, M. Hayes, and M. Svoboda, 2002. Drought monitoring with NDVI-Based Standardized Vegetation Index. *Photogrammetric Engineering and Remote Sensing*, 68:71–75.

Romm, J., 2011. The next dust bowl. *Nature*, 478: 450-451.

Rouse, J. W., R. Haas, J. Schell, and D. W. Deering, 1974. Monitoring vegetation systems in the Great Plains with ERTS," *in Proceedings of the Third Earth Resources Technology Satellite-1 Symposium*, 1: 48-62.

Rundquist, B. C. and J. A. Harrington, Jr., 2000. The effects of climatic factors on vegetation dynamics of tallgrass and shortgrass cover. *Geocarto International*, 15: 33-38.

United States Department of Agriculture (USDA) Economic Research Service, 2010, URL: http://www.ers.usda.gov/Briefing.

USDA-NASS. 2009. 2007 Census of Agriculture. Retrieved from United States Department of Agriculture-National Statistics Service-The Census of Agriculture: http://www.agcensus.usda.gov/Publications/2007/Full_Report/usv1.pdf

USDA (U.S. Department of Agriculture), 2002, "Weekly Weather and Crop Bulletin" [http://www.usda.gov/oce/weather/pubs/Weekly/Wwcb/index.htm], last accessed December 15, 2011.

Wang, J., K. P. Price, and P. M. Rich, 2001. Spatial Patterns of NDVI in response to precipitation and in the Central Great Plains. *International Journal of Remote Sensing*, 22: 3827-3844.

Wang, X., H. Xie, H. Guan, and X. Zhou, 2007. Different responses of MODIS-derived NDVI to root-zone soil moisture in semi-arid and humid regions. *Journal of Hydrology*, 340: 12- 24.

Wilhite, D. A., 2000. Preparing for drought: A methodology. *in Drought: A Global Assessment, Routledge Hazards Disaster Ser.*, vol. 2, edited by D. A. Wilhite, pp. 89– 104, Routledge, Boca Raton, Fla.

Wilhite, D. A. and M. H. Glantz, 1985. Understanding the drought phenomenon: The role of Definitions. *Water International*, 10: 111-120.

Wilhite, D.A., 1982. Measuring drought severity and assessing impacts. International Symposium on Hydrometeorology, *American Water Resources Association*, 333-335.

Wilhite, D. A., M. J. Hays and M. D. Svoboda, 2000. Drought monitoring and assessment: Status and trends in the United States. *Drought and Drought Mitigation in Europe,* J.V. Vogt and F. Somma (eds.), Kluwer Publishers: 149-160.

CHAPTER 2

NON-INVASIVE ESTIMATION OF RELATIVE WATER CONTENT IN SOYBEAN LEAVES USING INFRARED THERMOGRAPHY

Abstract

Infrared thermography is a useful technology for examining water status in terrestrial vegetation. The objective of this chapter is to estimate relative water content (RWC) in soybean plants (*Glycine max*), grown under greenhouse conditions using high resolution thermal infrared images. The plants were subjected to a range of moisture stress treatments in order to evaluate the water content in sampled leaves. The plants were irrigated with 8 different treatment levels (control (i.e., fully irrigated) and 1 to 7 days of water being withheld). One specific trifoliate (three leaves) was segmented from each of the thermal images for every plant sample, and both mean temperature and Crop Water Stress Index (CWSI) were computed for each plant. Leaf discs were taken from the same trifoliate to gravimetrically measure RWC. RWC had statistically significant correlation coefficients with both CWSI ($r = -0.92$, $n = 56$; $P < 0.001$) and raw mean temperature ($r = -0.84$, $n = 56$; $P < 0.001$). Two separate regression models were developed to predict RWC using mean raw trifoliate temperature and CWSI. Our results document that a CWSI-based regression model was better in predicting RWC than a model based on mean raw trifoliate temperature.

2.1. Introduction

Water deficit poses a serious threat to both the survival and productivity of crops. Plants experience water stress when the transpiration demand exceeds the amount of moisture available in the root zone (Kacira et al., 2002). Determination of water status in plants is important to agriculturalists, particularly as it relates to irrigation management, in order to optimize plant productivity (crop yields). Relative Water Content (RWC) is a biophysical variable that quantitatively expresses water volume per leaf. It is expressed as a ratio of the amount of water present in the leaf at sampling time to the amount when the leaf is turgid (Smart and Bingham, 1974). Traditionally, water status in plants is evaluated either by measuring *in situ* soil water status (such as soil water content, or soil water potential) or by measuring *in situ* physiological variables that characterize water status in leaves (e.g., RWC, leaf water potential, stomatal conductance, or photosynthetic rate). However, these methods are time consuming, labor-intensive, and often require destructive sampling. Additionally, such measurements are point based, and often provide a poor representation of field conditions, especially when the sample size is small (Jackson, 1982).

Remote sensing offers a non-destructive method of quantifying the amount of water present in plants, and several investigators have examined the utility of various portions of the electromagnetic spectrum for measuring the amount of liquid water in vegetation. The potential utility of vegetation indices based upon the near-infrared (NIR, 700 to 1300 nm) and middle-infrared regions (MIR, 1300 to 2500 nm) of the spectrum for retrieving leaf water content is well documented (Gao, 1996; Ustin et al., 1998; Jackson et al., 2004; Chen et al., 2005). Spectral reflectance of vegetation in the NIR

region is determined by leaf tissue, cell structure, canopy architecture, and the presence of two weak water absorption bands (at 970 and 1200 nm). Reflectance in the MIR is primarily controlled by the volume of water in leaf cells, with strong water absorption bands centered at 1450, 1950, and 2250 nm (Tucker, 1980; Carter, 1991; Sims and Gamon, 2003). Under water stress conditions, plant reflectance increases throughout the visible, NIR and MIR regions (Hunt and Rock, 1989; Carter, 1991; Inoue et al., 1993). Numerous vegetation indices have been developed using spectral bands in the NIR and MIR to quantify liquid water content in vegetation. Examples include the Moisture Stress Index (Rock et al., 1986), the Normalized Difference Infrared Index (Hardisky et al., 1983), and the Normalized Difference Water Index (Gao, 1996). Although widely used as surrogates for water content in vegetation, NIR and MIR based indices are not sensitive to RWC differences of 6% or less (Riggs and Running, 1991), which are critical for identifying the onset of drought stress in vegetation. MIR based indices, particularly those using spectral signals within the strong water absorption regions, tend to saturate when a vegetation canopy closes, or when the leaf area index reaches 4 or greater (Lillesaeter, 1982), which suggests that such indices may not be sensitive to the full range of RWC. Bowman (1989) showed that relationships between NIR (810 nm) or MIR (1665 and 2212 nm) and RWC were weak and sometimes statistically non-significant when RWC ranged between 92 and 100%.

The thermal infrared portion of the spectrum provides an alternate opportunity to analyze plant water status. Use of canopy temperatures for stress assessment is based on the principle that availability of adequate moisture enables plants to transpire at potential rates, thus resulting in leaf temperatures lower than air temperatures. During

transpiration, a substantial amount of the energy that is required for converting each mole of liquid water into water vapor is removed from the leaf in the form of latent heat, which keeps the leaf surface cool (Jones et al., 2009). When moisture in the root zone diminishes, the stomata close to prevent the diffusion of water vapor from the leaf to the atmosphere through transpiration. Thus, incident radiation on the leaf is primarily converted to sensible heat (instead of latent heat), which increases leaf temperatures so they then exceed the air temperatures (Fuchs, 1990; McVicar and Jupp, 1998; Anderson and Kustas, 2008). The onset of water stress, resultant stomatal resistance, and elevated temperature responses in plants can be more quickly detected than water stress related changes in NIR reflectances (e.g., Jackson and Ezra, 1985).

A number of previous water-stress studies were based upon canopy temperatures being measured by either hand-held or vehicle-mounted infrared thermometers (IRT's) (Idso et al., 1981; Jackson et al., 1981; Fuchs, 1990; Jones, 1999; Payero and Irmak, 2006). Often the measured canopy temperature is combined with meteorological data to further refine the quantification of water stress. For example, the Crop Water Stress Index (CWSI), one of the most widely used indices for quantifying water deficit in agricultural crops, combines canopy temperatures measured using IRT's in conjunction with ambient meteorological conditions such as air temperature and humidity (Idso et al., 1981; Jackson et al., 1981; Jackson et al., 1988). Although canopy temperatures as measured with an IRT may be used to estimate temperature at field scales, one of the limitations inherent in such a procedure is that the data are spatial averages of the emittances from all materials found within the field-of-view of the sensor. Therefore, the measured temperature may not represent canopy only, particularly during the early stages

of plant growth when the leaf area index is low, leading to the sensor field-of-view including non-leaf materials (e.g., stems or background soil). As the leaf temperature increases linearly with increased absorbed radiant energy (keeping other factors constant) (Jones et al., 2009), internal shading within the canopy is another issue potentially increasing the bias of the IRT based temperature measurements. Several thermal image based studies on grapevines, in both field (Jones et al., 2002; Grant et al., 2007) and greenhouse (Leinonen and Jones, 2004) settings, have reported temperature differences between the sunlit and shaded components of the canopies. The widespread availability of high resolution, lightweight, portable thermal cameras provides an opportunity to examine the temperatures of individual plant leaves; thus eliminating, or at least isolating, the influence of background materials. Thermal images have been used at both leaf and canopy levels for not only visually analyzing the impact of water stress on individual leaf surfaces but also for computing temperature-based indices as a means of quantifying water stress in leaves. Hashimoto et al. (1984) were among the first to use thermal imaging techniques to monitor the short-term (two minute intervals up to 22 minutes) changes in the leaf temperatures of root-pruned sunflower plants under moisture deficit. Jones (1999b) also used thermal imaging to monitor short-term changes (one minute intervals for an 11-minute period) in stomatal conductance over one detached leaf surface from a French bean plant. Ondimu and Murase (2008) combined imaging techniques in both the thermal infrared and visible spectrum to detect water stress in Sunagoke moss. They achieved good correlations among the CWSI derived from thermal imagery, visible reflectance from the Sunagoke moss, and water content.

Previous studies have reported the use of field or greenhouse based thermal imaging approaches in estimating stomatal conductance of grapevine canopies (Jones et al., 2002), French beans, and lupins (Grant et al., 2006), leaf water potential in cotton plants (Cohen et al., 2005; Alchanatis et al., 2010), and both stomatal resistance and stem water potential in olive trees (Ben-Gal et al., 2009). While a reduction in stomatal conductance is considered to be a very sensitive and early indicator of a plant experiencing a water deficit, RWC is a more direct measure of water status in plant tissue because it compares the actual water content in a leaf against the content at full turgor. Jones (2007) argues that cell elasticity or cell turgor, which directly drives cell expansion and contraction, is the real indicator of water status and that RWC is a good proxy for cell turgor. Although past studies have documented a strong relationship between leaf temperature and stomatal conductance (e.g. Jones et al., 2002, Grant et al., 2006), and considering the significance of RWC as an indicator of plant water status, the potential relationship between RWC and leaf temperature needs to be examined. In this study, we used RWC as an indicator of plant water status and tested the utility of high spatial resolution thermal images for non-destructive estimation of RWC in soybean leaves (*Glycine max*). More specifically, we used both raw leaf temperature and CWSI derived from the thermal images to develop and test our models.

2.2. Materials and Methods

2.2.1 Plant Material

The experiment was conducted in a greenhouse at the University of Nebraska-Lincoln (40.82°N, 96.68°W, and elevation 370.03 m above sea level), USA, during April and early May of 2011. Sixty soybean plants (Pioneer 92Y-70) were grown in identical

black plastic pots, with the capacity of each pot being 1.4 liters (length 10.7 cm; width 10.2 cm, and height 12.5 cm). To maintain uniform plant growth and development, an equal amount of soil (Bergers BM1 potting soil mix with 80% peat and 20% pearlite) was inserted into each pot, along with three soybean seeds. Plants emerged 6 days after the seeds were sown and at the emergence (VE) stage, the plants were thinned to retain one plant per pot. The pots were arranged in 5 columns and 12 rows with spacing of 0.2 m on an elevated netted platform. Positions of the plants were changed randomly to minimize the impact of any solar radiation differences occurring in the greenhouse. On day 21 after emergence (V3: third trifoliate stage of development), the plants were supplied with a fertilizer solution (Hoaglands modified nutrient solution) to maintain their nutrient sufficiency.

2.2.2 Meteorological Measurements

The environmental conditions within the greenhouse were monitored carefully. Two quantum sensors (Li-Cor Biosciences, Lincoln, NE, USA) were placed at both sides of an elevated platform (1 m above the soybean canopy) to record the amount of photosynthetically active radiation (PAR) available to the plants. The average of the two sensors was used in this study. Ancillary measurements included ambient air temperature and relative humidity (RH). Air temperature was measured using a thermistor (model 107, Campbell Scientific, Logan, UT, USA) and RH was measured (model HMP50, Campbell Scientific, Logan, UT, USA). PAR, air temperature and RH were sampled every minute and recorded by a data acquisition system (CR850, Campbell Scientific, Logan, UT, USA). Plants were grown under sunlight throughout the day and with air temperature and relative humidity ranging between 20 and 38 °C and 10–75%,

respectively. Variations in PAR and air temperature during the 8-day experimentation period are shown in Figure 2.1. No artificial lighting was used during the entire experimentation period.

2.2.3 Irrigation Treatments

All plants were watered every day to maintain the field capacity of the soil mixture, and excess water was allowed to drain through the bottom of the pots and the nets of the platform. A moisture-deficit strategy was implemented on day 38 after emergence. Most plants had developed pods (3/4 inch or longer) on one of the four upper nodes of the main stem, and thus, from a phenological standpoint, they were at the R4 stage of growth. R4 is the most crucial period for seed yield and any stress during this period can cause a significant reduction in yield (McWilliams et al., 2004). The plants (total 58) were randomly grouped into 8 classes and were subjected to 8 different irrigation treatments; control and water stressed day-1 (WS 1) through water stressed day-7 (WS 7). The treatment groups WS 1 through WS 7 had 7 replicates each (7 replicates x 6 treatments = 42), and control and WS 7 treatment groups contained 8 replicates each (8 replicates x 2 treatments = 16). In this experiment, each replicate is a single plant. It is noted that we kept one additional replicate in both the control and WS 7 treatment groups. These two “extra” plants were later used as fully transpiring (control replicate) and non-transpiring (WS 7 replicate) plants during the image acquisition to facilitate the computation of the thermal image based CWSI (more description is presented in the image acquisition and processing section).

On the first day of the water stress regimen, WS 7 plants were excluded from irrigation, while the remaining plants continued to receive water daily at the field

capacity of the soil. On the following day, WS 7 and WS 6 plants were both excluded from watering while the remaining plants were irrigated at field capacity. On each successive day, one more group of plants was excluded from irrigation in order (WS 5, WS 4, WS 3, WS 2, and WS 1). The process continued until only the control plants were left in the original lot, and these plants received water at field capacity each day of the 7-day water stress experiment period (May 5 to May 11, 2011).

2.2.4 Thermal Image Acquisition and Processing

Thermal images were acquired and measurements of relative leaf water content were taken on day 8 after the initiation of the moisture deficit program (45 days after plant emergence). Images of the plant canopies were acquired using a thermal camera (FLIR ThermaCAM 640, FLIR Systems, Inc.). The spectral range and resolution of the instrument are 7.5 to 13 μm and 0.65 milliradians, respectively. The acquired images were 640×480 pixels at 14-bit radiometric resolution. The instrument is sensitive to a temperature range between – 40 $^{\circ}$C and + 120 $^{\circ}$C with an accuracy of ±2°C**.** The FLIR instrument had an 8 mm lens with an angular field of view of 32°. Emissivity was set at 0.96, corresponding to the normally accepted value for vegetation (Jensen, 2007). The camera was mounted on a tripod and pointed vertically downward at a fixed position for each image. The distance between the camera and the plant canopy was approximately 0.85 meter, yielding images with a spatial resolution of 0.05 cm. This high spatial resolution allowed a precise distinction to be made between individual leaves and both stem and non-vegetated materials in the image. Narrow strips of aluminum foil were wrapped around the node (or petiole) of the fourth trifoliate of each plant to identify the leaves of interest in each thermal image. Leaf temperature varies with air temperature,

humidity, wind speed, and downwelling irradiance, and these conditions may change rapidly in not only the field but also in greenhouse settings (Jones et al., 2009). During image acquisition, two plants, one control (non-stressed) and one fully stressed (WS 7), were placed on either side of the plant of interest (within the field-of-view of the camera) in order to calibrate the leaf temperature against the same for a fully transpiring as well as a non-transpiring plant under the given environmental conditions. These two plants, representing fully transpiring and non-transpiring plants for the computation CWSI, remained constant for all thermal imaging. The thermal images were collected from a total of 56 soybean plants, grouped into 8 treatments with 7 replications (plants) per treatment. The plants from a single treatment were imaged sequentially. Several studies have recommended midday as the ideal time for thermal image acquisition when the plants experience maximum water stress, and the environmental variables (air temperature, irradiance, and RH) that affect the leaf temperatures are relatively stable (e.g. Grant et al., 2006; Ben-Gal et al., 2009; Alchanatis et al., 2010). However, thermal images for this study were acquired between 9:50 and 12:15 hours local time (Figure 2.2a) as we were interested in understanding the extent to which the thermal image based CWSI computation approach would normalize the influence of environmental variables on leaf temperatures. The conditions on the day of thermal imaging were quite typical of a day in mid-May in the Midwestern U.S. A major part of the experimentation day (Day 8) was marked by intermittent cloud cover and consequent sporadic variations in PAR. Air temperature remained fairly uniform compared to other days, especially from day-2 to day-7 (Figure 2.1). We hypothesized that since leaf temperatures at a particular time are dependent on the concurrent environmental conditions, the CWSI based method,

which normalized the leaf temperature, would be more responsive to the actual water content in leaves. The greenhouse environmental conditions that primarily drive the leaf temperature (i.e. PAR, air temperature, and relative humidity) showed some variations during the data collection period (Figure 2.2). PAR remained below 1000 µmol/s/m^2 during most of the data-collection period with some occasional spikes due to clouds. Air temperature ranged from 24° to 29°C between 9:30 and 12: 15 hours. Overall, RH showed a decreasing trend up to 11:30 hours and then increased toward the latter part of the data collection period (approximately between 11:20 and 11:45 AM).

The raw thermal images, one for each plant (total 56) were processed using FLIR systems proprietary software (ThermaCamResearcher), and were subsequently analyzed with ENVI image processing software (version 4.7; Environmental Systems, Boulder, CO). In each thermal image, the pixels comprising the fourth trifoliate of the control plant, fully stressed plant, and specific sampled plant of interest were manually segmented and the pixels were extracted. Mixed pixels along the edge of the leaf comprising the thermal signals from both leaf and other background materials were manually excluded. The CWSI index, developed by Idso et al. (1981) and Jackson et al. (1981), was used and is defined as:

$$\mathrm{CWSI} = \frac{(T_l - T_{wet})}{(T_{dry} - T_{wet})} \qquad (2.1)$$

Where, T_l is the actual leaf temperature under given environmental conditions; T_{wet} is the lower boundary for canopy temperature, corresponding to a well-watered plant with fully open stomata. T_{dry} is the upper boundary for canopy temperature, representing the

temperature of a non-transpiring plant with stomata completely closed. All temperature measurements were in °C.

Although Equation 2.1 was employed in this study, we made use of a different baseline for the computation of T_l, T_{wet}, and T_{dry} as described in Grant et al. (2006). We used the mean temperature of the 4th trifoliate of the plant of interest (Mean T_{leaf}) as T_l, minimum 4th trifoliate temperature of the control plant (Min T_{wet}) as T_{wet}, and maximum 4th trifoliate temperature of the fully stressed plant (Max T_{dry}) as T_{dry} in order to compute CWSI for each plant. Thus, the CWSI was calculated for this study as:

$$\text{CWSI} = \frac{(\text{Mean } T_l - \text{Min } T_{wet})}{(\text{Max } T_{dry} - \text{Min } T_{wet})} \tag{2.2}$$

2.2.5 Measurement of Leaf Gas-exchange

Leaf gas exchange measurements were made on specific leaves immediately after the acquisition of thermal images using a portable open-path gas exchange measurement system (model LI-6400, Li-Cor Inc., Lincoln, NE, USA). Three plants, each from control and treated (WS 1 through WS 6), were selected to measure the leaf photosynthetic rate (A), stomatal conductance (g_s), and intercellular CO_2 concentration (C_i). Because a number of leaves in WS 7 plants visually appeared to have shriveled because of the intensity of water stress, and to prevent any potential further damage to the leaves during the measurement process, the gas exchange data were not collected from those plants. The node leaf of the 4th trifoliate of the sampled plants was used, and 6 readings per leaf were obtained, with the average values of these three variables per leaf being reported upon in this study.

2.2.6 Measurement of Relative Water Content

The measurements of leaf gas exchange were immediately followed by the gravimetric measurements of RWC. Five leaf disc (1.0 cm diameter) samples were taken from each of the 4th trifoliate leaves (5 discs × 3 leaves = 15 discs per replicate). The leaf discs were immediately sealed in pre-weighed vials (one vial per replicate) to prevent any evaporative loss of water from the samples and then weighed on a balance (Leco-250, Leco/Sartorius Corp.). Fresh weights (FW) of the samples were determined by subtracting the empty vial weight from the filled vial weight. Subsequently, the vials were filled with distilled water and refrigerated at 5 $^{\circ}$C for 15 hours to allow the samples to fully rehydrate (Zygielbaum et al., 2009). The samples were then removed from the vials, placed on an absorbent paper towel and gently patted to remove any water from their surfaces. The leaf discs were immediately weighed again to obtain the full turgor weights (TW). The samples were again put in the vials, with caps loosely in place. The vials were kept in an oven for 36 hours at 105°C, and then weighed again to derive the dry weights (DW). The RWC was determined by using the following equation:

$$\mathrm{RWC} = \frac{(\mathrm{FW} - \mathrm{DW})}{(\mathrm{TW} - \mathrm{DW})} \times 100 \qquad (2.3)$$

2.2.7 Data Analyses

IBM SPSS Statistics 19 (2010) software was used for data analyses and Microsoft Excel (2010) was used for producing graphics. Data were tested for normality and homogeneity of variances using Shapiro-Wilk and Levene's tests, respectively. Differences among the treatments were examined with one-way Analysis of Variance (ANOVA). Welch results for equality of means were reported where the variances within

groups were not equal. Dunnet T3 tests were conducted to identify significant treatment differences where equal variances were not assumed. Conversely, Scheffe tests were reported where equal variances were assumed. Variation from the mean is reported as ± one standard error.

2.3. Results

The response of the soybean plants to water stress treatments, as detected by RWC, mean T_{leaf}, and CWSI methods is presented as Figure 2.3. The top graphic (Figure 2.3a) shows the mean RWC values of the control and the water stressed plants (WS 1 – WS 7). The Welch test shows significant differences in RWC among the treatments [$F(7, 20.21) = 749.63$; $P < 0.001$]. Overall, the RWC values decreased with increasing water stress in plants. The differences between control versus WS 1 and WS 2 were not statistically significant, while the difference between control and WS 3 was significant ($P = 0.002$). The rate of decrease in RWC was relatively low from control up to WS 4 plants, with a mean RWC difference of 14% ($P = 0.001$). The RWC of the WS 5 plants experienced a sharp decline compared to those of WS 4, which had a mean difference of 36%. This dramatic decrease in RWC from WS 4 to WS 5 indicates that under a stress condition, the plants lost water at a relatively slow rate up to 4 days. Beyond the fourth day without water, plants may require irrigation to maintain their water status. However, compared to the rest of the treated and control groups, the WS 5 plants experienced the greatest variance in their RWC values. As expected, the WS 7 plants experienced the lowest mean RWC value, which is about 68% less than that of control plants.

The mean T_{leaf} and the corresponding CWSI values for the control and water stressed plants are shown in Figs. 3b and 3c, respectively. Leaf temperatures exhibit an

increasing trend from control up to WS 5, while WS 6 and WS 7 plants experienced lower temperatures than those of WS 5. Conversely, CWSI values reveal an inconsistent trend from control up to WS 3, and then exhibit a consistent rising trend with increased levels of water stress. The differences in mean temperatures among the control and WS 1 through WS 3 were not statistically significant. The mean CWSI differences among the control and WS 1 through WS 4 were also not statistically significant. However, statistically significant differences in mean CWSI values were obtained between control and WS 5 (0.3, $P < 0.001$); control and WS 6 (0.35, $P < 0.001$); and control and WS 7 (0.41, $P < 0.001$).

Figure 2.4 illustrates the average photosynthetic rate, stomatal conductance, and C_i responses of the control and treated (WS 1 to WS 6) plants. Photosynthetic rate (Figure 2.4a) decreased slowly from control to WS 3 plants, and then exhibited a steep decline from WS 3 to WS 4. There were no statistically significant differences in photosynthesis rate detected between control and WS 1, WS 2, WS 3 plants. However, control plants experienced significant differences in photosynthetic rate with WS 4 ($P = 0.017$), WS 5 ($P < 0.001$), and WS 6 ($P < 0.001$). Stomatal conductance (Figure 2.4b) showed a decreasing trend with a near linear decline from control to WS 5, and a slight decline with higher variance from WS 5 to WS 6. Statistically significant differences in stomatal conductance were observed between the control and WS 4 ($P = 0.031$); control and WS 5 ($P = 0.003$); and control and WS 6 ($P = 0.002$). C_i rates were relatively stable from control to WS 3, and then they experienced an increasing trend up to WS 6 (Figure 2. 4c). Control plants had a significantly different C_i rate than those of WS 5 ($P < 0.001$) and WS 6 ($P < 0.001$).

To examine the robustness of the RWC measurement protocol adapted in this study, regression models were developed to relate photosynthetic rate, stomatal conductance, and C_i with their corresponding RWC values (Figure 2.5). Results documented a small increase in both stomatal conductance and photosynthetic rate between RWC measurements of 15% and 40%, but between RWC values of 60% and 85%, both these variables increased at near-linear rates with increasing RWC. Overall, RWC accounted for 85% of the variation in photosynthetic rate, 75% of the variation in stomatal conductance, and 90% of the variation in C_i. All regressions models were statistically significant with $P < 0.001$.

Pearson Product Moment Correlation coefficients were used to evaluate the relationship between RWC and mean T_{leaf} and CWSI, respectively. Results indicated that RWC had highly significant ($P < 0.001$) relationships with both CWSI and raw mean temperature. However, the correlation between RWC and CWSI was better (r = -0.92, n = 56) than that between RWC and raw mean temperature (r = -0.84, n = 56). We developed and validated regression models to predict RWC using both leaf mean temperature and CWSI. The data collected from the plants were divided into calibration and validation data sets. The first five replicates of each treatment (8 treatments × 5 replications = 40) were used for developing the calibration model and the remaining 2 replicates were used for validating the models (8 treatments × 2 replications = 16). Figure 2.6 shows the relationships between mean T_{leaf} and RWC (a) and between CWSI and RWC (c). The feature space of T_{leaf} and RWC exhibited scatter from the regression line (especially WS 4 and WS 6), while the feature space of CWSI and RWC is more closely distributed along the regression line. Although both models are highly significant ($P < 0.001$), higher

coefficient of determination (R^2) and lower RMSE values indicate that RWC may be better estimated using CWSI rather than using T_{leaf}. Validation of models led to the conclusion that CWSI (Figure 2.6d) is a better predictor of RWC than T_{leaf} (Figure 2.6b).

2.4. Discussion

The potential of using high spatial resolution thermal images for estimating RWC in soybean leaves was examined in this study. The mean temperatures of the leaves (T_{leaf}), as well as a temperature-based index (CWSI) calculated from the data extracted from thermal images, were used separately to predict RWC. Significant differences in mean T_{leaf} and CWSI values were obtained between control and water stressed plants (those experiencing at least four days of irrigation withdrawal). With the exception of some minor variations, T_{leaf} and CWSI were consistent with the gravimetrically measured RWC values (i.e., increasing T_{leaf} and CWSI values with decreasing RWC) (Figure 2.3). This also suggests that plants under water stress can be detected by thermal-image-based T_{leaf} and CWSI. Slight differences in RWC, T_{leaf}, as well as CWSI values were obtained between control and WS 1 treatments. This may be due to variations in environmental factors. Day 7 of the experiment, when water was withheld from the WS 1 group of plants, was a day with consistent cloud cover and afternoon thunderstorms. That resulted in both relatively low PAR and air temperatures as compared to the rest of the days of the experiment (Figure 2.1), and might have caused the WS 1 plants to be less water stressed. RWC values of WS 5, 6, and 7 are almost the opposite and mirror those of CWSI, while T_{leaf} values of WS 5, 6, and 7 are inconsistent. It should be especially noted that, although the thermal images of WS 6 and 5 plants were taken during 09:50 to 10: 16 hours and 10:18 to 10:44 hours, respectively, the mean T_{leaf} of WS 5 was higher than that of WS 6

(Figure 2.2a and Figure 2.3b). This indicates the potential combined influence of variables like irradiance, air temperature, and RH during the image acquisition time on the leaf temperature (Jones, 1999a). Compared to WS 6, average PAR was about 60µmol/s/m^2 higher, average air temperature was about 0.2°C higher, and average RH was about 5% lower when the thermal images of WS 5 plants were taken (Figure 2.2). Moreover, the impact of these variables was normalized by the computation of CWSI, and this is demonstrated in a gradual increase in CWSI values with increasing intensity of water stress (Figure 2.3c). The results indicate that calibration of T_{wet} and T_{dry} using the methods described in this study could make thermal image based indices more responsive to water stress.

The relationships between RWC and other leaf-physiological variables (photosynthetic rate, stomatal conductance, and intercellular CO_2 concentration) related to water status were examined in order to assess the accuracy of RWC in representing the water status of plants, as well as to test the RWC extraction procedure adapted in this study. Regression analyses showed that significant variations in photosynthetic rate, stomatal conductance, and intercellular CO_2 content were explained by variations in RWC.

Both T_{leaf} and CWSI exhibited significant correlations with RWC. T_{leaf} and CWSI were tested by means of regression analysis and validated separately to compare their relative performances in estimating RWC. A slightly lower R^2 value of T_{leaf} versus RWC regression again emphasizes the impact of varying meteorological conditions on the leaf temperature, and therefore uncertainty in estimating the water status of plants. This study demonstrates that a thermal image based CWSI that accounts for environmental

variations can be used for improved estimation of RWC in soybean plants with RMSE values of 10.8%. The RMSE values reported in this study are slightly lower than those obtained by Yu et al. (2000), who used reflectance ratios in the MIR (R_{1430}/R_{1650}; R_{1430}/R_{1850}; R_{1483}/R_{1650}) to estimate RWC in four plant species including soybeans. Comparable precision in estimating RWC in soybean leaves using a MIR-based spectral index was reported by Inoue et al. (1993). Previous thermal image based studies used both raw leaf temperature and CWSI for estimating plant water status and produced similar findings (i.e., they report the advantage of using CWSI relative to raw leaf temperature in evaluating plant water status). For example, Cohen et al., (2005) reported the greater accuracy of CWSI in estimating leaf water potential for field based cotton plants. CWSI-based indices also performed better for estimating soil water potential, stomatal resistance, and stem water potential for olive orchards (Ben-Gal et al., 2009).

The regression models developed using the calibration data sets were applied to the validation data sets to evaluate their accuracy in predicting the RWC of the soybean leaves. Predictions of RWC using the validation data sets resulted in higher R^2 values (T_{leaf} = 0.77; CWSI = 0.89) compared to those of the calibration data sets (T_{leaf} = 0.69; CWSI = 0.85). The results suggest that RWC in soybean leaves can be estimated accurately using the thermal image analysis procedures presented in this study, particularly with regard to CWSI computation. Use of maximum and minimum temperatures for the dry and wet reference leaves, respectively, minimized the excessive influence of some low temperature pixels particularly present near the edges of the leaves on the calculation of mean dry reference leaf temperature, which can lead to T_{dry} being lower than the T_{leaf} as suggested by Grant et al. (2006).

Future research will focus on investigating the accuracy of the CWSI model in estimating RWC in field conditions and in different phenological stages of soybean plants using both close-range and airborne thermal images.

References

Alchanatis, V., Y. Cohen, S. Cohen, M. Moller, M. Sprinstin, M. Meron, J. Tsipris, Y. Saranga, and E. Sela, 2010. Evaluation of different approaches for estimating and mapping crop water status in cotton with thermal imaging. *Precision Agriculture*, 11:27-41.

Anderson, M., and W. Kustas, 2008. Thermal remote sensing of drought and evaporation. *Eos Transactions, American Geophysical Union*, 89: 133-240.

Ben-Gal, A., N. Agam, V. Alchanatis, Y. Cohen, U. Yermiyahu, I. Zipori, E. Presnov, M. Sprintsin, and A. Dag, 2009. Evaluating water stress in irrigated olives: correlation of soil water status, tree water status, and thermal imagery. *Irrigation Science*, 27: 367-376.

Bowman, W., 1989. The relationship between leaf water status, gas exchange, and spectral reflectanec in Cotton leaves. *Remote Sensing of Environment*, 30: 249-255.

Carter, G. A., 1991. Primary and secondary effects of water content on the spectral reflectance of leaves. *American Journal of Botany*, 78: 916-924.

Chen, D., J. Huang, and T. J. Jackson, 2005. Vegetation water content estimation for corn and soybeans using spectral indices derived from MODIS near- and short-wave infrared bands. *Remote Sensing of Environment*, 98: 225-236.

Cohen, Y., V. Alchanatis, M. Meron, Y. Saranga, and J. Tsipris, 2005. Estimation of leaf water potential by thermal imagery and spatial analysis. *Journal of Experimental Botany*, 56: 1843-1852.

Fuchs, M., 1990. Infrared measurement of canopy temperature and detection of plant water stress. *Theoretical and Applied Climatology*, 42: 253-261.

Gao, B. 1996. NDWI-A normalized difference water index for remote sensing of vegetation liquid water from space. *Remote Sensing of Environment*, 58: 257-266.

Grant, O. M., M. M. Chaves, and H. G. Jones, 2006. Optimizing thermal imaging as a technique for detecting stomatal closure induced by drought stress under greenhouse conditions. *Physiologia Plantarum*, 127: 507–518.

Grant O. M., L. Tronina, H. G. Jones, and M. M. Chaves, 2007. Exploring thermal imaging variables for the detection of stress responses in grapevine under different irrigation regimes. *Journal of Experimental Botany*, 58: 815–825.

Hardisky, M. A., V. Klemas, and R. M. Smart, 1983. The influences of soil salinity, growth form, and leaf moisture on the spectral reflectance of Spartina alterniflora canopies. *Photogrammetric Engineering & Remote Sensing*, 49: 77-83.

Hashimoto, Y., T. Ino, P. Kramer, A. Naylor, and B. Strain, 1984. Dynamic analysis of water stress of Sunflower leaves by means of a thermal image processing system. *Plant Physiology*, 76: 266-269.

Hunt, E. R. Jr, and B. N. Rock, 1989. Detection of changes in leaf water content using near- and middle-infrared reflectances. *Remote Sensing of Environment*, 30: 43-54.

Idso, S. B., R. D. Jackson, P. J. Pinter Jr., R. J. Reginato, and J. L. Hatfield, 1981. Normalizing the stress degree day for environmental variability. *Agricultural Meteorology*, 24: 45–55.

Inoue, Y., S. Morinaga, and M. Shibayama, 1993. Non-destructive estimation of water status of intact crop leaves based on spectral reflectance measurements. *Japanese Journal of Crop Science*, 62: 462-469.

Jackson, R. D., 1982. Canopy temperature and crop water stress. *Advances in Irrigation*, 1: 43-85.

Jackson, R. D., and C. E. Ezra, 1985. Spectral response of Cotton to suddenly induced water stress. *International Journal of Remote Sensing*, 6:177-185.

Jackson, R. D., Idso, S.B., Reginato, R.J. 1981. Canopy temperature as a crop water stress indicator. *Water Resources Research*, 17: 1133–1138.

Jackson, R. D., W. P. Kustas, and B. J. Choudhury, 1988. A reexamination of the crop water stress index. *Irrigation Science*, 9: 309–317.

Jackson, T. J., D. Chen, M. Cosh, F. Li, M. Anderson, C. Walthall, P. Doriaswamy, and E. R. Hunt, 2004. Vegetation water content mapping using Landsat data derived normalized difference water index for corn and soybeans. *Remote Sensing of Environment*, 92: 475-482.

Jensen, J. R. Remote Sensing of the Environment: An Earth Resource Perspective, 2nd Ed., Prentice Hall: Upper Saddle River, New Jersey, USA, 2007, pp 592.

Jones, H. G., 1999a. Use of infrared thermometry for estimation of stomatal conductance as a possible aid to irrigation scheduling. *Agricultural and Forest Meteorology*, 95: 139-149.

Jones, H. G., 1999b. Use of thermography for quantitative studies of spatial and temporal variation of stomatal conductance over leaf surfaces. *Plant, Cell and Environment*, 22: 1043– 1055.

Jones, H. G., 2007. Monitoring plant and soil water status: established and novel methods revisited and their relevance to studies of drought tolerance. *Journal of Experimental Botany*, 58:119-130.

Jones, H. G., R. Serraj, B. R. Loveys, L. Xiong, A. Wheaton, and A. H. Price, 2009. Thermal infrared imaging of crop canopies for the remote diagnosis and

quantification of plant responses to water stress in the field. *Functional Plant Biology*, 36: 978–989.

Jones, H. G., M. Stoll, T. Santos, C. D. Sousa, M. M. Chaves, and O. M. Grant, 2002. Use of infrared thermography for monitoring stomatal closure in the field: application to Grapevine. *Journal of Experimental Botany*, 53: 2249-2260.

Kacira, M., P. Ling, and T. H. Short, 2002. Establishing Crop Water Stress Index (CWSI) threshold values for early, non-contact detection of plant water stress. *Transactions of the ASAE*, 45: 775-780.

Leinonen, I., and H. G. Jones, 2004. Combining thermal and visible imagery for estimating canopy temperature and identifying plant stress. *Journal of Experimental Botany*, 55: 1423–1431.

Lillesaeter, O., 1982. Spectral reflectance of partly transmitting leaves: laboratory measurements and mathematical modeling. *Remote Sensing of Environment*, 12:247-254.

Mcvicar, T. R., and D. Jupp, 1998. The current and potential operational uses of remote sensing to aid decisions on drought exceptional circumstances in Australia: A review. *Agriculture Systems*, 57: 399-468.

McWilliams, D. A., D. R. Berglund and G. J. Endres, 2004. Soybean Growth and Management, NDSU Extension Service, North Dakota State University, Fargo, North Dakota 58105.

Ondimu, S., and H. Murase, 2008. Water stress detection in Sunagoke moss (Rhacomitrium canescens) using combined thermal infrared and visible light imaging techniques. *Biosystems Engineering*, 100: 4-13.

Payero, J. O., and S. Irmak, 2006. Variable upper and lower crop water stress index baselines for corn and soybean. *Irrigation Science*, 25: 21–32.

Riggs, G. A., and S. W. Running, 1991. Detection of canopy water stress in conifers using the airborne imaging spectrometer. *Remote Sensing of Environment*, 35:51-68.

Rock, B. N., J. E. Vogelmann, D. L. Williams, A. F. Vogelmann, and T. Hoshizaki, 1986. Remote detection of forest damage. *Bioscience*, 36:439-445.

Smart, R. E., and G. E. Bingham, 1974. Rapid estimates of relative water content. *Plant Physiology*, 53: 258-260.

Sims, D. A., and J. A. Gamon, 2003. Estimation of vegetation water content and photosynthetic tissue area from spectral reflectance: a comparison of indices based on liquid water and chlorophyll absorption features. *Remote Sensing of Environment*, 84: 526-537.

Tucker, C. J., 1980. Remote sensing of leaf water content in the near infrared. *Remote Sensing of Environment*, 10, 23-32.

Ustin, S. L., D. A. Roberts, D. A. Pinzo´n, S. Jacquemoud, M. Gardner, G. Scheer, C. M. Castan˜eda, and A. Palacios-Orueta, 1998. Estimating canopy water content of chaparral shrubs using optical methods. *Remote Sensing of Environment*, 65: 280–291.

Yu, G., T. Miwa, K. Nakayama, N. Matsuoka, and H. Kon, 2000. A proposal for universal formulas for estimating leaf water status of herbaceous and woody plants based on spectral reflectance properties. *Plant and Soil*, 227: 47-58.

Zygielbaum, A. I., A. A. Gitelson, T. J. Arkebauer, and D. C. Rundquist, 2009. Non-destructive detection of water stress and estimation of relative water content in maize. *Geophysical Research Letters*, 36: L12403 (doi:10.1029/2009GL038906).

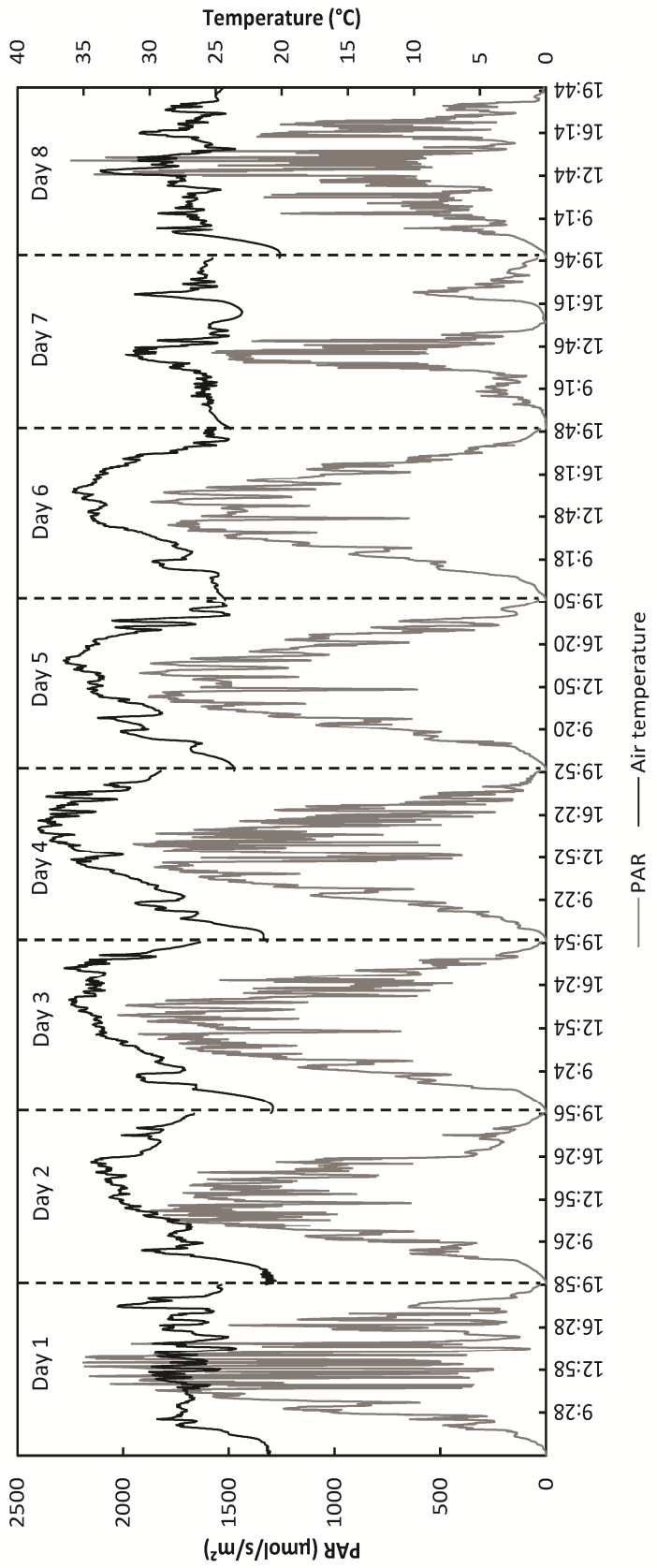

Figure 2.1. Variations in photosynthetically active radiation (PAR) and air temperature (per minute) during the 8-day experimentation period.

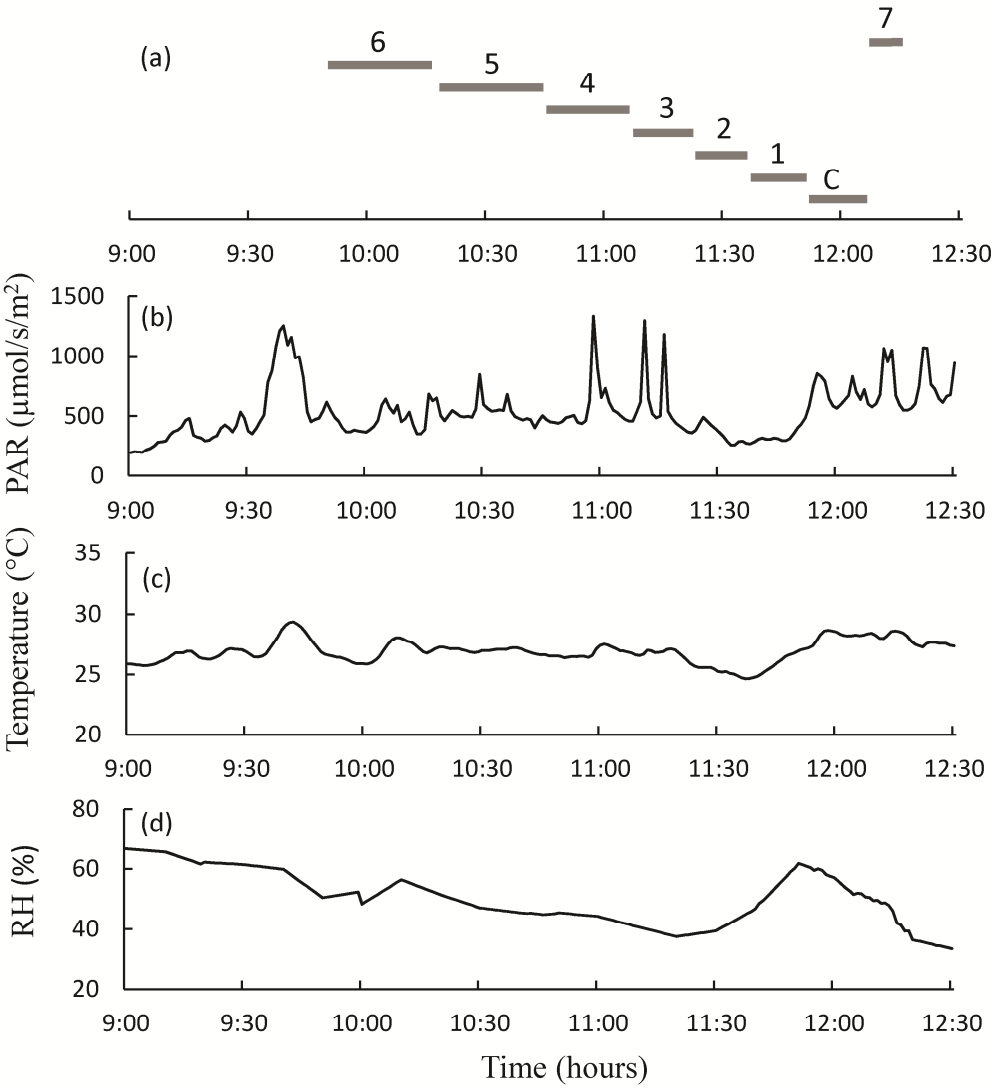

Figure 2.2. Time of thermal image acquisition, leaf gas exchange measurements, and leaf samples extraction for RWC measurements for each treatment (a) and greenhouse environmental conditions including PAR (b), air temperature (c), and RH (d) during the data collection period of May 12, 2011.

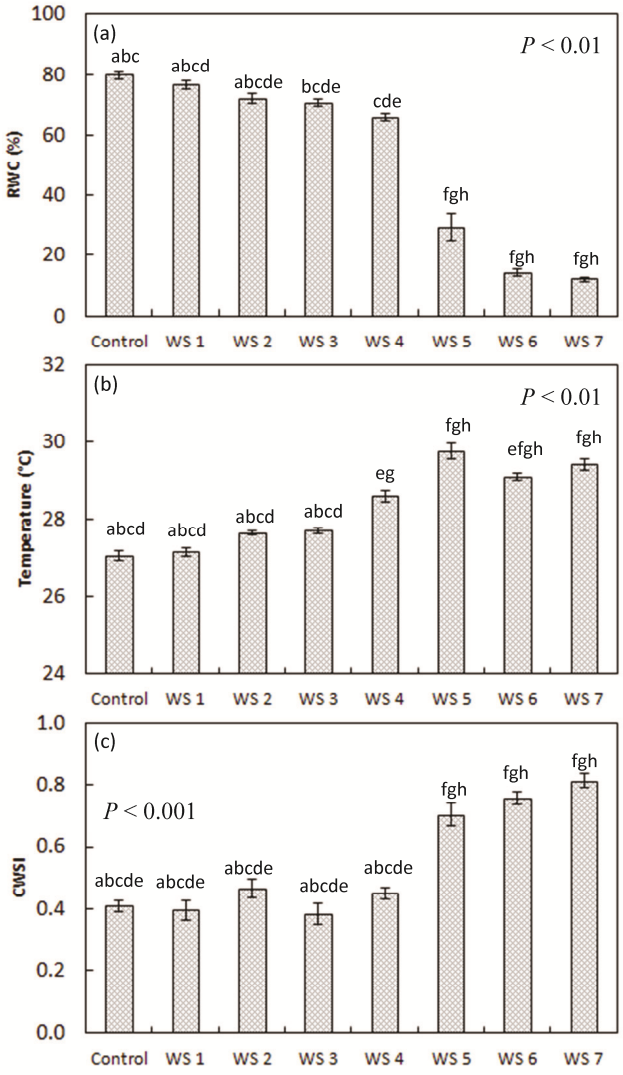

Figure 2.3. Average RWC (a), mean T_{leaf} (b), and CWSI (c) of control and water stressed (WS 1 – WS 7) soybean plants. Control plants were watered to the full capacity and the stressed plants were subjected to 1 (WS 1) through 7 (WS 7) days of water withdrawal. There were 7 plants (n=7) per treatment. Error bars represent mean ± SE. A significant difference between treatments is indicated in letters above the bars (following the ANOVA superscript method). Different treatments with the same lowercase letters are not significantly different according to the Dunnet T3 Test for RWC and the Scheffe Test for T_{leaf} and CWSI.

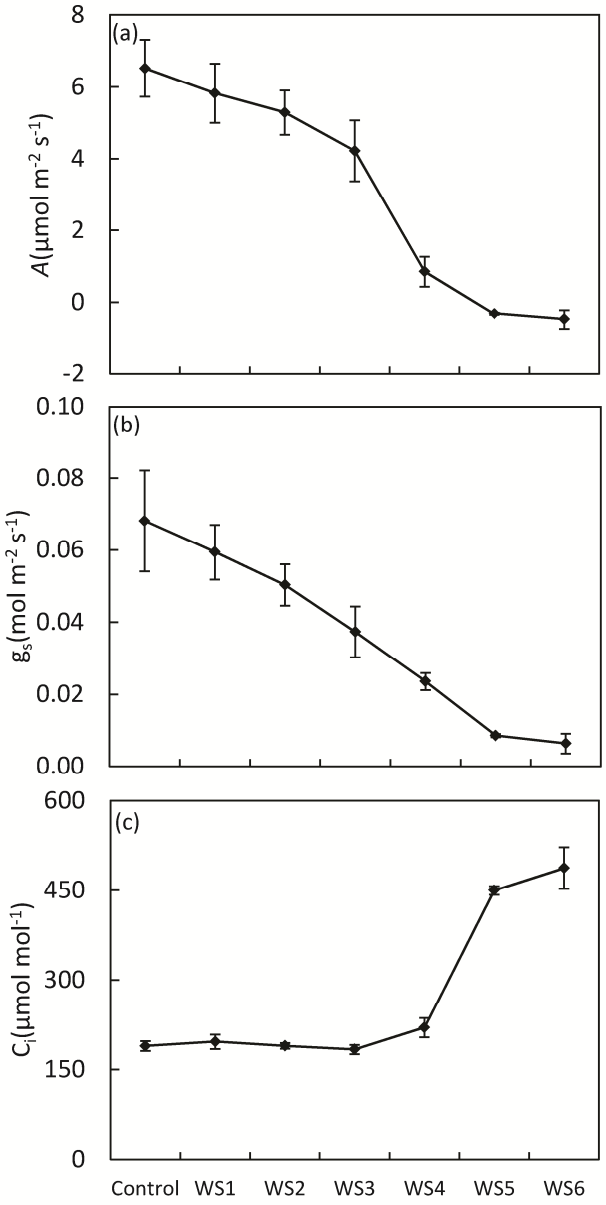

Figure 2.4. Average (a) photosynthetic rate (*A*), (b) stomatal conductance (g_s), and (c) intercellular CO_2 content (C_i) of control and water stressed (WS 1-WS 6) soybean plants (n=3 per treatment). Control plants were watered to the field capacity and the water stressed plants were subjected to 1 (WS 1) through 6 (WS 6) days of water withdrawal. Error bars represent mean ± SE.

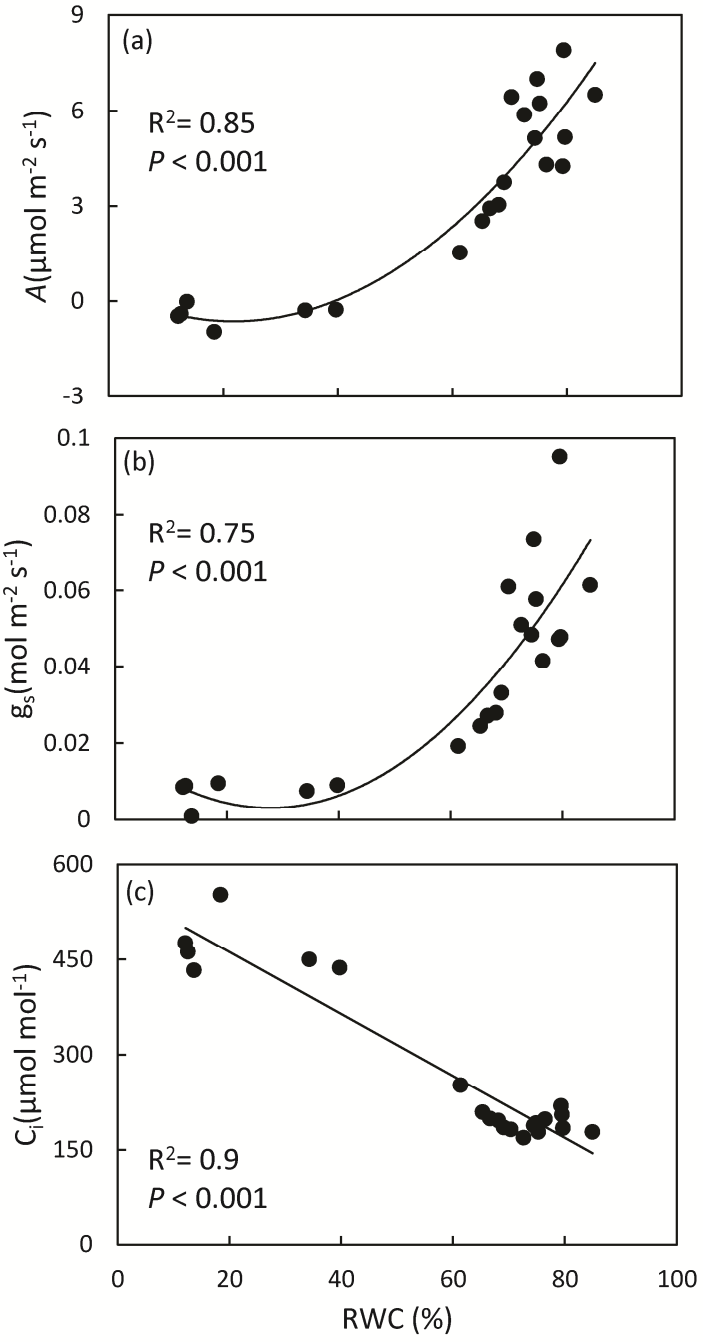

Figure 2.5. The relationship between RWC and (a) photosynthetic rate (*A*), (b) stomatal conductance (g_s), and (c) intercellular CO_2 concentration (C_i), respectively. Each data point represents an individual measurement on one leaf. Total sample size is 21 (7 treatments × 3 replicates). All regressions are highly significant ($P < 0.001$).

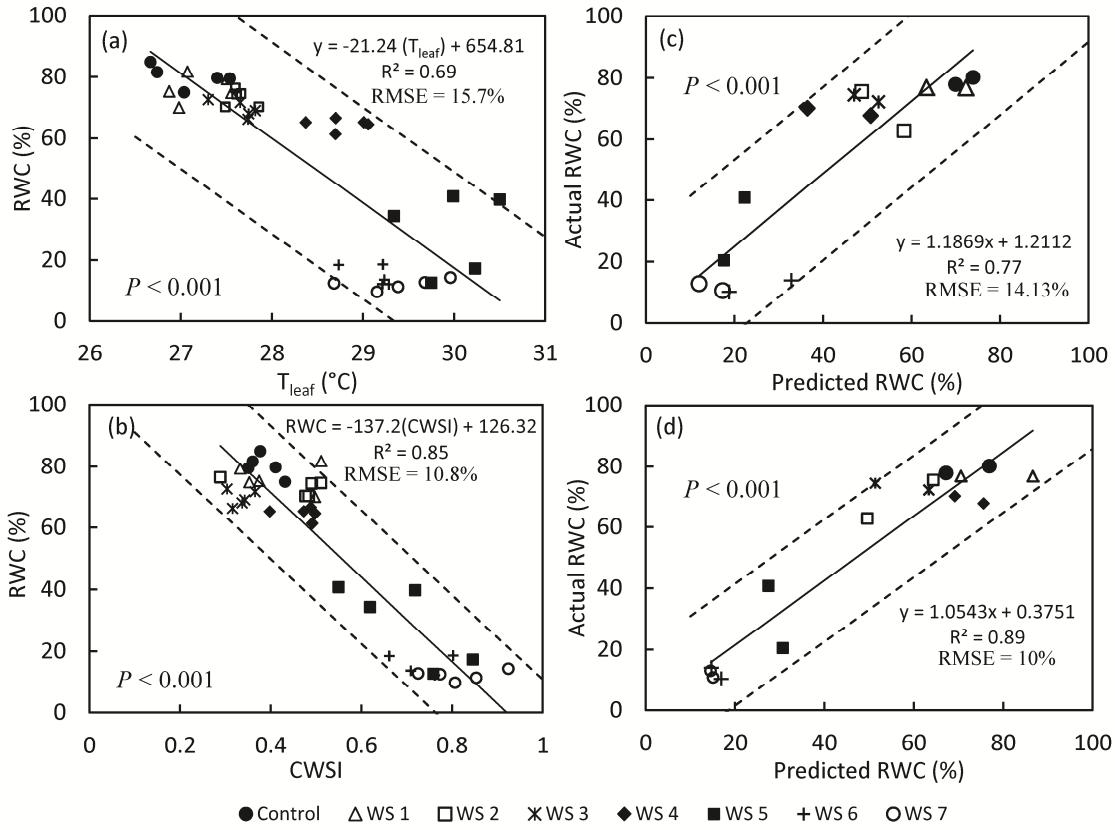

Figure 2.6. Regression models using calibration data sets to estimate RWC; RWC versus T_{leaf} (a) and RWC versus CWSI (c). RWC predicted versus RWC measured using T_{leaf} regression equation (b) and CWSI regression equation (d). The solid line in each graphic is the best fit function and the dashed lines represent the 95% confidence intervals for RWC prediction.

CHAPTER 3

RELATIONSHIPS BETWEEN VEGETATION INDICES AND ROOT ZONE SOIL MOISTURE UNDER CORN AND SOYBEAN CANOPIES IN THE U.S. CORN BELT: A COMPARATIVE STUDY USING CLOSE-RANGE SENSING APPROACH

Abstract

Understanding the connections between root zone soil moisture and vegetation spectral signals will enhance our ability to manage water resources and monitor drought-related stress in vegetation. In this paper, the relationships between vegetation indices (VIs) and *in situ* soil moisture under corn and soybean canopies were analyzed using close-range reflectance data acquired at a rainfed cropland site in the U.S. Corn Belt. Because of the deep rooting depths of corn plants, corn-based VIs exhibited significant correlations with soil moisture at a depth of 100 cm ($P < 0.01$) and kept soil moisture memory for a long period of time (45 days). Among the VIs applied to corn, the $CI_{Red\text{-}edge}$ correlated best with the 100 cm soil moisture depth ($P < 0.01$) at concurrent and up to 20-day lag periods. The same index showed a significant correlation with soil moisture at a 50 cm depth for lag periods from 10 ($P < 0.05$) to 60 days ($P < 0.01$). VIs applied to soybeans resulted in statistically significant correlations with soil moisture at the shallower 10- and 25-cm depths, and the correlation coefficients declined with increasing depths. As opposed to corn, soybeans held a shorter soil moisture memory as the correlations for all VIs versus soil moisture at 10 cm depth were strongest for the 5-day

lag period. WDRVI and NDVI performed better in characterizing soil moisture at the 10- and 25-cm depths under soybean canopies as compared to EVI and $CI_{Red\text{-}edge}$.

3.1. Introduction

Soil moisture is a key hydrological variable that influences the interactions and feedbacks occurring at the soil-vegetation-atmosphere interface. It controls the partitioning of incoming radiant energy into sensible and latent heat fluxes (Shukla and Mintz, 1982; Delworth and Manabe, 1989). A number of studies have shown the impacts of soil moisture on the atmosphere over a wide range of space and time scales. Namias (1989, 1991) noted that reduced soil moisture in spring in the Midwestern U.S.A. generates a high-pressure cell that results in a warm and dry summer; a condition conducive to the development of drought in this region. Mintz (1984) reported positive feedback existing between evaporation and precipitation on land. Similar positive feedback of soil moisture evaporation on precipitation has been observed in the central Great Plains of North America during the spring and summer months (Oglesby and Erickson, 1989; Findell and Eltahir, 1997; Koster et al., 2004).

Variations in soil moisture produce significant changes in hydrological processes including surface energy balances, vegetation productivity, flooding, runoff, and solute transport (Goward et al., 2002; Verstraeten et al., 2006). Accurate quantitative information on the spatial distribution of soil moisture using conventional *in situ* sensors is challenging as the data essentially represent measurements at discrete points that do not account for local-scale variations in soil properties, terrain, and vegetation cover. Thus, spatial extrapolation of these isolated soil moisture measurements to basin or watershed scales can produce large uncertainties (Western and Bloschl, 1999). Therefore, a dense

network of point observations is necessary to adequately characterize the spatial heterogeneity of soil moisture over extended geographic areas, which can be prohibitively expensive.

During the past three decades, remote sensing techniques have successfully supplemented data from ground-based sensors to retrieve spatially-integrated information on soil moisture over large areas with varying soil and land cover conditions (Schmugge et al., 1986; Jackson and Schmugge, 1989; Sandholt et al., 2002). Such studies have utilized the electromagnetic spectrum in the optical-thermal and microwave bands. A number of studies have demonstrated the utility of passive microwave radiometry and active microwave for assessing surface soil moisture over large areas (Jackson et al., 1996; Njoku et al., 2002). Despite having cloud penetration capabilities, microwave energy loses sensitivity to soil moisture in densely vegetated landscapes as the signals are influenced by foliage, stems, branches, and vegetation water content (Waring et al., 1996; Narayanan et al., 2004). In bare or sparsely vegetated surfaces microwave sensors can recognize water in a shallow near-surface soil layer; from 1-3 cm (C-band) to a maximal depth of 10 cm (L-band) (Waring et al., 1996; Njoku et al., 2003).

Root zone is the portion of the subsoil profile penetrated by vegetation roots, and availability of soil moisture in this zone can substantially influence vegetation health and surface energy balance through the process of transpiration. The depth of the root zone extends much deeper than the first few cm of the soil profile where the microwave energy cannot penetrate to retrieve the soil moisture. It is well known that vegetation spectral reflectance is sensitive to changes in plant biophysical properties including leaf water content, photosynthesis, or chlorophyll content (e.g. Carter, 1991; Gitelson et al., 2003;

Gitelson et al., 2005). Soil moisture is one of the major factors influencing these above mentioned plant biophysical properties; therefore, vegetation reflectance characteristics in the optical wavelengths can provide indirect information about the soil moisture status in the plant's root zone. However, cloud free conditions are required for obtaining reliable reflectance data in the optical wavelengths from aircraft or satellite platforms. Close-range sensing approach could potentially obviate some of the problems associated with cloud contamination and provide a basis for validating the satellite based data products that are affected by cloud cover.

Since the launch of the Landsat instrument in 1972, several vegetation indices (VIs) have been proposed by transforming the spectral reflectance of vegetation in the visible and near infrared wavebands. These VIs have been successfully applied to monitor terrestrial vegetation and to indirectly infer root zone soil moisture (e.g. Wang et al., 2007). The Normalized Difference Vegetation Index (NDVI) is sensitive to changes in the chlorophyll (Chl) content in the vegetation canopy through absorption of red wavelengths by the leaf Chl and related pigments and scattering of NIR radiation by the spongy mesophyll structure of green leaves (Rouse et al., 1974; Goward et al., 1985). Multi-temporal NDVI observations have been used extensively for monitoring global vegetation phenology (Justice et al., 1985), seasonality and annual net primary productivity in North American biomes (Goward et al., 1985; Goward and Dye 1987), drought (Kogan 1995) and desertification (Nicholson et al., 1998). While NDVI is widely used as an indicator of vegetative productivity, the index has several limitations for adequate characterization of vegetation bio-physical properties that include an apparent time lag between precipitation events and NDVI response (Di et al., 1994), effects from

the soil background (Huete et al., 1985), atmospheric attenuation (Kaufman and Tanré 1992), and asymptotic saturation over areas with moderate-to-high density of vegetation (Gitelson, 2004).

A number of new VIs were developed in order to overcome the inherent limitations and problems associated with the NDVI. For example, the Enhanced Vegetation Index (EVI) uses the blue, red, and NIR bands to increase the sensitivity of vegetation signals from high biomass regions while reducing canopy background noise along with effects from atmospheric aerosol scattering (Liu and Huete, 1995; Huete et al., 2002). EVI algorithm incorporates a canopy background adjustment factor that addresses nonlinear, differential NIR and red radiant transfer through a canopy, and two coefficients that describe the use of the blue band in correction of the band for atmospheric aerosol scattering (Huete and Justice, 1999). EVI is more responsive to variations in canopy structural parameters including leaf area index (LAI) and leaf morphology (Gao et al., 2000). EVI2 was recently proposed using red and NIR bands to facilitate the computation in the case of sensors without a blue band (Jiang et al., 2008). Performance of EVI2 was shown to be comparable with EVI when the atmospheric effects (including aerosol and residual clouds) are insignificant and data quality is good (Jiang et al., 2008). The Wide Dynamic Range Vegetation Index (WDRVI) was proposed to address the saturation of NDVI under moderate-to-high aboveground biomass conditions (Gitelson, 2004). WDRVI incorporates a weighting coefficient (α) in the NIR reflectance term in the NDVI formulation to account for the differential sensitivity of NDVI to red and NIR reflectances. WDRVI was shown to be linearly related to the green leaf area index of corn and soybeans (Gitelson, 2004; Gitelson et al., 2007). Recently,

Gitelson et al. (2005) proposed the Chlorophyll$_{Red\text{-}edge}$ Index ($CI_{Red\text{-}edge}$) to estimate Chl content in crops including corn and soybean. While the $CI_{Red\text{-}edge}$ has been successfully implemented for estimating GPP (Peng et al., 2011) and green leaf area in corn and soybean crops (Vina et al., 2011), its potential for root zone soil moisture characterization has not been explored.

The Corn Belt is a major corn growing region in the U.S. Within the Corn Belt, states such as Iowa, Illinois, Nebraska, Indiana, Minnesota, and Ohio collectively accounts for about three-fourths of the total corn produced in the U.S. (USDA-NASS, 2009). The major proportion of the corn growing areas in this region is rainfed rather than irrigated. For example, approximately all corn grown in Iowa, which is the leading corn producing state, is rainfed (Duvik and Cassman, 1999). Soybeans, also an important field crop in this region, primarily are grown in an inter-annual rotation with corn. Spatially-distributed estimations of root zone soil moisture in the U. S. Corn Belt may contribute to monitoring drought-related stress on corn and soybeans grown under rainfed farming systems. Previous studies have investigated the relationship of remotely sensed VIs with root zone soil moisture for corn and groundnut crops in India (Rao et al., 1993); croplands as well as forest cover types in the eastern U.S. Corn Belt (Adegoke and Carleton 2002); grassland and shrub sites in Texas, Arizona, and New Mexico (Wang et al., 2007; Schnur et al., 2010); and crop, pasture, and grassland sites in Oklahoma (Gu et al., 2008). However, a relatively limited body of research has demonstrated the linkages of root zone soil moisture with the spectral reflectance-based VIs for important agronomic crops such as corn and soybeans in the U.S. Corn Belt. Our objective is to evaluate the potential of proximally sensed VIs simulated to the band passes of

contemporary space-borne sensors such as Moderate Resolution Imaging Spectroradiometer (MODIS) and Medium Resolution Imaging Spectrometer (MERIS) in characterizing soil moisture at variable depths within the root zones of corn and soybean.

3.2. Data and Methods

3.2.1 Study Area

This study was conducted at the University of Nebraska Agricultural Research and Development Center (ARDC), located approximately 6 km south of Mead, Nebraska, USA (Figure 3.1a). The site includes a rainfed field (41°10'46.8″ N, 96°26'22.7″ W) covering an area of 65.4 ha with a yearly crop rotation pattern of corn (*Zea mays*) and soybeans (*Glycine max*). The research was undertaken using data acquired during the 2003, 2005, and 2007 growing seasons when the field was under corn cover and the 2002, 2006, and 2008 growing seasons when the field was planted with soybean. This area experiences a humid continental climate with warm summer months. The mean monthly precipitation during the past 30 year period (between 1981 and 2010) ranged from 14 mm in January to 106 mm in June (Figure 3.1b). Approximately 40% of the total annual precipitation is received during the months of April through June, crucial for soil moisture recharge and subsequent crop growth. The maximum monthly temperatures during the same period ranged between 1°C in January and 31°C in July. The soil types in the field are deep silty clay loams, typical of eastern Nebraska, and consist of four soil series including Yutan, Tomek, Filbert, and Filmore (Suyker and Verma, 2009).

3.2.2 Soil Moisture Data

Volumetric soil water content (hereafter referred to as soil moisture) was measured hourly at four Intensive Management Zones (i.e., IMZ-1, IMZ-2, IMZ-3, and

IMZ-5) within the field using Vitel (2002-03) and Theta probes (2005-08). These sensors comprise part of the automated weather data network (AWDN) operated by the High Plains Regional Climate Center (HPRCC) as implemented across parts of the U.S. Great Plains. The soil moisture sensors were installed at four depths: 10 cm; 25 cm; 50 cm; and 100 cm. Hourly soil moisture values were averaged to generate daily values for each of the four depths. Rigorous quality control tests have been conducted based on the properties of soil water, soil characteristics, and precipitation measurements to determine the accuracy of the daily soil moisture data (Hunt et al., 2009). After examining the data quality, we determined that IMZ-5 had the fewest soil moisture observations categorized as "bad data". For this reason, we used the soil moisture values measured at IMZ-5 for analysis. Soil types at this site at four depths were silty clay loam and fairly representative of the whole field.

3.2.3 Crop Spectral Reflectance Measurements

Close-range reflectance spectra were acquired over crop canopies using a motorized, all-terrain sensor platform (Rundquist et al., 2004). The platform has a ground clearance of 1.91 m and a width of 2.59 m. The wheels are positioned for movement through crops with 76.2 cm spaced rows. The sensors were deployed on a metal frame at the end of a 12 m long hydraulic boom attached to the platform. The boom can be rotated through 360° around the platform to collect above canopy data from the nadir position (Figure 3.2a).

A dual-fiber system, with two inter-calibrated Ocean Optics USB2000 radiometers attached to the sensor platform, was used to collect high spectral resolution reflectance data for the corn and soybean canopies. Both radiometers record spectral data

from 400 to 900 nanometers (nm) with an average wavelength spacing of about 1.5 nm. The first radiometer, with a 25° field-of-view, was pointed vertically downward to measure the upwelling radiance of the crop canopies. This field-of-view resulted in a sampling area with a diameter of around 2.4 m at the top of the canopy. The second radiometer, with a hemispherical field-of-view, was pointed upward to simultaneously measure incident irradiance (Gitelson et al., 2003). The two radiometers were positioned at approximately 6 m above the top of the canopies to measure the spectral reflectance of the respective crops. Calibration of the spectroradiometers was performed by measuring the total upwelling radiance of a white Spectralon reflectance standard (Labsphere, Inc., North Sutton, NH) simultaneously with incident irradiance. The radiometers were positioned at about 6 m above the top of the corn and soybean canopies, and the distance between the sensor and canopy was kept constant for all measurements across the growing season. Percent reflectance (ρ_λ) was calculated as:

$$\rho_\lambda = (L_\lambda^{crop}/E_\lambda^{inc}) \times (E_\lambda^{cal}/ L_\lambda^{cal}) \times 100 \times \rho_\lambda^{cal} \quad (3.1)$$

where, L_λ^{crop} is upwelling radiance of corn and soybean canopies, E_λ^{inc} is incident irradiance on the top of the canopies, E_λ^{cal} is incident irradiance and L_λ^{cal} is upwelling radiance of the white Spectralon reflectance standard during the time of calibration, and ρ_λ^{cal} is the reflectance of the Spectralon panel linearly interpolated to match the band centers of each radiometer (Rundquist et al., 2004).

A digital camera (Kodak DC-40) was mounted on the boom adjacent to the radiometers to acquire above-canopy true color images from the view of the spectroradiometer. A digital image was acquired concurrently for each of the reflectance

measurements. The reflectance measurements were taken at approximately one-week intervals from mid-May through the beginning of October each year to capture vegetative, reproductive, and senescence stages of crop development. A true color image of the field-of-view and the associated reflectance profile of a single scan made at a particular location within the field are shown in Figures 3.2b and 3.2c, respectively. On each measurement day, six sample locations were randomly selected within the field, and canopy reflectance measurements were made. The data were averaged to generate a single reflectance value, per wavelength, per field. This study is based upon a total of 76 field data collection campaigns (40 for corn and 36 for soybean) conducted in the 'core' growing season (between mid-June through mid-September) during the years 2002-2003 and 2005-2008.

3.2.4 Spectral Vegetation Indices

Hyperspectral reflectance data from the top of the crop canopies were transformed to four VIs including NDVI (Rouse et al., 1974), EVI2 (Jiang et al., 2009), WDRVI (Gitelson, 2004), and $CI_{Red\text{-}edge}$ (Gitelson et al., 2005) in order to compare their correlations with the root zone soil moisture. NDVI, EVI2, and WDRVI indices were computed by simulating the spectral channels of the MODIS system, on board NASA's Terra and Aqua satellites. These MODIS-simulated indices were calculated using the following equations:

$$NDVI = (R_{NIR} - R_{red}) / (R_{NIR} + R_{red}) \quad (3.2)$$

$$EVI2 = 2.5 \times (R_{NIR} - R_{red}) / (R_{NIR} + 2.4 \times R_{red}) \quad (3.3)$$

$$WDRVI = (\alpha \times R_{NIR} - R_{red}) / (\alpha \times R_{NIR} + R_{red}), \text{ with } \alpha = 0.2 \quad (3.4)$$

Where R_{NIR} and R_{Red} are the reflectance values corresponding to MODIS NIR (841-876 nm) and Red (620-670 nm) spectral channels, respectively.

Formulation of the $CI_{Red\text{-}edge}$ requires reflectances in the red edge and NIR channels, both of which are available via the MERIS system (onboard the polar orbiting Envisat Earth Observation Satellite). Therefore, $CI_{Red\text{-}edge}$ was calculated using the following equation:

$$CI_{Red\text{-}edge} = (R_{NIR} / R_{Red\text{-}edge}) - 1 \quad (3.5)$$

where R_{NIR} is the reflectance between 750-757.5 nm and $R_{Red\text{-}edge}$ is the reflectance between 703.75-713.75 nm.

In order to transform the close-range hyperspectral reflectance data to VIs as would be associated with other sensors, the reflectance values were averaged to the band passes of MODIS or MERIS sensors and used those values for computing the indices. For example, the mean reflectance value (for about 37 individual bands) between the wavelengths of 620 and 670 nm was calculated to determine the MODIS simulated red band reflectance. Similarly, MODIS simulated NIR reflectance was calculated by averaging the reflectance values (for about 28 bands) between the wavelengths of 841 and 876 nm. The simulated MODIS red and NIR values were then used to compute NDVI. The spatial resolution of MODIS red and NIR channels are 250m, while the pixel size of MERIS NIR and Red-edge full resolution (FR) product is about 260m × 290m. Considering the size of the study site, approximately 9 MODIS and 6 MERIS pixels can be located completely within the field. Since the field is planted to a homogenous mono-crop in a given growing season, we assume that the potential differences arising from the differences in the spatial resolutions are negligible when comparing the correlations of

MODIS and MERIS simulated VIs with measured soil moisture. In an earlier work, Gitelson et al. (2007) reported close relationships between the 250 m MODIS- and close-range reflectance-derived VI data (NDVI and WDRVI) at the same study site.

3.2.5 Correlation Analyses

Relationships between root zone soil moisture at four different depths and corn and soybean VIs were evaluated using the Pearson Product Moment Correlation (Korin 1975). VI observations were correlated with the concurrent (same day) soil moisture values. In order to evaluate the effect of antecedent soil moisture on the canopy reflectance signals, soil moisture lags up to 60 days at 5-day increments were also correlated with VIs. Lagged soil moisture values for different time lags were computed from the daily time series soil moisture data. For example, soil moisture of the 5-day lag period was computed by averaging the concurrent soil moisture (day of spectral measurement) and that of four previous days. The statistical significance of the relationships was tested using the probability (P) values of 0.05 and 0.01.

3.3. Results and Discussion

3.3.1 Growing Season Time Series Soil Moisture and VIs Profiles

Daily time series soil moisture profiles at four depths in the soil profile for the year 2005 are presented in Figure 3.3a to illustrate the temporal trends of soil moisture at the study site. Soil moisture at the shallower depths (10 and 25 cm) exhibited high frequency variations compared to those at the deeper depths (50 and 100 cm). Prior to the beginning of the growing season and early in the growing season (March-May), soil moisture content in the 50- and 100-cm depths remained constant. During that period, the

data for the shallower depths indicate variations due to snowmelt, precipitation, and direct evaporation from the soil as well as transpiration from the emerging plants (especially in late spring). In early June, the soil moisture content at the shallower depths progressively declined as the roots of the plants started extracting water. A similar trend was shown at the 50 cm depth beginning in early July as the roots penetrated deeper into the soil profile for water extraction. The 7-year (2002-2008), average seasonal soil moisture profile (Figure 3.3b) indicated a gradual decline from early June at 10- and 25-cm depths and from early and mid-July at 50- and 100-cm depths, respectively.

The growing season variations in the corn (2003) and soybeans (2002) scaled VIs are shown in Figure 3.4. The ranges of the four VI values across a given growing season were different. For example, corn NDVI values during the 2003 growing season ranged between 0.25 and 0.89, while corn CIRed-edge values during the same growing season ranged between 0.11 and 3.63. Therefore, to visually compare the changes in VIs across the growing season we scaled the index values between 0 and 1 (as shown in figure 3.4). During the vegetative stage of corn, the scaled VIs showed increasing trends and reached maximal values on DOY 202 (Figure 3.4a). The rate of increase in scaled NDVI (0.57 units) was maximum compared to the rate of increase in rest of the VIs, between DOYs 160 and 174. In the reproductive and senescence stages of corn, $CI_{Red\text{-}edge}$ showed a sharper decline than the rest of the VIs. Soybean VIs showed increasing trends (except for DOY 196) and reached maximal values on DOY 217 (Figure 3.4b). Soybean $CI_{Red\text{-}edge}$ values decreased rapidly during the reproductive and senescence stages compared to NDVI and WDRVI values. Among the four soybean VIs, EVI2 showed largest variations during the growing season, especially between DOYs 221 and 239. Similar temporal

patterns of corn and soybeans VIs were observed for other four year growing season data analysed in this study.

3.3.2 Correlation between Soil Moisture and VIs

Figure 3.5 illustrates the relationships between corn VIs and soil moisture at all four depths. Results show that the relationships of VIs with concurrent soil moisture (shown as time lag = 0) at 10-, 25-, and 50-cm were not statistically significant. The correlations of $CI_{Red\text{-}edge}$ (r = 0.57), NDVI (r = 0.52), WDRVI (r = 0.49), and EVI2 (r = 0.38) with concurrent soil moisture at 100 cm depth were highly significant ($P < 0.01$). Correlations of soybean VIs and soil moisture revealed that WDRVI ($P < 0.01$), NDVI ($P < 0.05$), and $CI_{Red\text{-}edge}$ ($P < 0.05$) exhibited significant relationships with soil moisture at 10 cm depth, while the relationships of the VIs with concurrent soil moisture at deeper depths were not statistically significant (Figure 3.5).

Previous studies have documented that, under rainfed farming systems in the U.S. Corn Belt, the amount of soil water present at the beginning of the growing season and during the early stages of crop cycles has a considerable impact on the overall vigour and productivity of crops during the later stages of the crop cycle (e.g. Grassini et al., 2010) and hence higher VIs. During the months of July and August, the amount of soil moisture in the soil profiles reduces because of the high plant transpiration rates (Figure 3.3b). Conversely, this period of the growing season is associated with pronounced greenness of the crops and hence maximal values of VIs. Based on these conditions; it was hypothesized that the relationship of VIs and soil moisture would be stronger if any inherent time delays (time lags) that plants require to respond to soil moisture changes were considered. We tested the hypothesis by correlating the VIs with the averaged soil

moisture values using lag periods up to 60 days. The results show that correlations of corn VIs at all four depths improved with increasing time lags (Figure 3.5). At 10- and 25-cm depths, corn EVI2 had a significant correlation ($P < 0.05$) with 45- and 50-day lagged soil moisture, respectively. At the intermediate depth of 50 cm, corn $CI_{Red\text{-}edge}$ was significantly related to 10-day lagged soil moisture ($P < 0.05$) and the relationship was highly significant for lag periods of 35 days or longer ($P < 0.01$). The relationships of corn NDVI and WDRVI with soil moisture at the 50 cm depth was significant from 30- and 40-day lag periods, respectively. This suggests that NDVI and WDRVI require a longer time lag to respond changes in soil moisture at the 50 cm depth compared to the $CI_{Red\text{-}edge}$. At 100 cm, peak correlations between corn VIs and soil moisture were primarily observed over a 45-day lag period (NDVI r = 0.7; $CI_{Red\text{-}edge}$ r = 0.66; WDRVI r = 0.63; EVI r = 0.54) and then showed a decreasing trend. This finding agrees with Adegoke and Carleton (2002), who reported maximum correlations between AVHRR-derived crop NDVI and 100 cm depth soil moisture on an 8-week lag period. Among the four corn VIs, the $CI_{Red\text{-}edge}$ had the strongest correlations with the 100 cm depth soil moisture up to 20-day lag periods. Beyond 20 days, NDVI exhibited the strongest correlations with soil moisture. These findings suggest that $CI_{Red\text{-}edge}$ can provide the most accurate estimates of soil moisture, among the indices tested, for concurrent, as well as shorter lag periods (20 days) under corn cover.

In contrast to corn correlations, the correlation of soybean VIs including NDVI, WDRVI, and $CI_{Red\text{-}edge}$ peaked at the 5-day lag period ($P < 0.01$) for the 10 cm depth and then followed a decreasing trend with increasing time lags (Figure 3.6). At the 25 cm depth, both NDVI and WDRVI had statistically significant relationships with soil

moisture at 5- and 10-day lags, and the correlations were strongest on the 5-day lag period. Relationships of all VIs with deeper depth soil moisture (50- and 100-cm) were not statistically significant with the exception of $CI_{Red\text{-}edge}$ versus 100 cm depth soil moisture for 50-day or longer lag periods ($P < 0.05$). These results suggest that even when grown in the same soil type and climate conditions, VIs for soybeans can respond to changes in soil moisture more rapidly and can maintain a fairly short soil moisture memory (i.e., the time-lag up to which antecedent averaged soil moisture exhibited the strongest correlation with the VIs) compared to corn. Similar to soybean VIs, the highest correlation of VIs with soil moisture lagged to 5 days at 10-cm depth was reported for other plant species (e.g. Wang et al., 2007) for a shrub site in semi-arid Arizona.

Results of this study show that the water extraction patterns of corn and soybean plants within the root zones are clearly distinct. VIs derived from the corn canopies exhibited strong relationships with soil moisture at deeper depths (50 and 100 cm). Conversely, soybeans VIs were highly sensitive to changes in soil moisture at much shallower depths of 10- and 25-cm. This discrepancy between the crops reflects their different rooting depths and structure. Corn is a fairly deep rooted plant with roots extending to a depth of 100 cm and beyond, while the rooting depths of soybean plants are comparatively shallower (Dwyer et al., 1988). In the U.S. Corn Belt, corn roots can extend downward to a depth of 120 cm or more (Adegoke and Carleton, 2002; Kranz et al., 2008). However, variations in the depth and distribution of roots are caused by differences in climate, soil properties, and management practices such as irrigation and tillage treatments. Dwyer et al. (1988) monitored the rooting depths of corn and soybeans plants grown on four different soil types for data over 3-year growing seasons and

reported that on each soil type, the rooting depths of corn were deeper than those of soybeans. In clayey-textured soil with a no-till system, Venzke Filho et al. (2004) reported that the mean root length density of soybean plants was significantly higher in the top 50 cm of the soil profile, and in the 0-10 cm depth the root length density of soybean plants was twice higher than that of corn ($P < 0.05$). Tufekcioglu et al. (1999) showed that the density of soybean roots was higher (versus corn) in the top 50 cm depth, and the density of corn root was higher (versus soybean) in 50-100 cm depth in the soil profile at a riparian buffer site in central Iowa. Such evidence is consistent with the findings of our study, where soybean canopy VIs respond to the soil moisture in the 10- and 25-cm depths while corn canopy VIs respond to soil moisture in deeper depths (100- and 50-cm).

We suggest that both $CI_{Red\text{-}edge}$ and NDVI perform better than the other two indices in relating to corn root zone soil moisture. $CI_{Red\text{-}edge}$ may provide a better estimate of corn root zone soil moisture both concurrently and for shorter time lags (20-days) when compared to NDVI. However, the relation of $CI_{Red\text{-}edge}$ to soybean ($CI_{Red\text{-}edge}$ peak r =0.39 at 10 cm depth) root zone soil moisture was found to be lower than that of corn ($CI_{Red\text{-}edge}$ peak r =0.66 at 100 cm depth). This differential sensitivity of $CI_{Red\text{-}edge}$ to corn and soybean root zone soil moisture could be attributed to the distinct leaf angle distribution (heliotropic in soybean versus hemispherical in corn), leaf structure, and total canopy Chl content between corn and soybean plants (Gitelson et al., 2005, 2006). Gitelson et al. (2005), using the data from the 2002 growing season for irrigated corn and soybean plots located close to our study site, showed that the canopy Chl content of corn plants was consistently higher than that of soybean throughout the growing season. The

higher Chl content of the corn canopies could have caused the corn $CI_{Red\text{-}edge}$ to be more sensitive to root zone soil moisture than that of soybean canopies.

3.4. Conclusions

In this study, we explored the potential of three simulated MODIS VIs (NDVI, WDRVI, and EVI2) and a simulated MERIS VI ($CI_{Red\text{-}edge}$) in characterizing root zone soil moisture under corn and soybean canopies using spectral data collected at a close-range (6 meters above the top of the canopy) in the U.S. Corn Belt. Time-series VI data for six growing seasons were correlated with concurrent as well as antecedent soil moisture (up to 60 days) at four different depths (10, 25, 50, and 100 cm) in the soil profile.

The corn VIs were found to be significantly related to the concurrent soil moisture at the 100-cm depth. Among the VIs analyzed in this study, $CI_{Red\text{-}edge}$ showed strongest correlation with the soil moisture at this depth. Relationships of corn VIs with soil moisture improved when the time lag that the plants require to respond to changes in soil moisture were taken into consideration. At 50-cm depth, $CI_{Red\text{-}edge}$ showed a statistically significant correlation with 10-day lagged soil moisture, and the r values increased with increasing time lags. Maximum correlations of corn VIs, including $CI_{Red\text{-}edge}$ and NDVI with the 45-day lagged soil moisture at 100-cm depth, indicated that corn VIs integrated the antecedent soil moisture conditions up to 45 days in their spectral signals.

Correlations of soybean VIs with soil moisture showed that WDRVI and NDVI were significantly related to concurrent soil moisture at 10- and 25-cm depths and may serve as better proxies for characterizing soil moisture at these depths than $CI_{Red\text{-}edge}$ and

EVI2. Correlations of soybean WDRVI and NDVI were highest with 5-day lagged soil moisture at 10- and 25-cm depths. These findings suggest that unlike corn, soybean VIs are highly sensitive to soil moisture at shallow depths in the soil profile and responsive to antecedent soil moisture conditions during the past 5 day period.

The results presented in this study should lead to a more accurate characterization of root zone soil moisture, which influences crop conditions and may contribute to vegetation stress assessment efforts in support of drought investigations. The relationships between soil moisture and VIs shown in this study can form the basis to build models for estimating root zone soil moisture in corn and soybean croplands in the U.S. Corn Belt where in situ soil moisture observation sites are sparse. Although MODIS-based 8-day and 16-day composited products have been used for estimating root zone soil moisture under crop, grass and shrub cover types (Wang et al., 2007; Gu et al., 2008; Schnur et al., 2010), the potential relationships of a daily surface reflectance product (MOD09GQ) and MERIS-based Chl related indices with root zone soil moisture has not been evaluated extensively. This study, performed using the close-range reflectance data, provides the first phase of the evaluation of such products. However, further research using the actual MODIS and MERIS products, with longer time-series data is proposed for continued evaluation of soil moisture and VI relationships in the U.S. Corn Belt. Future extension of this work by using the actual MODIS and MERIS products should include a few considerations. Firstly, the soil moisture and VI relationships established using the close-range reflectance data (as the case in this study) are expected to be similar when the above mentioned satellite sensor based data products acquired under clear sky conditions are used. Secondly, different spatial resolutions of

MODIS and MERIS data products mean that careful selection of pixel window centered near the middle of the field is necessary to avoid any mixed pixel (a single pixel containing more than one species) effects on the soil moisture and VI relationships.

References

Adegoke, J. O., and A. M. Carleton, 2002. Relations between soil moisture and satellite vegetation indices in the U. S. Corn Belt. *Journal of Hydrometeorology*, 3: 395-405.

Carter, G. A., 1991. Primary and secondary effects of water content on the spectral reflectance of leaves. *American Journal of Botany*, 78: 916-924.

Delworth, T., and S. Manabe, 1989. The influence of soil wetness on near surface atmospheric variability. *Journal of Climate*, 2: 1447-1462.

Di, L., D. Rundquist, and L. Han, 1994. Modelling relationships between NDVI and precipitation during vegetative growth cycles. *International Journal of Remote Sensing*, 15: 2121-2136.

Duvick, D.N. and K. G. Cassman, 1999. Post-green revolution trends in yield potential of temperate corn in the North-Central United States. *Crop Science*, 37: 1622-1630.

Dwyer, L. M., D. W. Stewart, and D. Balchin, 1988. Rooting characteristics of corn, soybeans and barley as a function of available water and soil physical characteristics. *Canadian Journal of Soil Science*, 68: l2l-132.

Findell. K. and E. Eltahir, 1997. An analysis of the soil moisture-rainfall feedback, based on direct observations from Illinois. *Water Resources Research*, 33: 725-735.

Gitelson, A.A., 2004. Wide dynamic range vegetation index for remote quantification of crop biophysical characteristics. *Journal of Plant Physiology*, 161: 165-173.

Gitelson, A. A., S. B. Verma, A. Viña, D. C. Rundquist, G. Keydan, B. Leavitt, T. J. Arkebauer, G. G. Burba, and A. E. Suyker, 2003. Novel technique for remote estimation of CO2 flux in corn. *Geophysical Research Letters*, 30, 486, doi:10.1029/2002GL016543.

Gitelson, A. A. , A. Vina, S. B. Verma, D. C. Rundquist, T. J. Arkebauer, G. Keydan, B. Leavitt, V. Ciganda, G. G. Burba, and A. E. Suyker, 2006. Relationship between gross primary production and chlorophyll content in crops: Implications for the synoptic monitoring of vegetation productivity. *Journal of Geophysical Research*, 111, D08S11, doi:10.1029/2005JD006017

Gitelson, A. A., A. Vina, T, J. Arkebauer, D. C. Rundquist, G. Keydan, and B. Leavitt, 2003. Remote estimation of leaf area index and green leaf biomass in corn canopies. *Geophysical Research Letters*, 305, 1248, doi:10.1029/2002GL016450.

Gitelson, A. A., A. Vina, V. Ciganda, D. C. Rundquist, and T. J. Arkebauer, 2005. Remote estimation of canopy chlorophyll content in crops. *Geophysical Research Letters*, 32, L08403, doi:10.1029/2005GL022688.

Gitelson, A. A., B. D. Wardlow, G. P. Keydan, and B. Leavitt, 2007. An evaluation of MODIS 250-m data for green LAI estimation in crops. *Geophysical Research Letters*, 34, L20403, doi:10.1029/2007GL031620.

Goward, S. and D. Dye, 1987. Evaluating North American net primary productivity with satellite observations. *Advances in Space Research*, 7: 165-174.

Goward, S., C. Tucker, and D. Dye, 1985. North American vegetation patterns observed with the NOAA-7 advanced very high resolution radiometer. *Vegetatio*, 64: 3-14.

Goward, S., Y. Xue, and K. Czajkowskic, 2002. Evaluating land surface moisture conditions from the remotely sensed temperature/vegetation index measurements: An exploration with the simplified simple biosphere model. *Remote Sensing of Environment*, 79: 225-242.

Grassini, P., J. You, K. G. Hubbard, and K. G. Cassman, 2010. Soil water recharge in a semi-arid temperate climate of the Central U.S. Great Plains. *Agricultural Water Management*, 97: 1063-1069.

Gu, Y., E. Hunt, B. D. Wardlow, J. B. Basara, J. F. Brown, and J. P. Verdin, 2008. Evaluation of MODIS NDVI and NDWI for vegetation drought monitoring using Oklahoma Mesonet soil moisture data. *Geophysical Research Letters*, 35, L22401, doi:10.1029/2008GL035772.

Huete, A., K. Didan, T. Miura, E. P. Rodriguez, X. Gao, and L. G. Ferreira, 2002. Overview of the radiometric and biophysical performance of the MODIS vegetation indices. *Remote Sensing of Environment*, 83: 195−213.

Huete, A., R. D. Jackson, and D. F. Post, 1985. Spectral response of a plant canopy with different soil backgrounds. *Remote Sensing of Environment*, 17: 37-53.

Hunt, E. D., H. G. Hubbard, D. A. Wilhite, T. J. Arkebauer, and A. L. Dutcher, 2009. The development and evaluation of a soil moisture index. *International Journal of Climatology*, 29: 747–759.

Jackson, T., and T. Schmugge, 1989. Passive microwave remote sensing system for soil moisture: some supporting research. *IEEE Transactions on Geoscience and Remote Sensing*, 27: 225-235.

Jackson, T., J. Schmugge, and E. Engman, 1996. Remote sensing applications to hydrology: soil moisture. *Hydrological Sciences*, 41: 517-530.

Jiang, Z., A. Huete, K. Didan, and T. Miura, 2008. Development of a two-band enhanced vegetation index without a blue band. *Remote Sensing of Environment*, 112: 3833-3845.

Justice, C., J. Townshend, B. Holben, and C. Tucker, 1985. Analysis of the phenology of global vegetation using meteorological satellite data. *International Journal of Remote Sensing*, 68: 1271-1318.

Kaufman, Y. J., and D. Tanré, 1992. Atmospherically resistant vegetation index ARVI for EOS-MODIS. *IEEE Transactions on Geoscience and Remote Sensing*, 30: 261−270.

Kogan, F. N., 1995. Droughts of the late 1980s in the United States as derived from NOAA polar orbiting satellite data. *Bulletin of the American Meteorological Society*, 76: 655-668.

Korin, B.P., 1975. Statistical Concepts for the Social Sciences, Winthrop publishers, Inc., Cambridge.

Koster, R., P. Dirmeyer, Z. Guo, G. Bonan, E. Chan, P. Cox, C. Gordon, S. Kanae, E. Kowalczyk, D. Lawrence, P. Liu, C. Lu, S. Malyshev, B. McAvaney, K. Mitchell, D. Mocko, T. Oki, K. Oleson, A. Pitman, Y. Sud, C. Taylor, D. Verseghy, R. Vasic, Y. Xue, and T. Yamada, 2004. Regions of strong coupling between soil moisture and precipitation. *Science*, 305: 1138-1140, doi:10.1126/science.1100217.

Kranz, W. L., S. Irmak, S. J. Donk, C. D. Yonts, and D. L. Martin, 2008. Irrigation management for corn, NebGuide, Institute of Agriculture and Natural Resources, University of Nebraska-Lincoln Extension, G1850. Available online at: http://www.ianrpubs.unl.edu/epublic/live/g1850/build/g1850.pdf (accessed 14 September 2011).

Liu, H. Q., and A. Huete, 1995. A feedback based modification of the NDVI to minimize canopy background and atmospheric noise. *IEEE Transactions on Geoscience and Remote Sensing*, 33: 457-465.

Mintz, Y., 1984. The sensitivity of numerically simulated climates to land-surface boundary conditions. *In The Global Climate*, J. Houghton (Ed.), pp. 79-105 (Cambridge University Press).

Namias, J., 1989. Cold waters and hot summers. *Nature*, 338: 54-57.

Namias, J., 1991. Spring and summer 1988 drought over the contiguous United States – causes and prediction, *Journal of Climate*, 4: 54-65.

Narayan, U., V. Lakshmieni, and E. Njoku, 2004. Retrieval of soil moisture from passive and active L/S band sensor (PALS) observations during the soil moisture experiment in 2002 (SMEX02). *Remote Sensing of Environment*, 92: 483–496.

Nicholson, S., C. Tucker, and M. Ba, 1998. Desertification, drought, and surface vegetation: An example from the West African Sahel. *Bulletin of the American Meteorological Society*, 79: 815-829.

Njoku, E., W. Wilson, S. Yueh, S. Dinardo, F. Li, T. Jackson, V. Lakshmi, and J. Bolten, 2002. Observations of soil moisture using a passive and active low-frequency microwave airborne sensor during SGP99. *IEEE Transactions on Geoscience and Remote Sensing*, 40: 2659-2673.

Njoku, E., T. J. Jackson, V. Lakshmi, T. Chan, and S. Nghiem, 2003. Soil moisture retrieval from AMSR-E. *IEEE Transactions on Geoscience and Remote Sensing*, 41: 215-229.

Oglesby, R. J., and D. E. Erickson III, 1989. Soil moisture and the persistence of North American drought. *Journal of Climate*, 2: 1362-1380.

Peng, Y., A. A. Gitelson, G. Keydan, D. C. Rundquist, and W. Moses, 2011. Remote estimation of gross primary production in corn and support for a new paradigm based on total crop chlorophyll content. *Remote Sensing of Environment*, 115: 978-989.

Rao, P.V.N., L. Venkataratnam, P. V. K. Rao, K. V. Ramana, and M. N. Singarao, 1993. Relation between root zone soil moisture and normalized difference vegetation index of vegetated fields. *International Journal of Remote Sensing*, 4: 441-449.

Rouse, J. W., R. H. Haas Jr., J. A. Schell, and D. W. Deering, 1974. Monitoring vegetation systems in the Great Plains with ERTS, *in 3rd ERTS-1 Symposium*, vol. 1, NASA Spec. Publ. NASA SP-351, pp. 309-317.

Rundquist, D. C., R. Perk, B. Leavitt, G. P. Keydan, and A. A. Gitelson, 2004. Collecting spectral data over cropland vegetation using machine-positioning versus hand-positioning of the sensor. *Computers and Electronics in Agriculture*, 43: 173-178.

Sandholt, I., K. Rasmussen, and J. Andersen, 2002. A simple interpretation of the surface temperature/vegetation index space for assessment of surface moisture status. *Remote Sensing of Environment*, 79: 213-224.

Schmugge, T., P. O'neill, and J. Wang, 1986. Passive microwave soil moisture research. *IEEE Transactions on Geoscience and Remote Sensing*, 24: 12-22.

Schnur, M. T., H. Xie, and X. Wang, 2010. Estimating root zone soil moisture at distant sites using MODIS NDVI and EVI in a semi-arid region of south western USA. *Ecological Informatics*, 5: 400-409.

Shukla, J., and Y. Mintz, 1982. Influence of Land-Surface Evapotranspiration on the Earth's Climate. *Science*, 215: 1498-1501.

Suyker, A. E. and S. B. Verma, 2009. Evapotranspiration of irrigated and rainfed corn-soybean cropping systems. *Agricultural and Forest Meteorology*, 149: 443-452.

Tufekcioglu, A., J. W. Raich, T. M. Isenhart, and R. C. Schultz, 1999. Fine root dynamics, coarse root biomass, root distribution, and soil respiration in a multispecies riparian buffer in Central Iowa, USA. *Agroforestry Systems*, 44: 163-174.

USDA-NASS. 2007, United States Department of Agriculture-National Statistics Service-The Census of Agriculture: United States Summary and State Data. Available online at:

http://www.agcensus.usda.gov/Publications/2007/Full_Report/usv1.pdf (accessed 05 October 2011).

Venzke Filho, S. P., B. J. Feigl, M. C. Piccolo, L. Fante Jr., M. S. Neto, and C. C. Cerri, 2004. Root systems and soil microbial biomass under no-tillage system. *Scientia Agricola*, 61: 529-537.

Verstraeten, W. W., F. Veroustraete, M. Sande, I. Grootaers, and J. Feyen, 2006. Soil moisture retrieval using thermal inertia, determined with visible and thermal space borne data, validated for European forests. *Remote Sensing of Environment*, 101: 299-314.

Vina, A., A. A. Gitelson, A. Nguy-Robertson, and Y. Peng, 2011. Comparison of different vegetation indices for the remote assessment of green leaf area index of crops. *Remote Sensing of Environment*, doi:10.1016/j.rse.2011.08.010.

Wan, Z., P. Wang, and X. Li, 2004. Using MODIS Land Surface Temperature and Normalized Difference Vegetation Index products for monitoring drought in the southern Great Plains, USA. *International Journal of Remote Sensing*, 25: 61-72.

Wang, X., H. Xie, H. Guan, and X. Zhou, 2007. Different responses of MODIS-derived NDVI to root-zone soil moisture in semi-arid and humid regions. *Journal of Hydrology*, 340: 12– 24.

Waring, R., J. Way, E. R. Hunt, L. Morrissey, K. J. Ranson, J. F. Weishampel, R. Oren, and S. Franklin, 1995. Imaging radar for ecosystem studies. *BioScience*, 45: 715-723.

Western, A. W. and G. Bloschl 1999. On the spatial scaling of soil moisture. *Journal of Hydrology*, 217: 203-224.

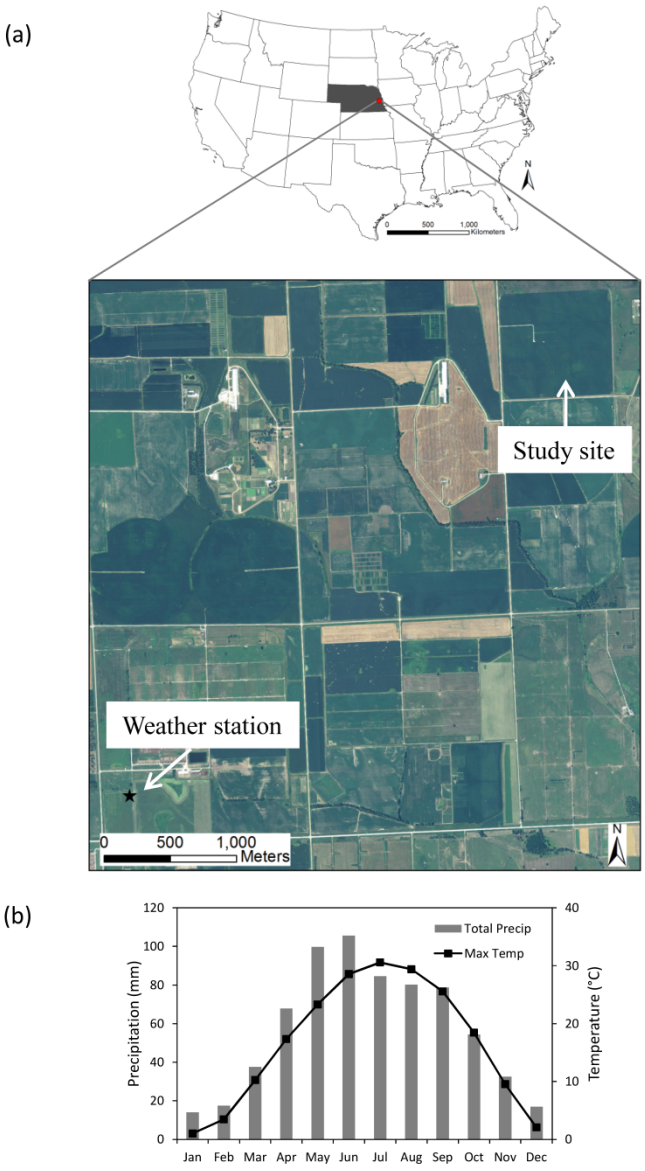

Figure 3.1. Location of study site at the University of Nebraska-Lincoln Agricultural Research and Development Center (a). The image is a segment of a natural color digital ortho quarter quad (DOQQ) taken in 2009. Average monthly total precipitation and maximum air temperature (between 1981 and 2010) as recorded at a nearby weather station (Source: High Plains Regional Climate Center, University of Nebraska-Lincoln) (b).

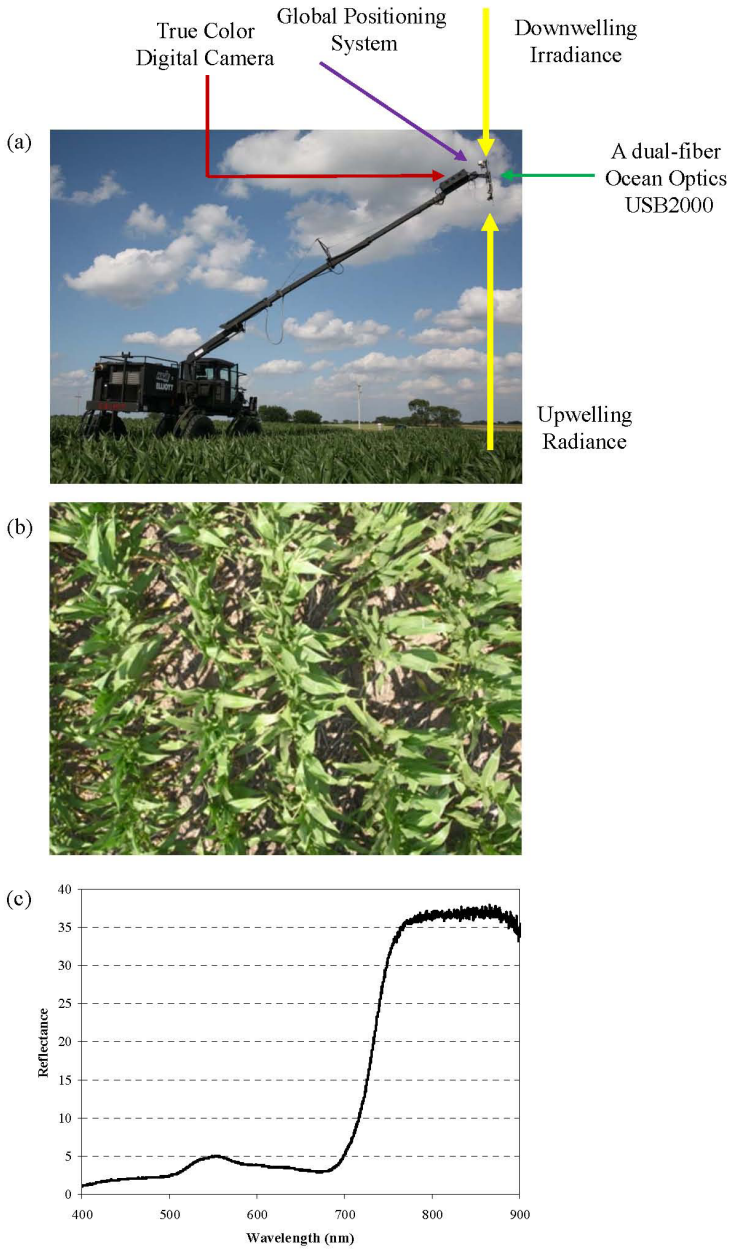

Figure 3.2. All-terrain sensor platform equipped with a dual-fiber Ocean Optics USB2000, a true color digital camera, and a global positioning system (a) A true color image, taken by the digital camera and the associated reflectance profile of a single Ocean Optics scan, made at a particular location within the field is shown in (b) and (c), respectively.

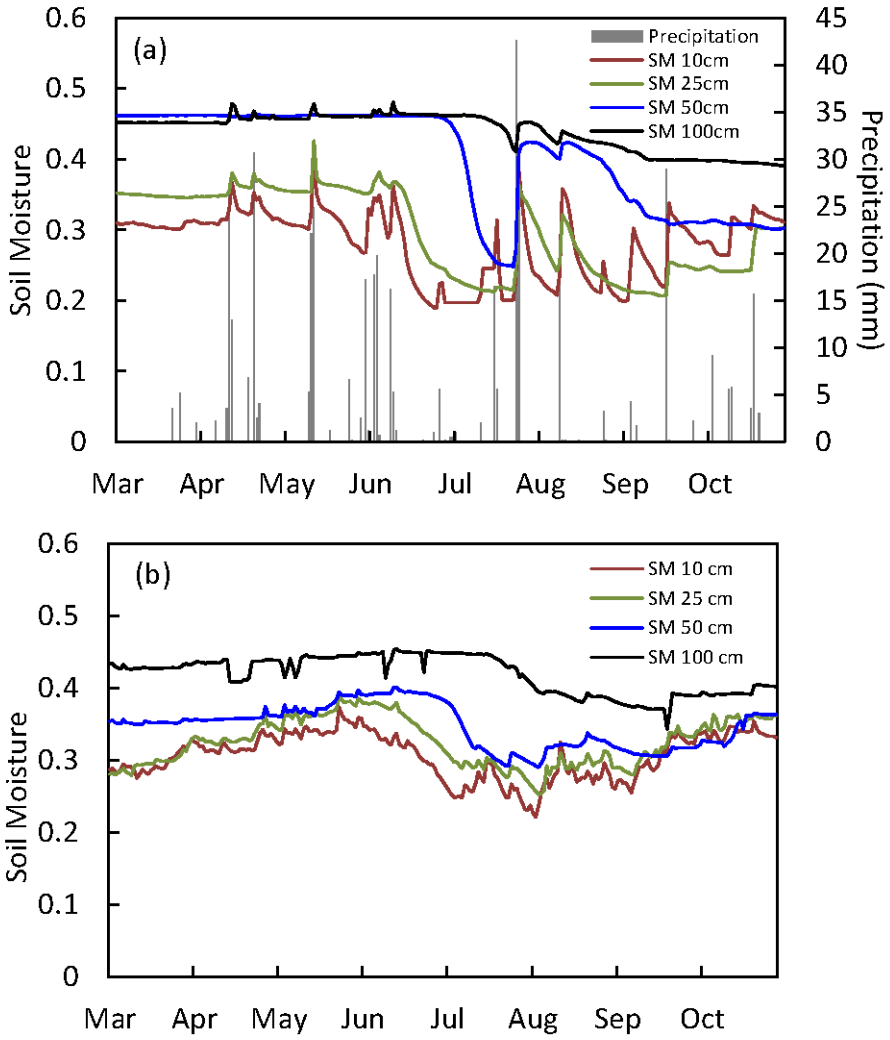

Figure 3.3. Daily time-series soil moisture as measured at the study site during March through October of 2005 and daily precipitation as recorded at a nearby weather station (a) and average daily time-series soil moisture from 2002 to 2008 measured at the study site (b). Soil moisture is the volumetric ratio of liquid water to soil and has no unit.

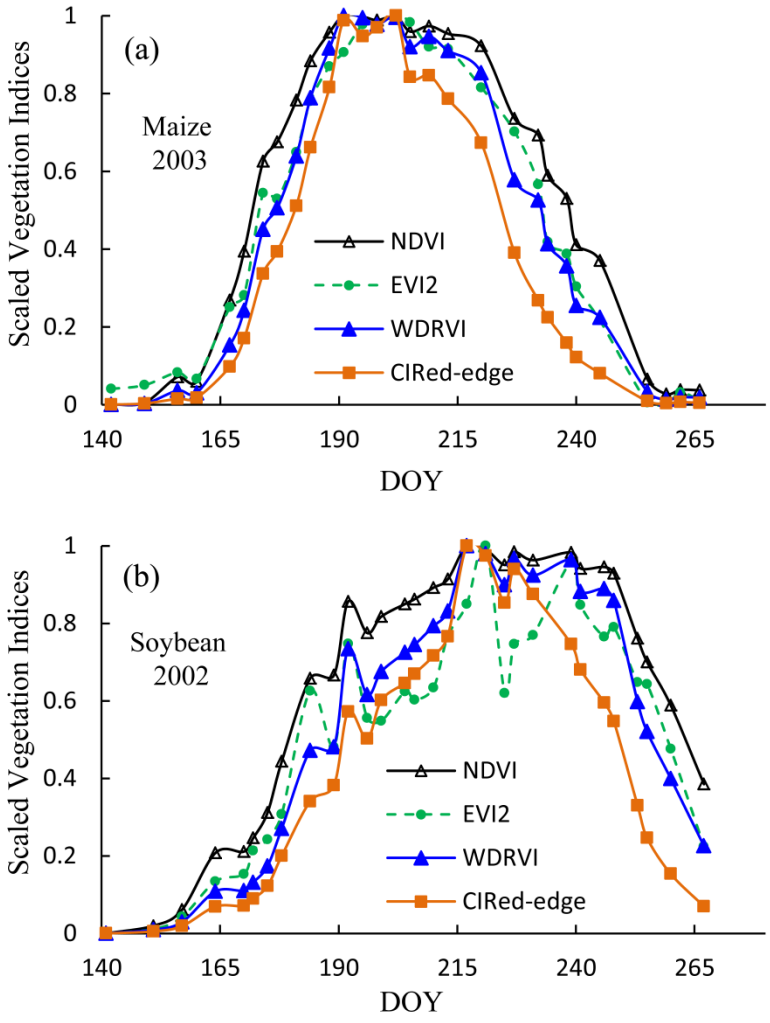

Figure 3.4. Temporal variations of scaled [(VI–VI_{min})/(VI_{max}–VI_{min})] vegetation indices (VI) for corn during the growing season of 2003 (a) and for soybean during the growing season of 2002 (b).

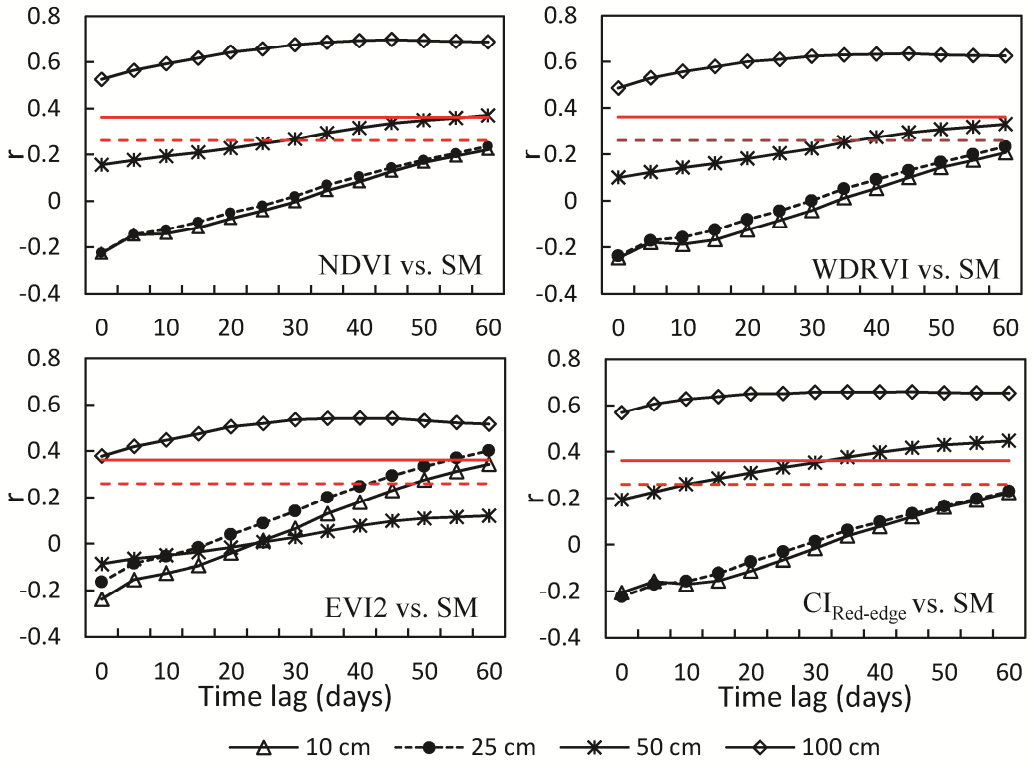

Figure 3.5. Correlation coefficient (r) between soil moisture (SM) at 10-, 25-, 50-, and 100-cm depths and corn vegetation indices with time lags up to 60-day during the growing season (mid-June through mid-September). The thresholds for r to reject the null hypotheses are 0.26 (P = 0.05, N = 40; broken red lines) and 0.36 (P = 0.01, N = 40; solid red lines).

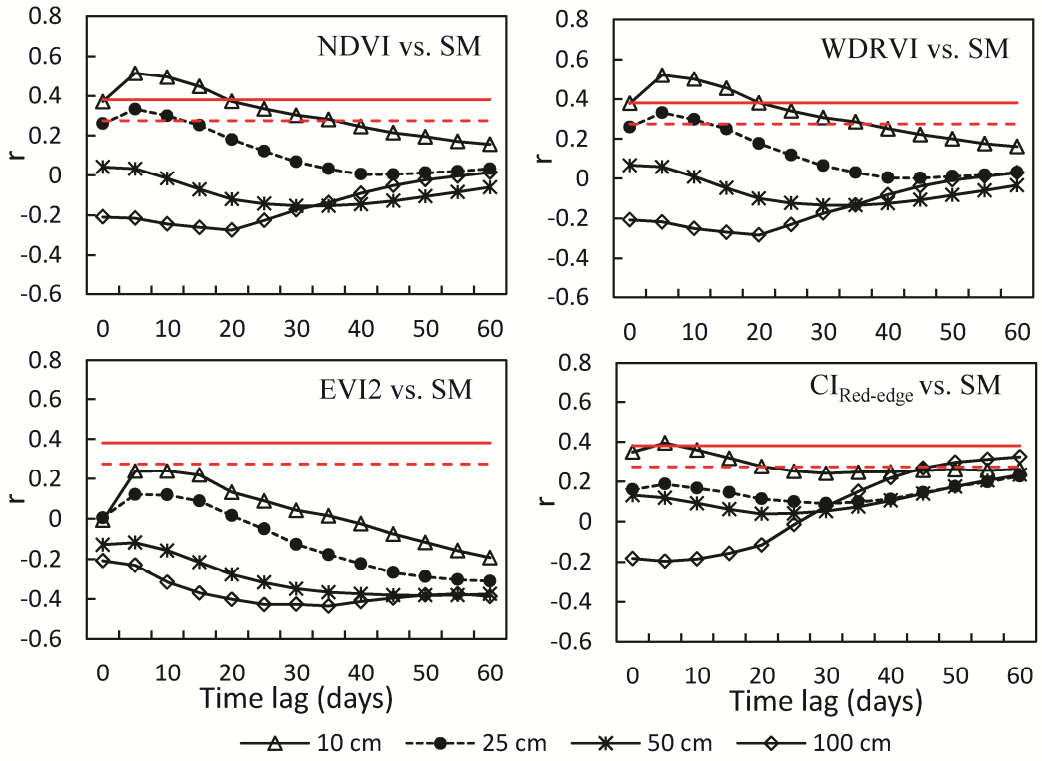

Figure 3.6. Correlation coefficient (r) between soil moisture (SM) at 10-, 25-, 50-, and 100-cm depths and soybean vegetation indices with time lags up to 60-day during the growing season (mid-June through mid-September). The thresholds for r to reject the null hypotheses are 0.2746 (P = 0.05, N = 36; broken red lines) and 0.381 (P = 0.01, N = 36; solid red lines).

CHAPTER 4

ASSESSMENT OF VEGETATION RESPONSE TO DROUGHT IN NEBRASKA USING TERRA-MODIS LAND SURFACE TEMPERATURE AND NORMALIZED DIFFERENCE VEGETATION INDEX

Abstract

The objective of this chapter is to investigate the changes in the spectral and thermal properties of cropland and grassland cover types to drought in Nebraska. Eight-day composite time-series Land Surface Temperature (LST) and Normalized Difference Vegetation Index (NDVI) time-series data derived by Terra-Moderate Resolution Imaging Spectroradiometer (MODIS) were analyzed to identify differences in the spectral and thermal responses of irrigated and non-irrigated crops and various grassland types during the growing season (mid-May through September) of a drought year (2002) and a non-drought year (2007). NDVI is responsive to changes in the amount of green biomass and chlorophyll in the vegetation canopy, while LST is sensitive to variations in available soil moisture and evapotranspiration rates contributing to overall vegetation growth and vigor. A total of 490, 1-km MODIS pixels that included irrigated and non-irrigated corn and soybeans and grassland cover types (sandhills upland prairie, little bluestem-grama mixedgrass prairie, and western short grass prairie) from three ecoregions were selected across the state of Nebraska. Statistical analyses revealed that a majority of the land cover pixels experienced significantly higher daytime and nighttime LSTs and lower NDVI during the drought year growing season ($P < 0.01$). Among the land cover types analyzed, grassland experienced the highest increase in daytime LST

and decrease in NDVI. The results indicate that LST combined with NDVI can assist in identifying and monitoring drought stress on crop and grassland cover types across the Central Great Plains of the U.S.A.

4.1. Introduction

Droughts are complex natural hazards that primarily develop because of the deficiency of precipitation over an extended period of time. Less than normal precipitation during the growing season can have profound impacts on the economy and environment through losses of agricultural production and natural resources (Kogan, 1997; Gu et al., 2007). Timely information about onset, magnitude, and duration of drought during a crop cycle is critical for mitigating economic and environmental impacts. Researchers have developed numerous drought indices to quantify the extent and intensity of drought. Most drought indices involve a single numerical value derived from a number of climatological or hydrologic variables and are often used in drought related decision-making processes (Wilhite et al., 2000). Traditional drought monitoring indices such as the Palmer Drought Severity Index (PDSI) (Palmer, 1965), Standardized Precipitation Index (SPI) (McKee et al., 1995), Crop Moisture Index (CMI) (Palmer, 1968), and Surface Water Supply Index (SWSI) (Shafer and Dezman, 1982) use point-based meteorological observations and regional hydrologic records. The accuracy of such approaches greatly depends on the data quality, location, and density of weather stations across the landscape (Kogan, 1997) and the use of spatial interpolation techniques (Mendelsohn et al., 2007).

Satellite-based remote sensing systems provide a spatially contiguous and temporally repetitive view of the earth surface, essential for monitoring short- and long-

term vegetation dynamics over large spatial units. During the past several decades, remotely sensed data have been used in plant biophysical and climate change–related studies, including drought monitoring (Ji and Peters, 2003; Bayarjargal et al., 2006). Numerous satellite-derived vegetation indices (VIs) have been designed to monitor vegetation conditions by quantifying foliage density and canopy properties within the field of view of the sensor. VIs are useful in the assessment of active photosynthesizing and transpiring vegetation and thus are related to composite canopy properties such as leaf area, fraction of vegetation cover, and total chlorophyll content (Glenn et al., 2007).

One of the most extensively used indices, the Normalized Difference Vegetation Index (NDVI), is based on the normalized difference between the absorption of radiation in red wavelengths by the chlorophyll pigments and the reflectance in the near infrared (NIR) in the spongy mesophyll layer within the leaf (Rouse et al., 1974; Tucker, 1979). NDVI values range from –1 to +1, with high values (closer to one) being associated with a greater level of photosynthetic activities. Since 1979, NDVI data derived from the Advanced Very High Resolution Radiometer (AVHRR) and more recently the Moderate Resolution Imaging Spectroradiometer (MODIS) have been widely used to monitor terrestrial vegetation health (Goward et al., 1985; Justice et al., 1985; Tucker et al., 1985; Kogan, 1997; Wang et al., 2001a; Ji and Peters, 2003; Wan et al., 2004); crop type mapping (Wardlow et al., 2007; Wardlow and Egbert, 2008), and crop phenology monitoring (Masialeti et al., 2010). The role of AVHRR- and MODIS-based NDVI in drought monitoring has been investigated extensively for a diversity of ecological settings. Ji and Peters (2003) found that the NDVI had significant relationships with the SPI, a precipitation-based drought index, for the croplands and grassland cover types in

the northern and central U.S. Great Plains. Wang et al. (2001a) found that spatial patterns of the NDVI exhibited significant relationships with an east-west gradient in precipitation for the grassland, cropland, and forest cover types in the central U.S. Great Plains. Several studies have been based on the normalization of time-series NDVI to emphasize the per-pixel relative changes in the NDVI over a long period of time. For example, Kogan (1995) computed the Vegetation Condition Index (VCI) on a pixel-by-pixel basis using average, minimum, and maximum NDVI of each pixel over a temporal composite period of interest. Relative Greenness (RG) was introduced by Burgan and Hartford (1993), which assigns a percentage value to the current NDVI observation in relation to the historical average NDVI for that pixel. Peters et al. (2002) developed the Standardized Vegetation Index (SVI) by quantifying the per-pixel deviation of the current NDVI from the "normal," computed from the historical NDVI data record. A normalization approach allows for a relative comparison for each given pixel over a temporal period, reducing the impact of spatial variability in NDVI phenology between different land cover types and climatic conditions (Karnieli et al., 2010).

Land Surface Temperature (LST) retrieved from remotely sensed thermal data (8 to 14 μm) represents surface skin temperature. LST is strongly influenced by evaporation and thus provides valuable information about surface soil moisture conditions (Anderson et al., 2007). Because of direct linkage with net radiation flux, LST is a good indicator of the energy balance at the earth's surface (Park et al., 2004; Wan et al., 2004). Remotely sensed LST has been used in estimating surface soil moisture (Feldhake et al., 1996; McVicar and Jupp, 1998), evapotranspiration (Granger, 2000; Anderson et al., 2007), surface vapor pressure deficit (VPD) (Hashimoto et al., 2008), and leaf water potential of

cotton plants (Cohen et al., 2005). Several indices have been developed by using satellite-derived LST observations. For example, Kogan (2001) proposed an AVHRR-based temperature condition index (TCI) by normalizing the pixel specific brightness temperature data over a long historical period. Anderson et al. (2007) developed an evaporative stress index (ESI) by using a model derived from potential and actual evapotranspiration from remotely sensed LST data.

VIs have often been integrated with LSTs to improve their effectiveness in detecting, quantifying, and monitoring drought stress on vegetation. While NDVI provides an assessment of the amount of vegetation present in a pixel, LST provides information about the surface moisture status. Studies suggest that NDVI has a delayed response to precipitation or soil moisture deficit, which means that initial deficiency in soil moisture is not apparent in the NDVI signals (Di et al., 1994; Rundquist and Harrington, 2000; Wang et al., 2001a). Conversely, the vegetated surface temperature has greater sensitivity to initial water stress (Goetz, 1997). However, amount of vegetation present in a pixel is critical for accurate estimation of surface temperature (Sandholt et al., 2002). The complementary information provided by these visible, near infrared, and thermal wave bands has been the focus of many vegetation water stress studies. Kogan (2002) developed the AVHRR-based Vegetation Health Index (VHI) by combining the Vegetation Condition Index (VCI) and Temperature Condition Index (TCI). The VHI was successfully applied globally for drought assessment in parts of Asia, Africa, Europe, and the Americas. McVicar and Bierwirth (2001) used the ratio of AVHRR-derived NDVI and brightness temperature to assess drought conditions in the cloudy environment of Papua New Guinea and reported that the ratio remained higher during the drought

period compared to the non-drought period. Trapezoid (Moran et al., 1994) or triangle (Price, 1990; Carlson et al., 1994; Sandholt et al., 2002) methods were developed from the scatter plots of LST and NDVI on a pixel-by-pixel basis to quantitatively extract information related to surface moisture conditions. Wang et al. (2001b) developed the Vegetation Temperature Condition Index (VTCI) using AVHRR-derived LST and NDVI scatter plots to identify spatial distribution of drought in Northwest China. Subsequently, Wan et al. (2004) applied VTCI derived from Terra-MODIS LST and NDVI for monitoring drought stress across the Great Plains of the United States.

Previous studies that investigated vegetation response to drought or climatic variables such as precipitation and temperature in the Great Plains of the United States and other parts of the world focused on broad spatial scales (e.g., the climate division level; Ji and Peters, 2003) or general land cover types (e.g., cropland, grassland, and forest cover types; Wang et al., 2001a; croplands and grasslands, Wan et al., 2004). Most of these studies used AVHRR-derived long-term brightness temperature or NDVI observations with an assumption that no changes in land cover/crop types or management practices (irrigated/non-irrigated) occurred during that temporal period (Kogan, 2001; Ji and Peters, 2003, Wang et al., 2001a).

In this study, we conducted an in-depth analysis of the responses of irrigated and non-irrigated corn and soybeans and three grassland cover types (sandhills upland prairie, little bluestem-grama mixed grass prairie, and western shortgrass prairie) to drought stress in Nebraska. The eight-day composite NDVI and thermal signals were extracted for the pixels representing the aforementioned land cover types during the growing seasons (mid-May through September) of a drought (2002) and a non-drought (2007) year.

Cumulative LST and NDVI values were computed and compared for both years. Specifically, this research addressed the following two research questions pertaining to drought stress on vegetation. Are there any differences in the daytime and nighttime LST and NDVI of irrigated and non-irrigated croplands and grasslands between the drought and non-drought years? Are croplands and grasslands distinct in their response to drought stress?

4.2. Study Area

The state of Nebraska in the United States covers an area of about 200 thousand km^2. It is situated approximately between 95°25' W and 104° W Longitudes and between 40° N and 43° N Latitudes and constitutes a part of the Central Great Plains region of North America. The physiography is characterized by minor topographic variations, with gentle, undulating landscapes. Being landlocked, the state experiences a temperate continental climate with sharp seasonal variations in temperature and precipitation. The average annual precipitation shows a strong east-west gradient with an increasing trend from northwest (330 mm) to southeast (889 mm) (HPRCC, 2010). Average annual maximum air temperatures range between 29° C and 34° C; maximum air temperatures above 32° C are primarily experienced in the southern parts of the state and in some isolated pockets in the Panhandle region (GDG, 2010). Nebraska is divided into eight climate divisions (CDs) defined by National Climatic Data Center (NCDC), which represent relatively homogenous climatic regions based on uniformity in temperature and precipitation regime (Figure 4.1) (Guttman and Quayle, 1996).

Nebraska has an agriculture- and rangeland-based economy, with a landscape dominated by a mosaic of grassland and cropland. Grasslands constitute about 54% (10.9

million ha) of the state's land cover and range from tall grass in the east to mixed and short grass toward the west (Henebry et al., 2008). Precipitation is the primary driving factor for the east-west distribution of these grassland cover types. Mean annual precipitation ranges from 762 to 1016 mm from the eastern side of the tallgrass prairie to 305 to 508 mm in the shortgrass prairie, with a major proportion of precipitation falling in the growing season between April and October (Tunnell, 2004). Tall grasses in eastern Nebraska include big bluestem (*Andropogon gerardii*), little bluestem (*Schizachyrium scoparium*), Indiangrass (*Sorghastrum nutans*), and switchgrass (*Panicum virgatum*), whereas the shortgrass prairie in the western Nebraska is composed of blue grama (*Bouteloua gracilis*) and buffalograss (*Bouteloua dactyloides*).

Croplands constitute approximately 39% (7.9 million ha) of the state's total area and are primarily located in the southern, southwestern, and eastern one-half of the state (Henebry et al., 2008). Corn (*Zea mays*) and soybeans (*Glycine max*) are the major crops grown in the state, and the other minor crops include winter wheat (*Triticum aestivum*), sorghum (*Sorghum bicolor*), and alfalfa (*Medicago sativa*). Over the past decade, Nebraska has consistently remained among the top five states in corn production and among the top ten states in soybean production (USDA, 2002). Specific cropping pattern and management practices are strongly influenced by the amount of precipitation received during the major crop growing season and vary widely across the state. Because of a favorable precipitation regime, non-irrigated corn and soybeans thrive in the eastern part of the state. In contrast, the majority of crops in the much drier western and central Nebraska are irrigated from both surface and ground water sources. In this part of the state, center pivot irrigation is the primary delivery system being used, accounting for

approximately two-thirds of the state's total irrigated land base (Johnson, 2001). Irrigation water is primarily pumped from the Ogallala Formation of the High Plains Aquifer. Extensive use of irrigated water for crop production led to the declining water table of the aquifer over the years, making less water available for farmers, especially during drought periods.

4.3. Materials and Methods

4.3.1 Selection of Temporal Study Periods

In this study, the 2002 and 2007 growing seasons (mid-May through September) were selected to represent the drought year and the non-drought year, respectively. Selection of drought and non-drought years was primarily based on the weekly U.S. Drought Monitor (USDM) maps [http://drought.unl.edu/DM/MONITOR.html], which display the magnitude and spatial extent of drought with associated impacts on agriculture and hydrology across the United States (Svoboda et al., 2002) and weekly CMI maps (USDA, 2007b). In 2002, the USDM maps indicated that in the early phase of the growing season (June 11, 2002), extreme drought conditions were experienced in the Panhandle region of Nebraska. Moderate to severe drought conditions were shown toward the east, with about one-half the total area of the state under moderate to extreme drought categories. The subsequent series of weekly USDM maps indicated that the drought conditions continued to geographically expand and intensify as the growing season progressed. By July 30, 2002, the USDM map showed that the entire state was under moderate to exceptional drought, with approximately 98% of Nebraska's total area under extreme, exceptional, and severe categories of drought (Figure 4.2a). In contrast, on June 12, 2007, about 14% of the state (in the Panhandle CD) was under moderate to

severe drought conditions. By July 31, 2007, the USDM map showed approximately 9% of the total area of the state, which was confined to the northern Panhandle CD, to be under severe drought (Figure 4.2b).

The CMI maps were computed based on the mean temperature and total precipitation for each week within a CD together with the CMI value from the previous week. The CMI is an indicator of short-term moisture conditions in the plant root zone necessary for crop growth (Hayes, 2003). In 2002, the weekly CMI values indicated moisture deficiency in the topsoil to extreme dry conditions throughout the growing season for all CDs across Nebraska. Conversely, during 2007 all the CDs with the exception of the Panhandle experienced CMI values indicative of adequate to above normal moisture conditions throughout the growing season (Figure 4.3) (USDA, 2007b).

4.3.2 Remote Sensing Data

Terra-MODIS eight-day composite LST (MOD11A2, collection 5) and surface reflectance (MOD09Q1, collection 5) products spanning the 2002 and 2007 growing season periods (May 15 through September 28) covering Nebraska (tile h10v04) were used in this study. These data sets were acquired from the United States Geological Survey (USGS) Center for Earth Resources Observation and Science (EROS), Sioux Falls, South Dakota. The calibration, atmospheric correction for the effect of gaseous absorption, molecules, and aerosol scattering, coupling between atmospheric and surface bi-directional reflectance function (BRDF) and adjacency effect (Vermote et al., 2002) and comparatively high sub-pixel geolocational accuracy (~50 m (1σ) at nadir) (Wolfe et al., 2002) of MODIS data allow regular monitoring of vegetation dynamics over large areas. The eight-day time period provides dense temporal coverage to monitor

phenological changes in sufficient detail, eliminating short-term (daily) fluctuations and representing a period that allows plants to acclimatize to the surrounding surface air temperature and root-zone soil moisture conditions. The other advantages include relatively low data volume compared to the daily observations and reduced cloud contamination due to the temporal compositing technique that was used.

MOD11A2 is an eight-day composite, 1-km spatial resolution LST product comprising two bands representing day and night LST observations. The Terra-MODIS day local overpass time is between 1000 and 1100 h while the night overpass time is between 2200 and 2300 h. The eight-day composite LST was produced by using the average values of clear-sky LSTs during the corresponding eight-day period (Wan et al., 2002). A total of 72 images (36 daytime and 36 nighttime LST images) covering the growing seasons of 2002 and 2007 were re-projected from the Sinusoidal to Lambert Azimuthal Equal-Area (LAEA) and sequentially stacked to generate time-series 18-date time-series LST data for each year.

The surface reflectance product (MOD09Q1) contains red and near infrared reflectance data with a spatial resolution of 250 m. Each pixel contains the best possible reflectance value during an eight-day period based on high observation coverage, low view angle, the absence of clouds or cloud shadow, and aerosol loading (Vermote and Kotchenova, 2008). The data sets were re-projected from the Sinusoidal to LAEA and resampled to 1 km to match the spatial resolution of the MODIS LST images. For each eight-day time period, NDVI images were created using the following equation:

$$NDVI = (\rho NIR - \rho Red) / (\rho NIR + \rho Red) \quad (4.1)$$

where ρNIR (841–876 nm) and ρRed (620–670 nm) are the surface reflectance values received by the Terra-MODIS sensor.

A total of 36 NDVI images over the 2002 and 2007 growing seasons were sequentially stacked to produce an 18-date time-series data set for each growing season.

4.3.3 Selection of Land Cover Pixels

Cropland Data Layer (CDL) maps for Nebraska prepared by the USDA National Agricultural Statistics Service (NASS) for the 2002 and 2007 study years were used to locate land cover pixels representing cropland and grassland. The 2002 CDL was produced by using multi-date, multi-spectral Thematic Mapper (TM) and Enhanced Thematic Mapper (ETM+) instruments on Landsat 5 and 7, respectively, that have a ground resolution of 30 m. The 2007 CDL map was prepared by using multi-date, multi-spectral Advanced Wide Field Sensor (AWiFS) imagery with a ground resolution of 56 m (USDA, 2007a). In order to relate these data sets to 1-km MODIS data, a shape file comprising 1 km2 polygons was created in GIS, where each 1-km polygon corresponded to one pixel in LST and NDVI (resampled to 1 km) images. The polygon layer was then superimposed on the CDL layers and the area of each crop/cover type for both study years within every 1-km cell was tabulated and the percentage of each crop/cover type within each polygon was calculated.

4.3.3.1 Cropland Pixels

In all, 335 cropland pixels (303 corn and 32 soybeans) with more than 85% of the pixel area devoted to the same crop type during both years were selected. The threshold of 85% was chosen for identification of relatively homogenous pixels that would minimize the effect of other targets present in the pixel from the crop reflectance and

thermal signals. Selection of pixels that had the same crop type during both years was based on the rationale that the multi-temporal spectral and thermal signatures of the same crop would follow a similar seasonal pattern because of their similar planting dates, canopy structure and architecture, and other biophysical properties such as leaf area index (LAI). Any divergence between the two growing seasons might be attributed to drought-related stress. A 30-m spatial resolution land use map of Nebraska, prepared by the Center for Advanced Land Management Information Technologies (CALMIT), was used for further classifying the selected cropland pixels into irrigated and non-irrigated classes (Dappen et al., 2007). The fraction of irrigated and non-irrigated land within each of the selected cropland pixels was calculated. An individual pixel was designated as irrigated (or non-irrigated) if more than 85% of the 1-km area was classified as irrigated (or non-irrigated). Among the total cropland pixels, 18 (12 corn and 6 soybeans) were classified as non-irrigated and 144 pixels (138 corn and 6 soybeans) were classified as irrigated. The cropland pixels that were below the threshold (85% irrigated/non-irrigated) were discarded. Figure 4.4 presents the location of these pixels in various CDs of Nebraska. Spatial distribution of irrigated cropland pixels indicates that irrigated cropland is primarily located in the East-Central, Central, and Northeast CDs, and non-irrigated cropland pixels were mostly confined to the Northeast and East-Central CDs. From the CDL image maps of Nebraska for both years it can be observed that the individual field sizes of non-irrigated croplands located in central and western parts of the state are generally smaller than those of 1 km pixel size areas. A single 1-km MODIS pixel can encompass six or more individual farms, and the possibility of the same crop being grown

in all these fields in both the studied years is remote. Smaller sample sizes for non-irrigated corn and soybeans were chosen for this reason.

4.3.3.2 Grassland Pixels

In comparison to cropland, anthropogenic influence on grassland is minimal and the grassland species are less susceptible to change from year to year in a given region. Tabulation of the grassland area within each 1 km grid (method described in the first paragraph of this section) indicates that approximately 4,679 pixels contained more than 95% grassland cover type during both study years. A higher threshold was adopted for grassland pixels compared to corn, as relatively continuous expanses of grassland in Nebraska provided the possibility of finding more homogenous pixels. In the NASS CDL data layer, all the grassland cover types are identified as one thematic class: "Pasture/Range/CRP/Non Ag." In order to identify the dominant grassland cover type, a Gap Analysis Program (GAP) land cover image map of Nebraska was used (Henebry et al., 2008). Area and fraction of each grassland cover type within the selected 4,679 grassland pixels were calculated using the same method described earlier in this section. A threshold of 95% was again used to classify those grassland pixels (n = 4,679) into various grassland cover types as depicted in the GAP land cover image map, and the pixels that did not meet the threshold were discarded. Among those qualified pixels, 328 were randomly selected to represent sandhills upland prairie (hereafter sandhills upland; 160 pixels), little bluestem grama mixed-grass prairie (hereafter little bluestem; 71 pixels), and western shortgrass prairie (hereafter western shortgrass; 97 pixels) land cover categories. The dominant grassland species in the sandhills upland cover type are sand

bluestem and prairie sandreed. The little bluestem cover type is primarily composed of grass species such as little bluestem and sideoats grama. The prominent grass species in the western short grass cover type is blue grama. All these species are native perennial warm-season grasses that grow rapidly in late spring and remain green through the hot summer until the first killing frost, and the flowering seasons extend from July through September (Stubbendieck and Kottas, 2005).

4.3.4 Extraction of Time-Series Data

The selected crop and grassland pixels were geolocated on the MODIS imagery and the time-series daytime LST, nighttime LST, and NDVI data for the 2002 and 2007 growing seasons were extracted. The LST and NDVI values were sequentially integrated from the beginning of the growing season (day of year [DOY] 137) to the end (DOY 273) to obtain the cumulative LST and NDVI values for each eight-day composite period.

4.3.5 Data Analysis

4.3.5.1 Matched-Pair t-tests

Matched-pair t-tests (Dowdy et al., 2004) were performed to quantitatively compare the drought and non-drought cumulative time-series LST and NDVI observations for each land cover pixel. During a drought year, less than normal precipitation over the growing season leads to less water being available for the plants to use. In order to reduce the loss of water through evapotranspiration, stomatal pores in most plants close down partially or fully. This physiological change in the plants reduces the partitioning of the incident net radiation into latent heat flux and increases the sensible heat flux, which elevates the surface temperature of the vegetation. Based on this principle, we hypothesize that during the drought year the Terra-MODIS–derived

cumulative daytime and nighttime LST for the selected land cover types will be significantly higher than their corresponding non–drought year observations. Because the drought period is associated with less vegetation growth, we hypothesize that the cumulative NDVI observations of these cover types during the drought year will be significantly lower than the corresponding non-drought observations. Specifically, the following three alternative hypotheses were tested for each of the 490 land cover pixels and the p-values of 0.05 and 0.01 were used to reject the null hypotheses.

H_1: Terra-MODIS–derived cumulative daytime LST observations during the drought year (2002) were higher than those of the non-drought year (2007).

H_2: Terra-MODIS–derived cumulative nighttime LST observations during the drought year (2002) were higher than those of the non-drought year (2007).

H_3: Terra-MODIS–derived cumulative NDVI observations during the drought year (2002) were lower than those of the non-drought year (2007).

The test statistic was computed as:

$$t = \frac{\bar{y}_d - \mu_{d_0}}{S_d / \sqrt{n}} \tag{4.2}$$

where d is the difference between the pairs, y_d is the mean of the paired differences, μ_{d0} is the hypothesized difference between means which is zero, n is the number of pairs of data, and S_d is the standard deviation of the difference for paired sample data.

4.3.5.2 Correlation and Bivariate Linear Regression Analysis

To analyze the magnitude of drought-induced changes in cumulative LST and NDVI for the selected land cover types, four clusters of land cover pixels located in

different parts of Nebraska were selected (Figure 4.4). These clusters represented sandhills upland (number of pixels n = 55), little bluestem (n = 29), irrigated corn (n = 61), and non-irrigated corn (n = 6). Western shortgrass cover types located in northwestern Nebraska were excluded from this analysis because USDM maps (Figure 4.2) and CD-based CMI data (Figure 4.3) indicated dry conditions in this part of the state during the growing season of 2007. Our pixel based t-test analyses of LST and NDVI also indicated similar spatial patterns (see the results and discussion section). Because of smaller sample sizes and wide-area distribution, irrigated and non-irrigated soybeans cover types were not included in this analysis. The land cover–specific mean cumulative LST (MCL) and NDVI (MCN) for each eight-day composite period during the 2002 and 2007 growing seasons were computed by averaging the respective cumulative LST and NDVI values obtained for all the pixels within the land cover cluster. MCLs and MCNs obtained during 2007 were subtracted from those of 2002 to derive the MCL and MCN differences. The Pearson Product Moment Correlation (Korin, 1975) and bivariate least square regression model (Dowdy et al., 2004) were used to analyze the relationship between the MCL and MCN for the four land cover types.

4.4. Results and Discussion

4.4.1 Time-series LST and NDVI Profiles

Time-series LST and NDVI observations of irrigated croplands, non-irrigated croplands, and grassland pixels were plotted to analyze their temporal dynamics across the growing seasons of the drought and non-drought years. Figure 4.5 presents the temporal profiles of three pixels, representing irrigated corn (Central CD), non-irrigated corn (Northeast CD), and little bluestem (Southwest CD) cover types. Although the

example is limited to one pixel (for each cover type), the temporal behavior of LST and NDVI exhibited by these pixels across both growing seasons was fairly representative for other pixels of the same cover type.

LST and NDVI profiles of irrigated corn (Figure 4.5a) indicated that during the early growing season between DOYs 136 and 168, the daytime LSTs for the drought year were higher than those of non-drought year (except for DOY 136). The nearest weather station located within 8 km indicated that a total of 49 mm of precipitation was received during the preceding 15-day period of DOY 136 in the drought year compared to 57 mm received during the same period in the non-drought year. The observed higher LST on DOY 136 for the non-drought year could be attributed to the differences in the timing and amount of irrigation water applied during both years. NDVI during this period showed an increasing trend from 0.24 to 0.84 during the non-drought year and from 0.24 to 0.6 during the drought year, indicating the green-up and canopy development phase of crop cycle. Except for DOY 152, NDVI observations during the non-drought year were higher than those of drought year. DOY 176 through 224 represent the vegetative and reproductive stages of the corn plant growth cycle. During this period the daytime LST observations in the drought year were primarily higher than those of non-drought year. The observed higher LSTs could be the result of limited water availability and consequent reduced transpiration rates (Nemani et al., 1993; McVicar and Jupp, 1998). During this period the nighttime LST values did not exhibit any trend. NDVI values during this period ranged between 0.66 and 0.83 in the drought year and between 0.87 and 0.91 in the non-drought year. From DOY 232 to 272 (i.e., the maturation and subsequent senescence stage of corn) both daytime and nighttime LST values during the

non-drought year were primarily higher than those of the drought year. The NDVI values during this period showed decreasing trends, and lower NDVI values were experienced during the drought year compared to the non-drought year.

LST and NDVI profile of non-irrigated corn (Figure 4.5b) indicated that during the green-up stage between DOY 136 and 168, the daytime LSTs during the drought year were primarily higher than those of the non-drought year. NDVI values increased consistently from 0.23 to 0.59 during the non-drought year and from 0.23 to 0.57 during the drought year. Between DOYs 176 and 224, both daytime and nighttime LST observations were primarily higher and the NDVI values lower during the drought year than their corresponding non-drought observations. During this period, the daytime LST observations in the drought year were up to 7.4° C warmer (DOY 176) and nighttime LST values were up to 5.2° C (DOY 208) warmer than the corresponding non-drought observations.

Time-series daytime LST of little bluestem grassland cover type during the drought year shows a gradual increasing trend from 29° C (DOY 136) to 49° C (DOY 208) and then a decreasing trend up to 28° C (DOY 264) (Figure 4.5c). During June and July (DOY 152 through 208), which denotes the peak “greenness” period, daytime LST observations during the drought year were considerably higher than their corresponding non-drought observations. On DOY 176 and 208, the drought year LST was 6° C and 20° C higher, respectively. This suggests that among the three cover types, grassland experienced the highest daytime temperature increase during the drought year as compared to the non-drought year. The NDVI values during the drought-year growing season were consistently lower than those of the non-drought year, with a mean

difference of about 0.3 units for the entire growing season and 0.4 units during the peak "greenness" period.

4.4.2 Matched-pair t-tests

Matched-pair t-test results of H_1 (mentioned in the data analysis section) indicate that 412 (84%) of the land cover pixels experienced significantly higher cumulative daytime LST ($P < 0.01$) during the drought-year growing season (Figure 4.6a). Among the cropland cover types, about 96% of the irrigated corn, 83% of the irrigated soybeans, and all the non-irrigated corn and soybeans pixels experienced significantly higher cumulative daytime LST during the drought-year growing season ($P < 0.01$). Among the three grassland cover types, the cumulative LST observations of all little bluestem pixels, 97% of sandhills upland pixels, and 31% of western shortgrass pixels during the drought year were significantly higher than those of the non-drought year at $P < 0.01$. Spatial distribution of pixels indicated that land cover pixels that experienced significantly higher daytime LST during the drought year were distributed in all the CDs of Nebraska, and the non-significant pixels were primarily confined to the western shortgrass prairie cover type in the extreme northwestern part of the Panhandle CD.

The results of H_2 show that about 61% of the total land cover pixels experienced significantly higher nighttime LST during the growing season of the drought year at $P < 0.01$. About 4% of the total land cover pixels experienced significantly higher nighttime LST, with P values ranging between 0.05 and 0.01 (Figure 4.6b). This result suggests that during drought a greater number of pixels exhibited significantly higher daytime LST compared to those with significantly higher nighttime LST. The spatial pattern showed that 85% of the western shortgrass pixels primarily located in the northern Panhandle and

northwestern corner of the North Central CD did not experience significantly higher nighttime LST. Among the cropland pixels, the non-significant pixels are scattered in the eastern half of the state.

The results of H_3 show that about 85% of the total land cover pixels experienced significantly lower NDVI during the drought year compared to the non-drought year at $P < 0.01$ (Figure 4.6c). Among the cropland cover types, 68% of the irrigated corn, 92% of the non-irrigated corn, and the majority of the non-irrigated soybeans pixels recorded significant decreases in NDVI during the drought year at $P < 0.01$. This indicates that the rate of decrease in NDVI of irrigated corn during drought is less pronounced than the rate of increase in LST during the drought year growing season. Among the grassland pixels, all little bluestem pixels, 99% of sandhills upland, and 80% of western shortgrass pixels showed significantly lower NDVI during the growing season of the drought year.

Overall, the results of t-tests indicated that the majority of the land cover pixels, with the exception of western shortgrass pixels in the northern Panhandle, experienced significantly higher daytime LST during the drought year. Compared to the daytime LST, fewer pixels experienced significantly higher nighttime LST in the drought year. These non-significant pixels belonged to western shortgrass pixels located primarily in northern Panhandle, sandhill upland pixels in the northwestern corner of the North Central CD, and irrigated and non-irrigated corn and soybeans pixels located primarily in the Central and South Central CDs. The location of non-significant pixels (daytime and nighttime LST) in the northern Panhandle matched well with the area of persistent severe drought depicted on the series of USDM maps throughout the growing season of 2007 (for example, see Figure 4.2b). A large proportion of the irrigated corn pixels selected from

two counties (Hall and Buffalo) located in the southern part of the Central CD showed significantly higher day and nighttime LST and lower NDVI during drought. This is reflected in significant losses in irrigated corn production in this region. For example, the yields of irrigated corn in Buffalo County (165 bushels in 2002 compared to 191 bushels in 2007) and Hall County (172 bushels in 2002 compared to 190 bushels in 2007) were the lowest and second-lowest, respectively, in 2002 over the past decade (2000 to 2009) (USDA, 2002).

4.4.3 Response of Land Covers to Drought

Figure 4.7 shows the time-series MCL and MCN differences across the growing season for four land cover clusters. Based on the weekly USDM maps, the three land cover clusters representing little bluestem, sandhill upland, and irrigated corn (which primarily experienced similar drought stress throughout the growing season of the drought year) were chosen. These pixels experienced moderate to severe drought until mid-June, severe to extreme drought from mid-June through Mid-July, and then extreme to exceptional drought through the end of the growing season during the drought year. In contrast, those clusters were under near-normal (non-drought) conditions throughout the 2007 growing season. Compared to the three cover types in central and western Nebraska, drought stress on non-irrigated corn pixels selected from the Northeast CD was less severe throughout the 2002 growing season, but the drought severity experienced in this CD during this year was still maximum compared to those in the past decade (based on the weekly USDM maps from 2000 to 2009). In 2002, parts of the Northeast CD experienced abnormally dry conditions in May and June. The drought conditions further intensified and by the end of July the CD was primarily under the severe to extreme

drought categories. In 2007, the CD was primarily under near-normal conditions except for some temporary abnormally dry and moderate drought conditions experienced in the eastern part of the CD. Overall, the drought conditions for all land cover clusters were milder at the beginning of the growing season and gradually intensified as the growing season progressed. This is evident from our results, which indicate increasing trends in MCL difference over the growing season for all cover types (Figure 4.7a). Among the four land cover types, the cumulative LST difference for little bluestem increased up to 116° C (DOY 257), followed by sandhills upland with an increase up to 73° C (DOY 248). The cumulative difference of irrigated corn exhibited a minimum increase (up to 32° C on DOY 257). The majority (93%) of the time-series MCL differences were statistically significant with $P < 0.01$. Similarly, the MCN difference showed decreasing trends for all land cover types except irrigated corn, which showed an initial decrease followed by an increasing trend over the growing season (Figure 4.7b). This may suggest that the impact of progressive drought intensity on irrigated corn NDVI is not as evident as on the rest of the land cover types analyzed in this study. Increase in the amount and frequency of irrigated water applications in response to the extreme and exceptional drought conditions experienced in this region could be one possible factor for these lower MCN differences across the growing season. Little bluestem exhibited near linear decrease in MCN differences (up to –3.9 units on DOY 273), followed by sandhills upland (up to –1.8 units on DOY 273).

The results of time-series regression and correlation analyses between drought and non-drought differences in MCL and MCN for the four land cover clusters are shown in Figure 4.8. Several studies have reported a negative correlation between LST and

NDVI in the mid-summer months over the central Great Plains (Goetz, 1997; Sun and Kafatos, 2007; Karnieli et al., 2010). In this study, we observed strong negative relationships between MCL and MCN differences between drought and non-drought years at the growing-season scale for all land cover types, with Pearson correlation coefficients (r) ranging between –0.78 for irrigated corn to –0.99 for the little bluestem cover type. Correlation coefficients for all four land cover types are statistically significant at $P < .001$. In the water-limiting (as opposed to energy-limiting) environment, as is observed during the warmer summer months in the central Great Plains, the magnitude of the negative relationship between LST and NDVI is primarily controlled by the availability of soil water. The irrigated corn was less moisture stressed during drought based on the smaller range of MCL and MCN differences between the drought and normal years compared to the other rainfed land cover types. Although statistically significant, the irrigated corn data points display much more scatter from the regression line than the non-irrigated corn and the two grassland cover types. This suggests that the linear association between LST and NDVI is weaker for irrigated cropland compared to other land cover types. This is consistent with the work of Karnieli et al. (2010), who observed less significant correlations between LST and NDVI in the irrigated areas of the Mississippi River basin. In the case of non-irrigated corn, the range of MCL and MCN differences was higher than those of irrigated corn, but markedly lower than those of the two grassland cover types. This could be due to the less severe drought stress experienced in the Northeast CD in comparison to the North-Central and Southwest CDs as shown in USDM maps (Figure 4.2).

4.5. Conclusions

Canopy temperatures and surface reflectance detected from space offers an effective means of monitoring drought stress on vegetation. This paper analyzed the response of different land cover types to drought by comparing their Terra-MODIS–derived cumulative LST and NDVI signals during the summer growing season of a drought and a non-drought year. Results of matched-pair t-tests indicate that a majority of the land cover pixels in Nebraska experienced significantly higher cumulative day and nighttime LST coupled with lower NDVI during the drought year in all CDs of Nebraska except for the northwestern part of Panhandle ($P < 0.01$). For irrigated corn, NDVI is rather a conservative indicator of drought compared to LST, with more pixels experiencing significantly higher LST compared to those depicting significant NDVI decrease ($P < 0.01$). The time-series drought and non-drought differences in MCL and MCN for four land cover clusters were examined to analyze the magnitude of drought induced stress on these land cover types. The results indicated that the little bluestem grassland cover type exhibited the maximum increase in mean cumulative daytime LST and decrease in mean cumulative NDVI during the drought year, followed by sandhills upland grassland, suggesting that grassland cover types are more sensitive to drought.

The cross-correlations between time-series MCL and MCN differences were significant for all four land cover types ($P < 0.001$). The regression models depicting the relationship between cumulative LST and NDVI differences between the drought and non-drought periods for four land cover types can be used to predict the drought related stress in vegetation.

Overall, this study demonstrates that Terra-MODIS eight-day composite LST and NDVI products are sensitive to drought-related stress in vegetation. AVHRR-based vegetation condition monitoring indices such as VCI, TCI, VH, RG, and SVI require a longer period of LST and/or NDVI data. Considering the shorter temporal history of MODIS data, use of cumulative LST and NDVI to quantitatively compare drought and non-drought years as demonstrated in this study can assist in assessing the vegetation stress in the Central Great Plains region of the United States. As a part of future study, similar analysis for other land cover types in different geographical regions will be conducted to investigate the LST and NDVI responses during drought.

References

Anderson, M. C., J. M. Norman, J. R. Mecikalski, J. A. Otkin, and W. P. Kustas, 2007. A climatological study of evapotranspiration and moisture stress across the Continental United States based on thermal remote sensing: 2. Surface moisture climatology. *Journal of Geophysical Research*, 112, D11112 [doi:10.1029/2006JD007507].

Bayarjargal, Y., A. Karnieli, M. Bayasgalan, S. Khudulmur, C. Gandush, and C. J. Tucker, 2006. A comparative study of NOAA-AVHRR derived drought indices using change vector analysis. *Remote Sensing of Environment*, 105:9–22.

Burgan, R. E., and R. A. Hartford, 1993. Monitoring Vegetation Greenness with Satellite Data, Ogden, UT: U.S. Department of Agriculture, U.S. Forest Service, Intermountain Research Station, Gen. Tech. Rep. INT-297, 13 p.

Carlson, T. N., R. R. Gillies, and E. M. Perry, 1994. A method to make use of thermal infrared temperature and NDVI measurements to infer soil water content and fractional vegetation cover. *Remote Sensing Reviews*, 9:16–173.

Cohen, Y., V. Alchanatis, M. Meron, S. Saranga, and J. Tsipris, 2005. Estimation of leaf water potential by thermal imagery and spatial analysis. *Journal of Experimental Botany*, 56:1843–1852.

Dappen, P., J. Merchant, I. Ratcliffe, and C. Robbins, 2007. Delineation of 2005 land use patterns for the state of Nebraska, Lincoln, NE: Department of Natural Resources, Final Report

[http://dnr.ne.gov/Publications_Studies/2005_Landuse_FinalReport.pdf].

Di, L., D. C. Rundquist, and L. Han, 1994. Modeling relationships between NDVI and precipitation during vegetation growth cycles. *International Journal of Remote Sensing*, 15:2121–2136.

Dowdy, S., S. Wearden, and D. Chilko, 2004. Statistics for Research, third edition, New York, NY: John Wiley, 627 p.

Feldhake, C. M., D. M. Glenn, and D. L. Peterson, 1996. Pasture soil surface temperature response to drought. *Agronomy Journal*, 88(4):652–656.

GDG (Geospatial Data Gateway), 2010, "Annual Maximum Temperature by State" [http://datagateway.nrcs.usda.gov/GDGOrder.aspx], accessed July 20, 2010.

Glenn, E. P., A. R. Huete, P. L. Nagler, and K. K. Hirschboeck, 2007. Integrating remote sensing and ground methods to estimate evapotranspiration. *Critical Reviews in Plant Sciences*, 26:139–168.

Goetz, S. J., 1997. Multi-sensor analysis of NDVI, surface temperature and biophysical variables at a mixed grassland site. *International Journal of Remote Sensing*, 18:71–94.

Goward, S. N., C. J. Tucker, and D. G. Dye, 1985. North American vegetation patterns observed with the NOAA-7 Advanced Very High Resolution Radiometer. *Vegetatio*, 64:3–14.

Gu, Y., J. F. Brown, J. P. Verdin, and B. D. Wardlow, 2007. A five-year analysis of MODIS NDVI and NDWI for grassland drought assessment over the Central Great Plains of the United States. *Geophysical Research Letters*, 34, L06407 [doi:10.1029/2006GL029127].

Granger, R. J., 2000. Satellite-derived estimates of evapotranspiration in the Gediz basin. *Journal of Hydrology*, 229:70−76.

Guttman, N. B., and R. G. Quayle, 1996. A historical perspective of U.S. Climate Divisions. *Bulletin of American Meteorological Society*, 77:293–303.

Hashimoto, H., J. L. Dungan, M. A. White, F. Yang, A. R. Michaelis, S. W. Running, and R. R. Nemani, 2008. Satellite-based estimation of surface vapor pressure deficits using MODIS land surface temperature data. *Remote Sensing of Environment*, 112:142–155.

Hayes, M. J., 2003. Drought Indices," National Drought Mitigation Center, University of Nebraska–Lincoln [http://drought.unl.edu/whatis/indices.htm], last accessed May 18, 2010.

Henebry, G., M. Vaitkus, and J. Merchant, 2008. Nebraska Gap Analysis Project, Reston, VA: U.S. Geological Survey

[http://digitalcommons.unl.edu/cgi/viewcontent.cgi?article=1030&context=usgspubs].

HPRCC (High Plains Regional Climate Center), 2010. University of Nebraska–Lincoln [http://www.hprcc.unl.edu], last accessed January 16, 2010.

Ji, L., and A. J. Peters, 2003. Assessing vegetation response to drought in the Northern Great Plains using vegetation and drought indices. *Remote Sensing of Environment*, 87:85–98.

Johnson, B., 2001. Inventorying Nebraska's irrigation acres. Cornhuskers Economics, University of Nebraska Cooperative Extension, June 20, 2 p.

Justice, C. O., J. R. Townshend, B. N. Holben, and C. J. Tucker, 1985. Analysis of the phenology of global vegetation using meteorological satellite data. *International Journal of Remote Sensing*, 6:1271–1318.

Karnieli, A., N. Agam, R. Pinker, M. Anderson, M. Imhoff, G. Gutman, N. Panov, and A. Goldberg, 2010. Use of NDVI and land surface temperature for drought assessment: Merits and limitations. *Journal of Climate*, 23:618–633.

Kogan, F. N., 1995. Droughts of the late 1980s in the United States as derived from NOAA polar orbiting satellite data. *Bulletin of the American Meteorological Society*, 76:655–668.

Kogan, F. N., 1997. Global drought watch from space. *Bulletin of the American Meteorological Society*, 78:621–636.

Kogan, F. N., 2001. Operational space technology for global vegetation assessment. *Bulletin of the American Meteorological Society*, 82:1949–1964.

Kogan, F. N., 2002. World droughts in the new millennium from AVHRR-based Vegetation Health Indices. *EOS, Transactions, American Geophysical Union*, 83:557–564.

Korin, B. P., 1975. Statistical Concepts for the Social Sciences, Cambridge, UK: Winthrop Publishers.

McKee, T. B., N. J. Doesken, and J. Kleist, 1995. Drought monitoring with multiple time scales," *in Preprints 9th Conference on Applied Climatology*, Dallas, TX, 233–236.

Masialeti, I., S. Egbert, and Wardlow, B. D., 2010. A comparative analysis of phenological curves for major crops in Kansas. *GIScience & Remote Sensing*, 47: 241–259.

McVicar, T. R., and P. N. Bierwirth, 2001. Rapidly assessing the 1997 drought in Papua New Guinea using composite AVHRR imagery. *International Journal of Remote Sensing*, 22:2109–2128.

McVicar, T. R., and D. L. Jupp, 1998. The current and potential operational uses of remote sensing to aid decisions on drought exceptional circumstances in Australia: A review. *Agriculture Systems*, 57(3):399–468.

Moran, M. S., T. R. Clarke, U. Inoue, and A. Vidal, 1994. Estimating crop water deficit using the relation between surface-air temperature and spectral vegetation index," *Remote Sensing of Environment*, 49:246–263.

Mendelsohn, R., P. Kurukulasuria, A. Basist, F. Kogan, and C. Williams, 2007. Climate analysis with satellite verses weather station data. *Climatic Change*, 81:71–83.

Nemani, R. R., L. L. Pierce, S. W. Running, and S. Goward, 1993. Developing satellite-derived estimates of surface moisture status. *Journal of Applied Meteorology*, 32:548–557.

Palmer, W. C., 1965. Meteorological Drought, Washington, DC: U.S. Department of Commerce Weather Bureau, Research Paper No. 45.

Palmer, W. C., 1968. Keeping Track of Crop Moisture Conditions, Nationwide: The New Crop Moisture Index. *Weatherwise*, 21:156–161.

Park, S., J. J. Feddema, and S. L. Egbert, 2004. Impacts of hydrologic soil properties on drought detection with MODIS thermal data. *Remote Sensing of Environment*, 89:53–62.

Peters, A. J., E. A. Walter-Shea, L. Ji, A. Viña, M. J. Hayes, and M. D. Svoboda, 2002. Drought monitoring with NDVI-based Standardized Vegetation Index. *Photogrammetric Engineering and Remote Sensing*, 68:71–75.

Price, J. C., 1990. Using spatial context in satellite data to infer regional scale evapotranspiration. *IEEE Transactions on Geoscience and Remote Sensing*, 28:940–948.

Rouse, J. W., R. H. Haas, J. A. Schell, and D. W. Deering, 1974. Monitoring vegetation systems in the Great Plains with ERTS. *in Proceedings of the Third Earth Resources Technology Satellite-1 Symposium*, Vol. 1, 48–62.

Rundquist, B. C., and J. A. Harrington, Jr., 2000. The effects of climatic factors on vegetation dynamics of tallgrass and shortgrass cover. *Geocarto International*, 15(3):33–38.

Sandholt, I., K. Rasmussen, and J. Andersen, 2002. A simple interpretation of the surface temperature/vegetation index space for assessment of surface moisture status. *Remote Sensing of Environment*, 79:213–224.

Shafer, B. A., and L. E. Dezman, 1982. Development of a Surface Water Supply Index (SWSI) to assess the severity of drought conditions in snowpack runoff areas. *in Proceedings of the Western Snow Conference*, Colorado State University, Fort Collins, Colorado, 164–175.

Sun, D., and M. Kafatos, 2007. Note on the NDVI-LST relationship and the use of temperature-Related drought indices over North America. *Geophysical Research Letters*, 34, L24406 [doi:10.1029/2007GL031485,2007].

Stubbendieck, J., and K. L. Kottas, 2005. Common Grasses of Nebraska, Lincoln, NE: University of Nebraska Extension, EC05-170, 123 p.

Svoboda, M., D. LeComte, M. J. Hayes, R. Heim, K. Gleason, J. Angel, B. Rippey, R. Tinker, M. Palecki, D. Stooksbury, D. Miskus, and S. Stephens, 2002. The Drought Monitor. *Bulletin of American Meteorological Society*, 83(8):1181–1190.

Tucker, C. J., 1979. Red and photographic infrared linear combinations for monitoring vegetation. *Remote Sensing of Environment*, 8:127–150.

Tucker, C. J., C. Vanpraet, M. I. Sharman, and G. Van Ittersum, 1985. Satellite remote sensing of total herbaceous biomass production in the Senegalese Sahel: 1980–1984. *Remote Sensing of Environment*, 14:233–249.

Tunnell, T. R., 2004. Guide to Native Grassland Management, Wood River, NE: Nature Conservancy Management Guide.

USDA (U.S. Department of Agriculture), 2002. USDA National Agricultural Statistics Service (NASS)-Quick Stats.

[http://www.nass.usda.gov/QuickStats/Create_County_Indv.jsp], last assessed June 4, 2010.

USDA (U.S. Department of Agriculture), 2007a. USDA National Agricultural Statistics

Service (NASS)—Cropland Data Layer Metadata.

[http://www.nass.usda.gov/research/Cropland/metadata/meta.htm], last accessed March 15, 2010.

USDA (U.S. Department of Agriculture), 2007b. Weekly Weather and Crop Bulletin. [http://www.usda.gov/oce/weather/pubs/Weekly/Wwcb/index.htm], last accessed May 6, 2010.

Vermote, E., N. Saleous, and C. Justice, 2002. Atmospheric correction of MODIS data in the visible to middle infrared: First results. *Remote Sensing of Environment*, 83:97–111.

Vermote, E. and S. Kotchenova, 2008. MOD09 (Surface Reflectance) user's guide, Version 1.1.

[http://modis.datamirror.csdb.cn/resource/doc/MOD09_UserGuide.pdf],

last accessed November 18, 2010.

Wan, Z., P. Wang, and X. Li, 2004. Using MODIS land surface temperature and normalized difference vegetation index products for monitoring drought in the southern Great Plains, USA. *International Journal of Remote Sensing*, 25:61–72.

Wan, Z., Y. Zhang, Q. Zhang, and Z. Li, 2002. Validation of the land-surface temperature products retrieved from Terra Moderate Resolution Imaging Spectroradiometer Data. *Remote Sensing of Environment*, 83:163–180.

Wang, J., K. P. Price, and P. M. Rich, 2001a. Spatial patterns of NDVI in response to precipitation and temperature in the Central Great Plains. *International Journal of Remote Sensing*, 22:3827–3844.

Wang, P.-X., X.-W. Li, J.-Y. Gong, and C.-H. Song, 2001b. Vegetation temperature condition index and its application for drought monitoring. *in Proceedings of International Geoscience and Remote Sensing Symposium*, Sydney, Australia, 141–143.

Wardlow, B. D., and S. L. Egbert, 2008. Large-area crop mapping using time-series MODIS 250 m NDVI data: An assessment for the U. S. Central Great Plains, *Remote Sensing of Environment*, 112:1096-1116.

Wardlow, B. D., S. L. Egbert, and J. H. Kastens, 2007. Analysis of timeseries MODIS 250 m vegetation index data for crop classification in the U. S. Central Great Plains. *Remote Sensing of Environment*, 108: 290–310

Wilhite, D. A., M. J. Hayes, and M. D. Svoboda, 2000. Drought monitoring and assessment: Status and trends in the United States. *in Drought and Drought Mitigation in Europe*, Vogt, J. V. and F. Somma (Eds.), Dordrecht, The Netherlands: Kluwer Academic Publishers, 149–160.

Wolfe, R. E., M. Hishihama, A. J. Fleig, J. A. Kuyper, D. P. Roy, J. C. Storey, and F. S. Patt, 2002. Achieving sub-pixel geolocation accuracy in Support of MODIS land science. *Remote Sensing of Environment*, 83:31–49.

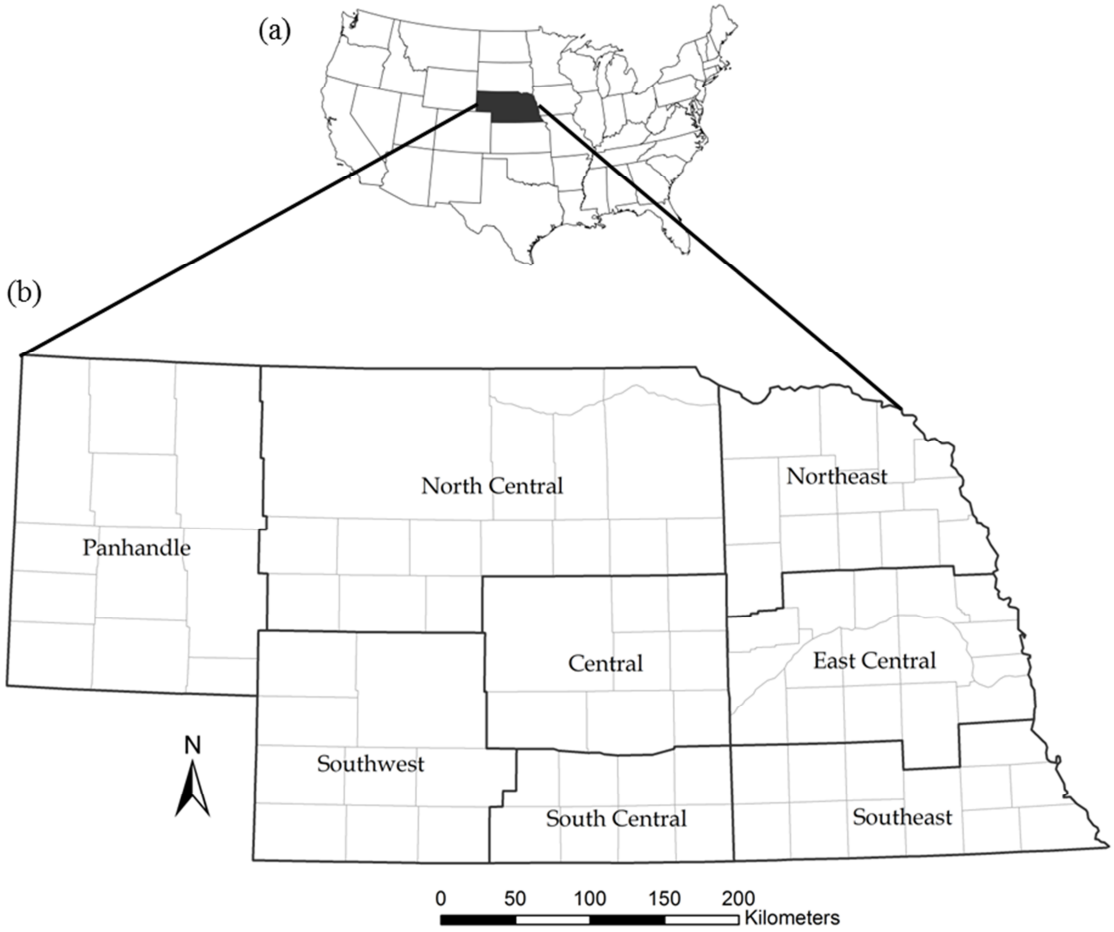

Figure 4.1. Location of study area, the state of Nebraska (a) and the climate division (CD) boundary map (b). The dark lines in (b) denote CD boundaries, and the lighter grey lines correspond to the county boundaries.

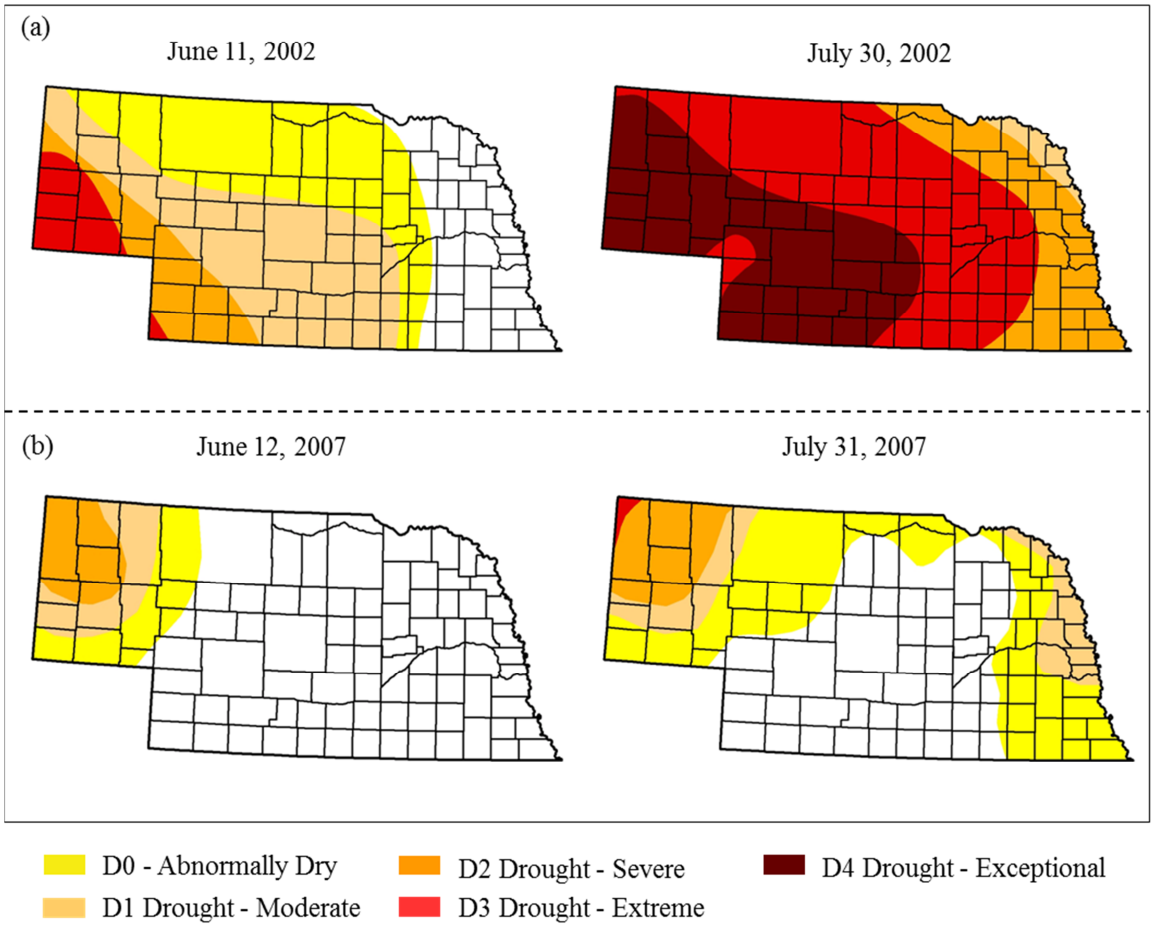

Figure 4.2. U.S. Drought Monitor maps showing the spatial patterns of drought with impacts on agriculture and water resources across Nebraska during the growing seasons of 2002 (a) and 2007 (b).

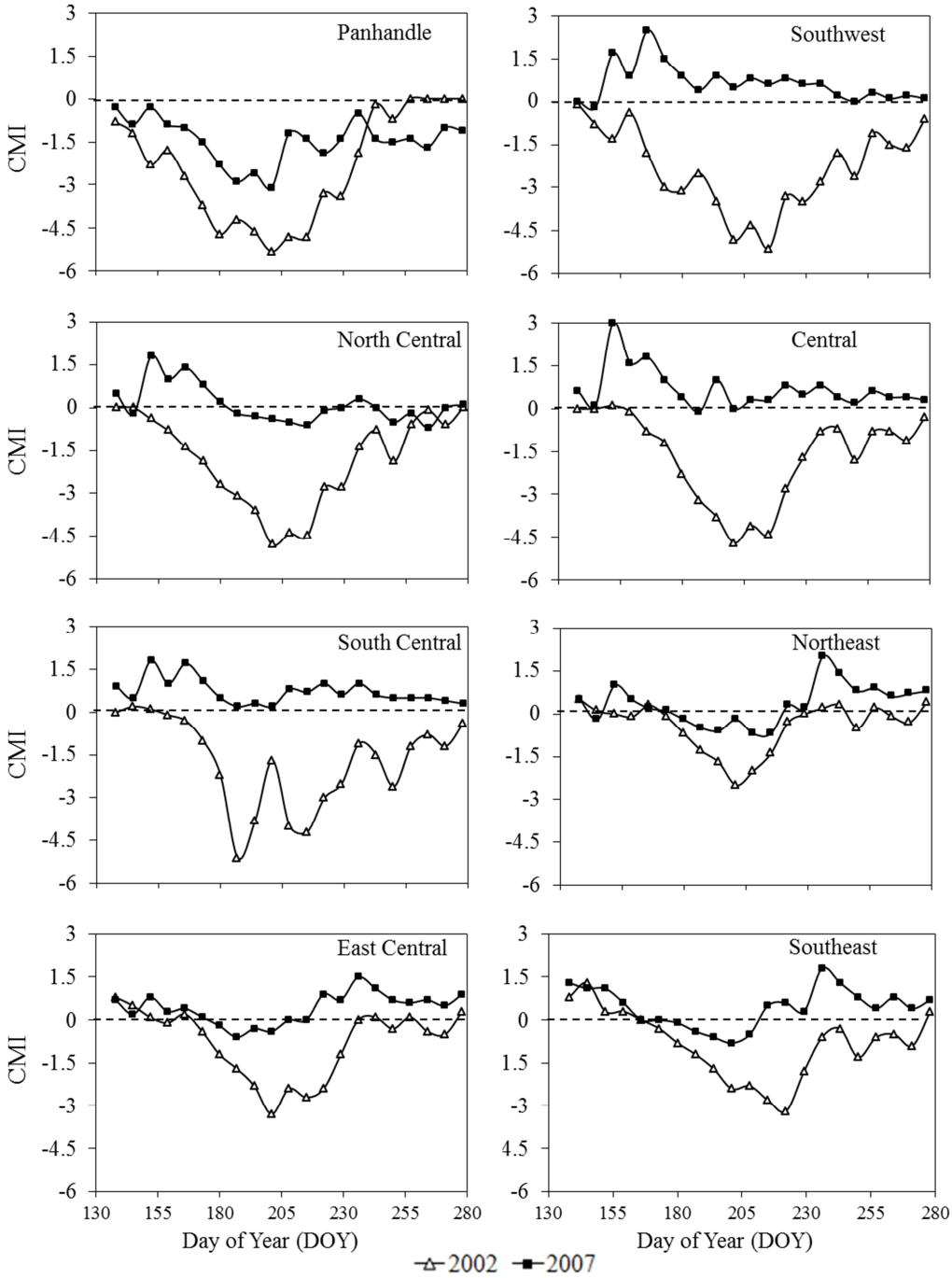

Figure 4.3. Weekly crop moisture index (CMI) values for each Climate Division (CD) of Nebraska during the growing seasons of 2002 and 2007 (Data source: Weekly Weather and Crop Bulletin, USDA).

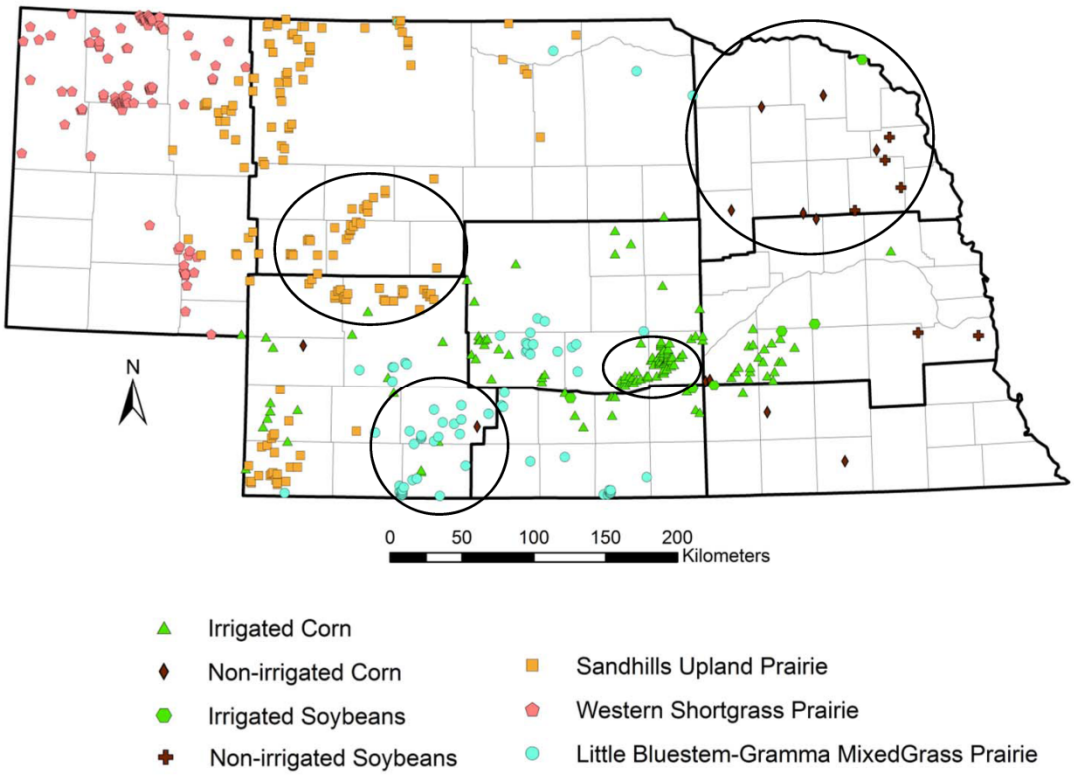

Figure 4.4. Spatial distribution of selected land cover pixels across Nebraska. The number of pixels in each of the land cover classes is as follows: irrigated corn (n = 138), non-irrigated corn (n = 12), irrigated soybeans (n = 6), non-irrigated soybeans (n = 6), sandhills upland prairie (n = 160), little bluestem-grama mixed-grass prairie (n = 71), and western shortgrass prairie (n = 97). The circles show the four land cover clusters (sandhills upland, n = 55; little bluestem, n = 29; irrigated corn, n = 61; and non-irrigated corn, n =6) selected for correlation and regression analyses.

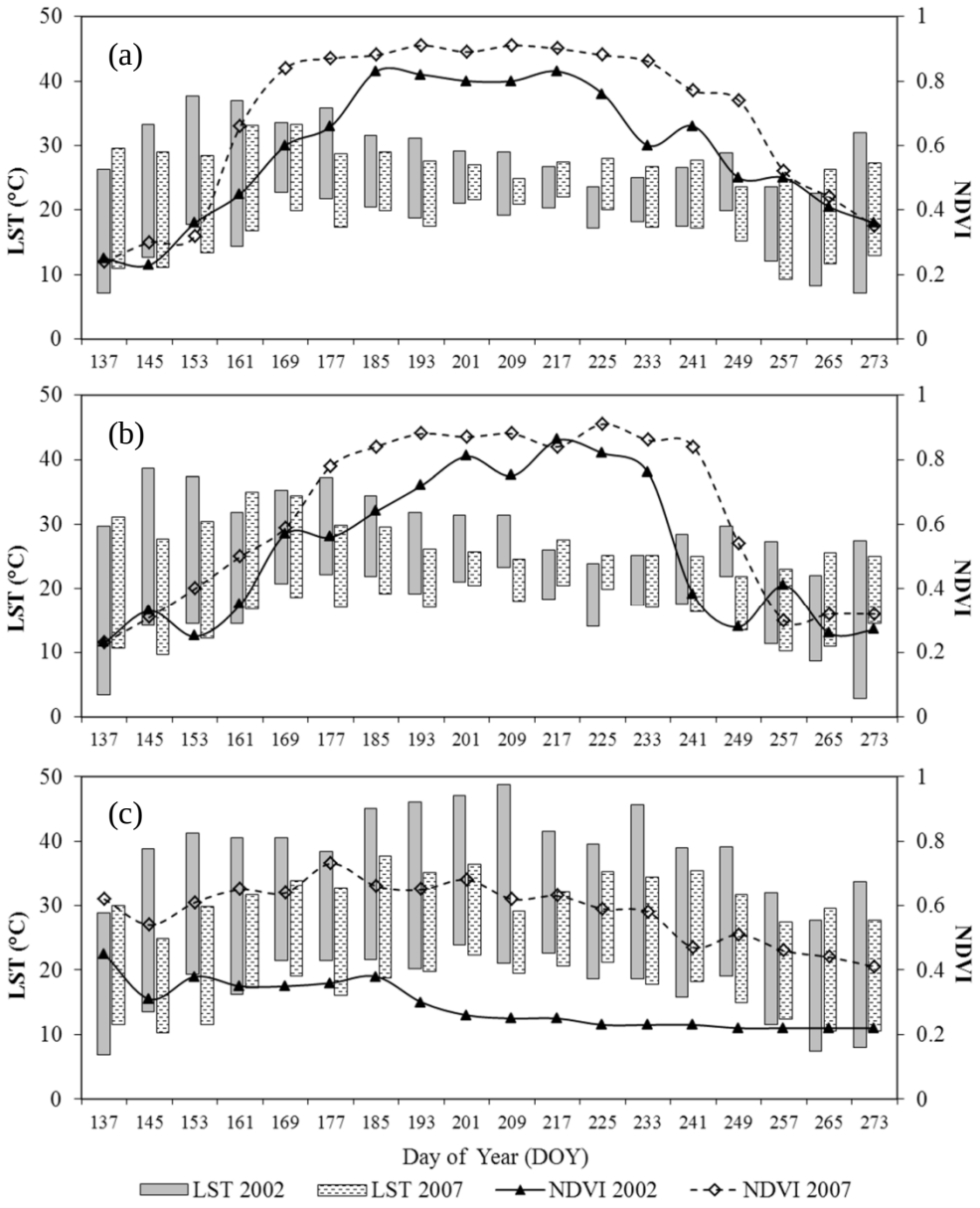

Figure 4.5. Time-series LST and NDVI profiles of an irrigated corn (a), a non-irrigated corn (b), and a little bluestem grassland (c) pixel during the growing seasons of a drought (2002) and a non-drought (2007) year. The bars show the eight-day composited LST observations across the growing season. Top of the bar indicates the daytime LST measured at about10:30 a.m. and the bottom of the bar indicates the nighttime LST measured at about 10:30 p.m. local time.

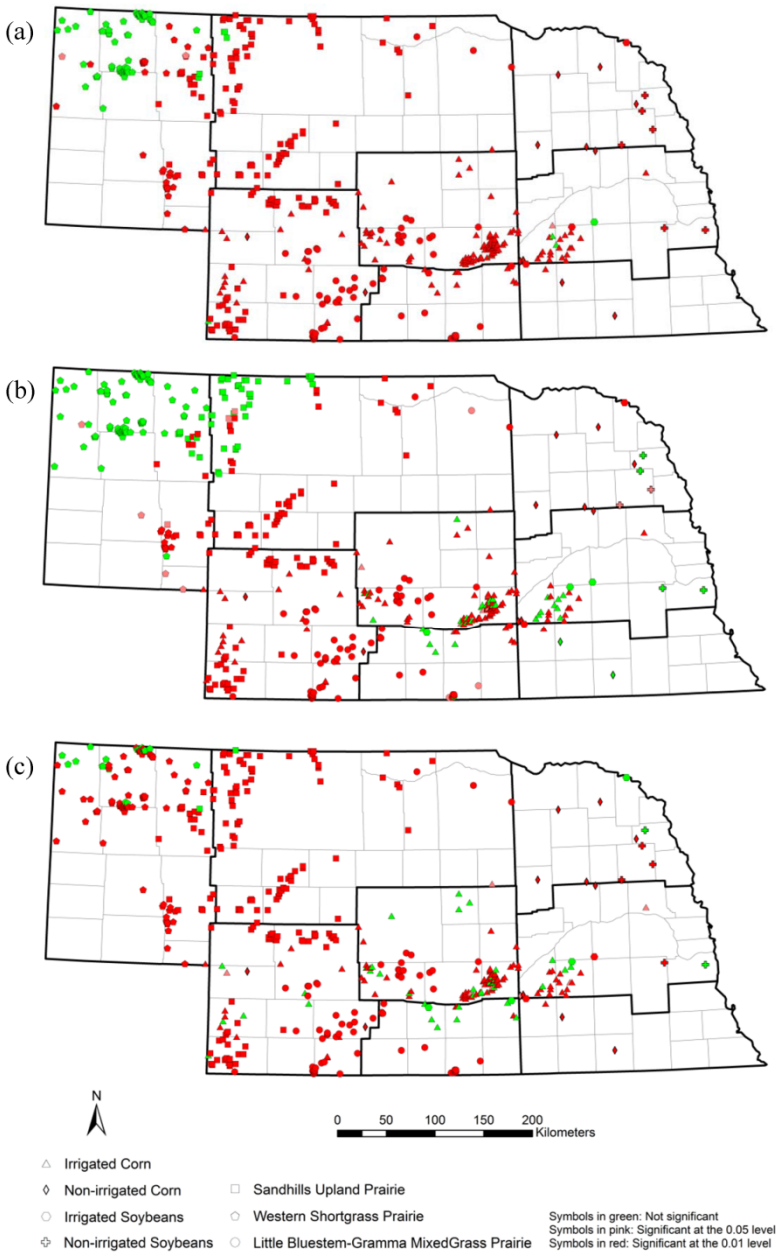

Figure 4.6. Matched-pair t-test results showing the spatial distribution of land cover pixels that exhibited significant and non-significant increase in cumulative daytime LST (a) and cumulative nighttime LST (b), and decrease in cumulative NDVI (c) during the drought year (2002).

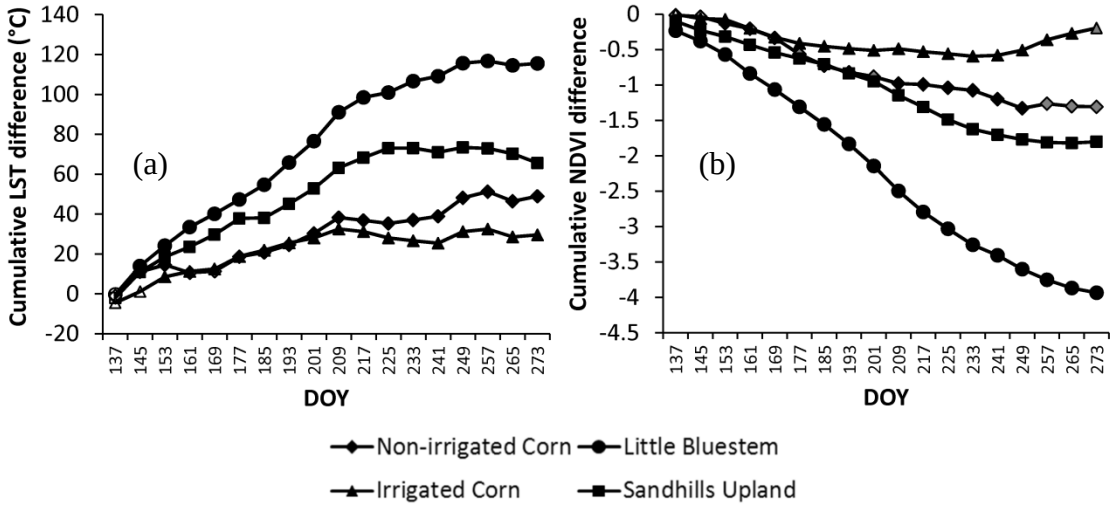

Figure 4.7. Time-series of mean cumulative LST (a) and mean cumulative NDVI (b) differences between the drought (2002) and the non-drought (2007) growing seasons for four selected land cover types. Solid symbols indicate that the mean cumulative LST during the drought year growing season was significantly higher than that of the non-drought year (black indicates $P < 0.001$ and grey $P < 0.01$) and open symbols indicate statistically not significant ($P > 0.05$).

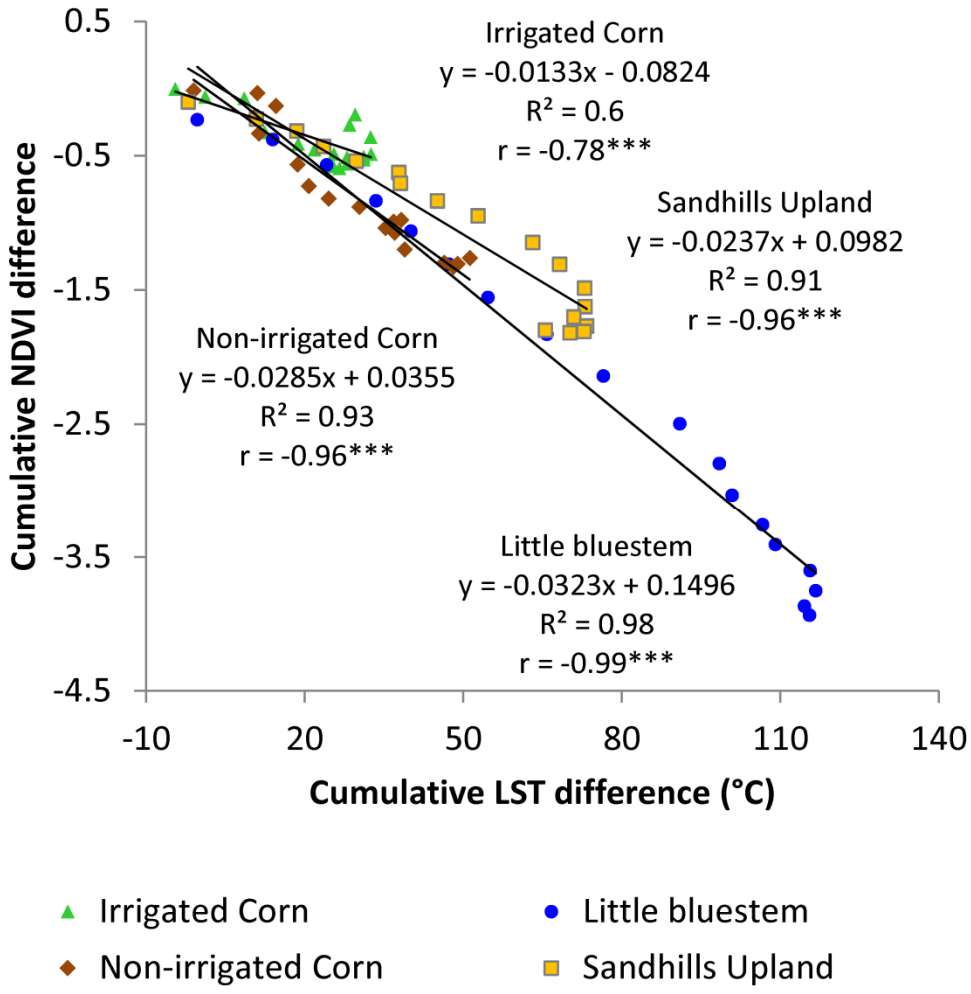

Figure 4.8. Regression models showing the relationship between time-series mean cumulative LST and mean cumulative NDVI differences between the drought and the non–drought year growing seasons for four selected land cover types; *** indicates statistically significant at $P < 0.001$ level.

CHAPTER 5

SUMMARY, CONCLUSIONS, AND RECOMMENDATIONS

The goal of this research was to evaluate the response of different vegetation types to drought-related water stress at multiple spatial scales using both close-range and satellite remote sensing techniques. Vegetation response to drought was evaluated at leaf, canopy, and landscape levels. The summary and key findings of these three studies are presented below.

5.1. Leaf Level Study

At the leaf level, high spatial resolution thermal images of the soybean plants were used to evaluate the effect of water stress on leaf temperatures and to develop a leaf temperature-based model to estimate the relative water content (RWC) in leaves. The soybean plants were grown under the greenhouse conditions and were subjected to eight levels of irrigation treatments. One specific leaf trifoliate was extracted from the thermal images for every plant sample. Mean leaf temperature (T_{leaf}) and Crop Water Stress Index (CWSI) were computed for a specific trifoliate of each plant and compared with the gravimetrically measured RWC as well as with leaf gas exchange measurements. Some of the key findings are presented below.

- The plants experienced decreased RWC with increased intensity of water stress. The differences between control versus WS 1 and WS 2 were not statistically significant, while the difference between control and WS 3 through WS 7 plants were

statistically significant ($P < 0.01$). The mean RWC of WS 7 plants was about 68% less than that of control plants.

- T_{leaf} and CWSI showed overall rising trends with increasing intensity of water stress. Statistically significant differences in the leaf temperatures were found between control and water stressed plants (WS 4 through WS 7). Control plants exhibited significantly different CWSI values than those of water stressed plants (WS 4 through WS 7). These results suggested that leaf temperature derived from the thermal imageries could be used to detect irrigation differences among the soybean plants.
- Separate regression models were calibrated and validated using T_{leaf} and CWSI to estimate RWC. CWSI based model that accounted for varying meteorological conditions such as air temperature, humidity, wind speed, and downwelling irradiance on leaf temperatures resulted in greater accuracy in RWC estimation compared to the model based on T_{leaf}.

Previous studies have been conducted to relate RWC with leaf spectral reflectance in the visible, middle infrared portions of the electromagnetic spectrum. Much of the vegetation water stress research that has used thermal imagery has focused on quantifying leaf biophysical properties such as stomatal conductance and leaf or stem water potentials. These studies were based primarily on grapevines, French beans, lupins, cotton, and olives trees. Despite an extensive scientific literature search, no previous thermal image based RWC determination studies were found. To the best of our knowledge, this research is one of the first studies that used thermal imagery for

estimating RWC in soybean plants. Since soybean is an important agronomic crop in the U.S. Corn Belt, the findings of this study can be applied for operational monitoring of drought in soybeans. In order to apply the findings for operational drought monitoring, some of the potential limitations of the study should be considered and addressed in future research. The results presented here are derived from an experiment conducted in a greenhouse. The variables affecting the plants growth and development were carefully controlled in the managed greenhouse environment, which is not representative of real-world field conditions. In a real-world setting, plants are exposed to uncontrolled air movement, solar radiation, and air temperature in the agricultural fields. Furthermore, the orientation of leaves in the agricultural fields, determined primarily by the wind speed and direction may be different than that at the greenhouse. That could potentially affect the leaf temperature measured by the thermal camera. More research is needed for rigorous validation of the CWSI model developed in this study for RWC estimation in the field conditions.

5.2. Canopy Level Study

Close-range corn and soybean canopy reflectance data were used to explore the potential of three simulated MODIS VIs (NDVI, WDRVI, and EVI2) and a simulated MERIS VI ($CI_{Red\text{-}edge}$) in characterizing root zone soil moisture in the U.S. Corn Belt. Time-series VI data for six growing seasons were correlated with concurrent as well as antecedent soil moisture (up to 60 days) at four different depths (10, 25, 50, and 100 cm) in the soil profile. The key findings are presented below:

- The corn VIs were significantly related to the concurrent soil moisture at the 100 cm depth and among the VIs analyzed in this study, $CI_{Red\text{-}edge}$ showed strongest correlation with the soil moisture at this depth.
- Relationships of corn VIs with soil moisture improved when the time lag that a plant requires to respond to changes in soil moisture were taken into consideration. Corn $CI_{Red\text{-}edge}$ exhibited statistically significant relationship with 10-day lagged soil moisture at 50 cm depth and the correlations increased with longer lag periods. At 100 cm, peak correlations between corn VIs and soil moisture were primarily observed over a 45-day lag period and then showed decreasing trends.
- Contrary to corn, soybean VIs including WDRVI and NDVI were sensitive to concurrent soil moisture at shallow depths of 10- and 25-cm.
- Strongest correlations of soybean WDRVI and NDVI with 5-day lagged soil moisture at 10- and 25-cm depths indicated that soybean VIs kept a relatively shorter soil moisture memory in their spectral signals.

The above findings suggest that accurate characterizations of root zone soil moisture that influences crop conditions can be made using close-range simulated MODIS and MERIS VIs. Spectral reflectance data recorded by the sensors on board satellites are largely contaminated by the intervening atmosphere such as cloud cover, water vapor, and aerosols. Close-range sensing approach adopted in this study overcomes these uncertainties associated with atmospheric impacts. This approach also helps improve our understanding with regard to using spectral signals (VIS and NIR) from crops to assess essential soil-moisture conditions. The relationships shown in this study can be applied to monitor vegetation stress using the satellite data for regional scale

drought assessment. However, the results derived from this study are based on the currently available reflectance data during three years of growing seasons each for corn and soybeans. It would be interesting to analyze corn and soybean VIs and soil moisture correlations with more growing season data using actual MODIS and MERIS data.

5.3. Landscape Level Study

At the landscape scale, the objective was to investigate the changes in the thermal and spectral responses of cropland and grassland cover types to drought across Nebraska. Terra-MODIS eight-day composite cumulative time series daytime LST, nighttime LST and NDVI data pertaining to irrigated and non-irrigated corn and soybeans, and three grassland cover types during a drought year (2002) and a non-drought year (2007) were compared. Some of the key findings are presented below.

- Majority (84%) of the land cover pixels across Nebraska experienced significantly higher cumulative daytime LST ($P < 0.01$) during the drought-year growing season. Fewer pixels (65%) experienced significantly higher nighttime LST in the drought year growing season. These findings suggested that cumulative daytime LST could be a more sensitive indicator of drought stress on vegetation than nighttime LST.
- The location of the non-significant pixels (cumulative daytime and nighttime LST) in northern Panhandle matched well with the area of persistent severe drought depicted on the series of USDM maps throughout the growing season of 2007.
- About 85% of the total land cover pixels experienced significantly lower NDVI during the drought year compared to the non-drought year at $P < 0.01$. A higher percentage of irrigated corn pixels (96%) experienced significantly higher cumulative daytime LST compared to lower cumulative NDVI during the drought year. This

indicates that the rate of decrease in NDVI of irrigated corn during drought is less pronounced than the rate of increase in LST during the drought year growing season.

- Land-cover specific analyses show that the mean cumulative drought year and non-drought year differences in daytime LST and NDVI of grassland cover types (little bluestem followed by sandhills upland) were higher than those of irrigated and non-irrigated corn. It suggests that grassland cover types are more sensitive to drought than irrigated and non-irrigated corn.

- The regression models depicting the relationship between cumulative LST and NDVI differences between the drought and non-drought growing seasons for four land cover types were statistically significant and can be used to predict the drought related stress in vegetation.

This study showed that Terra-MODIS eight-day composite LST and NDVI products are sensitive to drought-related stress in vegetation. By quantitatively comparing the drought and non-drought year growing season's cumulative LST and NDVI values, this study tested a new methodology for assessing drought stress at a landscape scale. The findings of this study can lead to the development of new or refinement of existing operational large-area vegetation drought monitoring tools (for example, Vegetation Drought Response Index (VegDRI)). VegDRI integrates historical weather station-based drought index data (SPI and PDSI) and satellite-based NDVI-derived products with other biophysical characteristics of land such as land cover, land use, and soils and depicts the geographic extent and severity of drought stress on vegetation in the contiguous U.S. at 1-km spatial resolution (Brown et al., 2008). VegDRI model in its current operational

form uses AVHRR-derived NDVI metrics and doesn't include a satellite-based thermal component. Recently, eMODIS-based (Jenkerson et al., 2010) VegDRI was developed to take advantage of better quality and higher temporal resolution NDVI data from MODIS. A pheno-region based, AVHRR-MODIS NDVI translation algorithm (Gu et al., 2010) was used to apply the AVHRR-based VegDRI models to MODIS-derived NDVI inputs. The sensitivity of LST to drought stress on croplands and grassland cover types as demonstrated in this study indicate the potential utility of incorporating MODIS-based LST in the eMODIS-VegDRI model for improved drought monitoring in the contiguous U.S. Compared to the previous remote sensing-based vegetation drought assessment studies in the U.S. Great Plains (Wang et al., 2001; Ji and Peters, 2003), this study is more detailed in the sense that it distinguished drought responses of different crop types (corn and soybeans) with distinct management practices (irrigated and non-irrigated).

However, this study encountered a number of challenges that could provide directions for future research. Since this study was focused on comparing drought year and non-drought year growing seasons to assess the response of vegetation to drought, it would have been ideal to select a growing season in which the entire state of Nebraska was drought free. Choosing such a year was challenging considering the short history of MODIS data availability. The growing season of 2007 was chosen to represent the non-drought year as most parts of the state with the exception of the Panhandle was drought free. Future study involving a different non-drought year may lead to improved vegetation drought stress assessment especially in the Nebraska panhandle region. In this study, the land cover information was spatially aggregated at 1-km level to match with the 1-km MODIS LST and NDVI data. In the eastern Nebraska, the individual crop fields

as identified from the Cropland Data Layers were much smaller than the size of MODIS pixel (1-km). Smaller field sizes together with high frequency crop rotations resulted in less number of non-irrigated corn and soybean pixels that had the same crop type (with >85% per pixel coverage) during both the study years. Future expansion of the study area to Iowa where large proportion of the croplands is non-irrigated may provide more sample pixels to analyze the drought responses of non-irrigated corn and soybeans. The utility of MODIS-derived LST and NDVI products in monitoring drought-related vegetation stress should be tested in other parts of the U.S. Corn Belt and Great Plains as well as in other major agricultural regions of the world. Additionally, this approach should be tested on other crops such as wheat and cotton.

References

Brown, J.F, B. D. Wardlow, T. Tadesse, M. J. Hayes, and B. C. Reed, 2008. The Vegetation Drought Response Index (VegDRI): A new integrated approach for monitoring drought stress in vegetation. *GIScience & Remote Sensing*, 45: 16-46.

Ji, L., and A. J. Peters, 2003. Assessing vegetation response to drought in the Northern Great Plains using vegetation and drought Indices. *Remote Sensing of Environment*, 87: 85-98.

Wang, J., K. P. Price, and P. M. Rich, 2001. Spatial patterns of NDVI in response to precipitation and temperature in the Central Great Plains. *International Journal of Remote Sensing*, 22:3827–3844.

Jenkerson, C. B., T. Maiersperger, and G. Schmidt, 2010. eMODIS: A user-friendly data source: U.S. Geological Survey Open-File Report 2010-1055, 10 pp.

Gu, Y., J. Brown, T. Miura, W. Van Leeuwen, B. Reed, 2010. Phenological classification of the United States: A geographic framework for extending multi-sensor time-series data. *Remote Sensing*, 2: 526-544.